# Ultrafast Optical Pulse Interactions in Active Disordered Condensed Matter

By

**Masood Siddique**

A dissertation submitted to the Graduate Faculty in Electrical Engineering in partial fulfillment of the requirements for the degree of Doctor of Philosophy, The City University of New York.

**2005**

INFORMATION TO USERS

The quality of this reproduction is dependent upon the quality of the copy submitted. Broken or indistinct print, colored or poor quality illustrations and photographs, print bleed-through, substandard margins, and improper alignment can adversely affect reproduction.

In the unlikely event that the author did not send a complete manuscript and there are missing pages, these will be noted. Also, if unauthorized copyright material had to be removed, a note will indicate the deletion.



ProQuest Information and Learning Company
300 North Zeeb Road
P.O. Box 1346
Ann Arbor, MI 48106-1346

This manuscript has been read and accepted for the Graduate Faculty in Engineering in satisfaction of the dissertation requirement for the degree of Doctor of Philosophy.

1/27/05

Date

Professor R. R. Alfano

Chair of Examining Committee

1/27/2005

Date

Executive Officer

Supervisory Committee:

Professor Prof. P. Ho (Electrical Engineering)

Prof. L. Issacs _(Chemical Engineering)

Prof. V. Petricevic (Physics)

Prof. W. Wang (IUSL, Senior Scientist)

Prof. Nan-Lo Yang_(Chemistry, College of Staten Island)

# ABSTRACT

## Ultrafast Optical Pulse Interactions in Active Disordered Condensed Matter

by

**Masood Siddique**

**Advisor: Professor Robert R. Alfano**

The goal of this research is to better understand the basic physics that governs the behavior of short-pulsed light propagating in scattering media where either the host medium or the scattering particles exhibit emission or absorption interact with the incident light in form of absorption or stimulated emission.

The temporal and spectral dynamics from the interactions of optically active disordered-media with ultrashort optical pulses is the focus of the research performed in this thesis. The interaction processes studied are optical gain, spectral narrowing, fluorescence and pulse lifetime reduction and transport of ultrashort optical pulses in disordered media containing optically active discrete scattering particles. Linear and nonlinear effects are presented where the propagation of picosecond and femtosecond laser pulses in active disordered media is measured experimentally and compared with the theories of Boltzmann radiative transport and diffusive propagation of radiation in disordered media.

Active media can be involved in optical processes in disordered media where either the propagation of optical radiation can result in gain or absorption upon optical

excitation. A study of optical scattering in non-discrete media such as the biological heterogeneously-continuous scattering tissues is carried out as well. Lasing in random media is one of the outcomes of these results. The optical gain of optically excited active media is divided into clear subdivisions of Amplified Spontaneous Emission, Stimulated Emission and Laser Emission by characterizing them by their temporal and spectral emission.

*Dedicated to the memory of my father*

Siddique Mohammad

# Acknowledgements

It is with great pleasure and deepest gratitude that I thank my mentor Prof. Alfano for his support throughout my research and thesis work. He has been my mentor in the truest sense of the word. He was always been open to helping and guiding me in academic and personal matters. He has always been available to me in his support and I could always count on him during very difficult times. It has been a great learning experience working under his tutelage. I hope I can live up to the trust and faith he has invested in me.

I take this opportunity to thank Dr. Lisa Samstag. I could not get through my difficult times without her unwavering and dedicated support.

I have been blessed with many good and supportive friends. Special thanks to my friends Dr. Imran Shah and Tinky Shah and their children Taimur, Anum, Shahryar and Tipu. Their love and support has been one of the brighter spots in my life. They have always been there for me in their love and friendship and not the least of which is the unfettered access to their fridge! I also thank Dr. Tahir Andrabi, Shaila Akbar and their children Nafeesa, Anisa and Mohi for their love and support.

I thank my family, especially my brothers Mahmood and Nadim for being there whenever I needed them and my nephews Abdullah, Humza, Taha and Rayan, whose zany antics are a constant source of pleasure.

This thesis is dedicated to the memory of my father. His absolute honesty, unshakeable faith and exemplary hard work has been the guiding light in my life. I can only aspire to highest standards of integrity he has set. I wish he could be here today, I miss him very much.

# Table of Contents

# List of Figures

# List of Tables

# CHAPTER 1

# INTRODUCTION

## 1.1 Introduction

The propagation of light in matter is still one of the most fundamental physical processes that enable us to interact with the world around us. A majority of the composition of the condensed matter in the universe is disordered in nature, which makes it important for us to better understand the underlying physical processes that effect the interaction of electromagnetic radiation with disordered turbid matter. The light scattering off materials around us makes us aware of their presence and proximity allowing us to see objects. Examples such as, light scattering off fog makes the image hazy or hard to see and sometimes interferes in the transmission of useful information. Multiple scattering blurs images of objects. This kind of undesirable scattering process is detrimental to many desirable and important activities such as communications, driving etc. and poses serious impediments to quick diagnosis for effective medical imaging and treatments.

Scattering arises from the particles located in a host medium. The nature of scattering depends on the relative size of the particle and the wavelength of the radiation involved and the presence of gain or absorption in the scattering medium. The study of light scattering is a field of great interest and since the advent of ultrashort-pulsed laser the research in this area of physics has been area of intense research activity. Light is characterized by several key properties; color (wavelength), directionality, travels at the ultimate speed, coherence, polarization and temporal duration. Despite the fundamental

nature of the light scattering processes, the physics behind the propagation of light in scattering media is still not well understood and fundamental universal physical laws that govern scattering processes have yet to be established. The main problem in modeling propagation of scattered light is the difficulty in specifying the radiation field in an atmosphere that scatters light in accordance with well-defined physical laws. The scattering medium can have active particles or host molecules.

One of the earliest attempts at quantifying the scattering process and specifying physical laws originated in 1871 from the investigations by Lord Rayleigh into the illumination and polarization of sunlit sky. The fundamental equations governing Rayleigh's problem was not formalized until Arthur Schuster formulated a problem in radiative transfer in the 1905 to explain the appearance of absorption and emission lines in stellar spectra[2] and the introduction of the concept of radiative equilibrium in stellar atmospheres by Karl Schwarzchild[3] in 1906. Since that time, the application of the Radiative Transfer Theory (RTE) has been the basis for the investigations by astrophysicists as the optical analogue of the Boltzmann-Transfer-Theory. More recently, RTE has formed the centerpiece for modeling diffusive processes by theoretical and experimental physicists studying disordered media in various fields since essentially the same problems arise in disparate fields such as the theory of diffusion in optical propagation in disordered media and in the diffusive propagation of neutrons. Over the past decade, the propagation of ultrafast optical pulses through highly scattering media has drawn great interest due to its wide range of potential applications in the medical, military and commercial fields. Scattering media with gain or absorptive particles alters

the pulse shape in the spectral and frequency domains as it is backscattered and transmitted. This thesis focuses on active scattering media.

A major advancement in the development of theory of light scattering has been the exact closed-form mathematical solution of amplitude and phase of the scattered radiation from a sphere of arbitrary size and dielectric constants by Mie[4] in 1906. The exact Mie solution facilitated in the accurate calculation the fundamental parameters of light scattering off a scattering particle such as the scattering and absorption cross-sections. Using the Mie theory, one can calculate the amplitude and intensity of scattered light off a spherical particle at any angle and the average cosine, which is a measure of the difference between of amount of light scattered in the forward and back direction. The scattering and absorption cross sections depend on the wavelength of the incident light and the size and dielectric constants of the scattering particle and the average cosine factor, $g$, has a value between 1 and –1. The incident laser radiation that enters the disordered scattering medium is characterized by its change in coherence, directionality, polarization, intensity and temporal duration. The incident pulse is altered as it loses its coherence, polarization, intensity and pulse broadening in time as it travels through the medium. The incident light is dispersed and decomposes into coherent and incoherent components and may change further depending on the optical gain or absorptive properties of the medium itself. The scattering medium can get altered itself as it might absorb the radiation and remit it as fluorescence or absorb the incident light. The emission process can alter the emission lifetime of the optically active species embedded in the medium and can induce optical gain to the fluorescent light as it travels through the system. The absorption can influence the incident pulse depending on how the absorption

is introduced into the system. The basic principles used in the modeling of scattering effects on the incident radiation in various types scattering media such as biological media, atmospherical media and interstellar dust, have been laid out in books of seminal importance by Chandrashekar[5], H. C. Van de Hulst[6], and Huffman[7]. The fundamental principles of light scattering and radiation transfer laid out in these books still form the basis of modeling of optical transport in scattering media.

The recent interest in the experimental investigation has been facilitated by the confluence of the development of the laser[8] and the theory of localization in scattering materials in the 1960's. The process of light scattering off a material can affect a change in the properties of the incident light or bring a change in the physical properties of the material it is interacting with. The experimental and theoretical research in emission radiation from scattering media containing optical gain has picked up further interest since the experimental demonstration of laser-like effects by Lawandy[9] et al and Alfano[10,11] et al in 1994. There has been intense activity in modeling the emission properties of scattering media since the publication of the results by Lawandy[9] and Alfano's[10,11] group the publication of the results presented in this thesis.

This thesis deals with two aspects of optical interaction with disordered media where the some part of the disordered medium is active and has either optical gain or absorption embedded in it. The optically active processes that were experimentally investigated in the thesis are optical amplification and optical absorption. The scattering medium generally consists of a host medium containing scattering particles randomly distributed through out the system. Two types of disordered scattering media were investigated as shown in figure 1.1. One type consists of an optically active host which is either

absorptive or has optical gain and the scattering particles are non-active (purely scattering), whereas in the second type, the scattering particles have absorption or gain and the host is transparent. The interaction of the active scattering medium with and incident optical pulse, $E_{in}(t,\lambda)$, resulting in the an output optical emission, $E_{out}(t,\lambda)$ can be written as,

$$E_{out}(t,\lambda) = M_s E_{in}(t,\lambda) \tag{1.1}$$

where $M_s$ is the modulation transfer function i.e. the property of the scattering medium that transforms the input pulse into the output radiation.

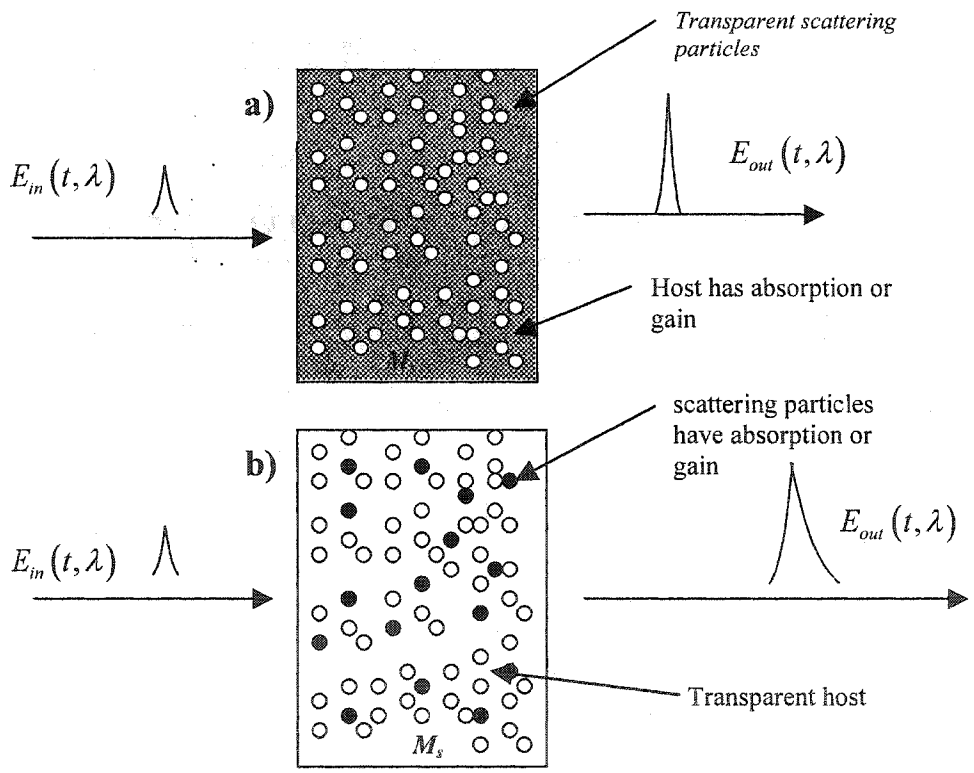


Figure 1.1 Two possible models of optically active scattering media, a) The host has absorption or gain, b) the scattering particles may have absorption or gain

In the optical amplification experiments, the excited disordered systems, the host is composed of lasing materials where the emission properties are altered due to the presence of scatterers in the medium. In optical absorption experiments, the scattering media is composed of scattering particles in a transparent host where some of the particles are replaced in part by absorptive particles.

Ever since the demonstration of laser emission by Townes[8] and establishment of operating principles for obtaining lasing threshold, the conventional wisdom dictates that any losses due to scattering in the gain media should be eliminated or minimized for efficient and effective lasing conditions and operation. This thesis deals with the emission dynamics of laser materials where the scattering was enhanced by adding scattering particles to the laser media. Letokhov[12] *et al* first proposed the idea of what he termed as "generation in an amplifying and scattering clouds" containing uniform gain in the 1960's as a model of a nonresonant feedback laser action. His group demonstrated the principles of incoherent feedback by using scattering media as an incoherent reflector replacing a cavity mirror. The work was further developed by the experimental investigations of the alterations in spectral profiles of emission of crushed laser crystals under varying excitation intensity by Markushev[13] and others. They demonstrated the dependence of emission lineshape as a function of incident intensity and the particle shape. Gouedard[14] analyzed the shift in emission lifetime in excited powder aggregates of laser powders in 1993 by measuring the temporal and spectral coherence from the contrast of near-field speckle pattern.

The laser-like emission from colloidal gain media was first termed as "random lasers" after demonstration of laser-like behavior of emission spectrum by Lawandy[9] et al and

the demonstration of drastic spectral and lifetime shortening under excitation by ultrashort intense pulses by Alfano[10,11] et al. Since the demonstration of laser-like emission in 1994, there has been a flurry of theoretical and experimental activity to investigate the lasing action in disordered media in different materials and configuration to better understand the transient dynamics of emission radiation. The underlying dynamics of lasing in scattering media are still being researched as the multiple scattering off particles can give rise to multiple lasing modes in the emission spectrum profile or act as a feedback conduit to enhance amplifying effect in bursts intense emission intensity.

The lasing process in scattering media was subdivided into two categories based on incoherent and coherent feedback. Cao[15] *et al* demonstrated the evolution of multiple laser lines in densely packed powder aggregates of ZnO particles. They have termed this process as coherent feedback random lasers. In extremely dense packing of lasing particles, when the transport mean free path length was of the order of the wavelength, the emission is effected by coherent interference of radiative emission from within the scattering particles.

The field of lasing in scattering media is still not well understood and there is a lot of interest in the scientific community to better model the processes involved in laser action in disordered media. Letokhov[12] had originally modeled the lasing process as amplification due to diffusion. The diffusion model did nor fully explain the nature of emission and since the renewed interest in lasing processes in the 1990's various other models have been proposed to better explain the experimental observations. Gouedard[14] proposed the idea of collective pulse emission from grains of powders on nanosecond scale similar to distributed feedback in lasers. Auzel and Goldner[16] further investigated

the idea of collective where they identified two processes, 1) amplification of spontaneous emission and 2) superradiance. Wiersma[17] and Lagendijk proposed a rate equation model where they measured the amplification of an incident pulse traveling through an excited powder slab. Berger and Genack[18] used Monte-Carlo simulations as a random walk problem of both the incident pump pulse and the emitted spontaneous emission.

The field of laser action is disordered media is still in its infancy and the physical laws governing the primary fundamental processes have yet to be established.

Optical absorption in scattering media poses a problem as to how should the absorption be accounted for in the RTE or the diffusion equation currently used to model the propagation of the light in scattering media. There is no consensus in the scientific community if the absorption should be accounted for in the diffusion constant of the diffusion equation or as a damping constant represented by an exponential containing the absorption constant. Yoo[19] demonstrated the effect of absorption by using it to enhance the coherent part over the diffuse component in a medium where the host contained absorption. Cai[20] has theoretically demonstrated the independence of the diffusion constant from the absorption coefficient whereas Fujirustu[21] claims to have shown the necessity to include the absorption in the diffusion constant. In this thesis, a scattering medium was used where part of the scattering particles had absorption in a transparent host and the transmitted profiles failed to fit either of the two models.

## 1.2 Thesis Statement

This thesis focuses on the experimental investigations of the temporal and spectral evolution of the transmitted and emitted optical radiation from an optically active disordered scattering media when excited by an incident ultrashort optical pulse. Two kinds of optically active media, scattering media where the host was optically active and scattering media where the scattering particles were optically absorptive, were studied. Experimental measurements were carried out to better understand the physics behind the transient dynamics of the emitted radiation or the effects of absorption on the incident pulse as it propagated through the scattering medium. The media where the host medium has optical gain under excitation by incident optical pulse at the absorption wavelength mainly emits the incident absorbed energy where the temporal and spectral dynamics are affected by the presence of scattering. The scattering media where the scattering particles were absorptive, the temporal diffusion of an ultrashort pulse that traverses the media is affected by the presence of optical activity. The radiation exiting from the optically active disordered media involves the reshaping of temporal and spectral profiles. The effect of the presence of scattering in the media with or without dyes was studied on picosecond scales by measuring the temporal and spectral profiles of emitted radiation. The emitted radiation shows significant pulse narrowing in both the temporal and spectral domain with lower input intensity thresholds as compared with the neat laser media. The aim of this thesis is to use the experimental measurements to study the counterintuitive effects brought about in the temporal behavior of radiation emitted from the disordered media in particular, in particular, improve imaging and mirrorless lasers. Different types of host

media such as discretely scattering colloidal media and continuously scattering bio-medical media have been used.

### 1.3 Organization of the Thesis

The thesis is divided into six chapters.

Chapter 2 describes the fundamental physical processes that are involved in the light interactions with condensed matter. The processes described cover both end of the scattering media, the effect on the light radiation and the effect on the atomic media which absorbs or emits radiation. The fundamental parameters involved in modeling of light scattering in scattering media such as scattering and transport cross section and scattering patterns are presented. The gain and absorption parameters, such as the calculation of absorption and stimulated emission cross sections, as a result of light interaction with atomic media are described

Chapter 3 describes the measured temporal dynamics of emission radiation from scattering media consisting of laser dyes and scattering particles. Intense ultrashort optical pulses produced from a mode-locked laser were used to optically excite the scattering media under study and the temporal profiles of the emitted radiation were measured by a streak camera. The measured results are compared with the model of conventional lasers under to explain the dynamics of the emitted radiation and further compared with the models of random lasers currently under consideration in literature.

Chapter 4 describes the temporal and spectral dynamics from excited scattering media when the scattering media is a continuously heterogeneous scattering medium consisting of bio-medical tissues.

Chapter 5 describes the measured temporal profiles of ultrashort laser pulses after having traveled through a scattering medium where the scattering particles consist of absorptive and non-absorptive particles in varying proportions. The ballistic and the diffuse components of the transmitted particles were measured and compared with the conventional diffusion models used in literature to explain the behavior of diffuse and incoherent component of the transmitted light.

Chapter 6 describes possible future directions and experiments for further research which can aid in further exploring the phenomena of optical interactions in active disordered media.

References


1. Rayleigh, Lord, *Phil. Mag.* 41, 107 (1871)
2. A. Schuster, *Astrophys. J.* 21, 1 (1905)
3. K. Schwarzchild, *Göttinger Nachrichten*, p. 41 (1906)
4. Mie, G., *Ann. Phys.*, 25, 377-445 (1908)
5. S.Chandrasekhar, "Radiative transfer", Dover 1960
6. H. C. van de Hulst, "Light scattering by small particles", Dover, 1981
7. C. F. Bohren and D. R. Huffman, "Absorption and scattering of light by small particles", Wiley-Interscience, 1983
8. A. L. Schawlow and C. H. Townes, *Phys. Rev.* 112, 1940-1949 (1958)
9. Lawandy, N. M. and Balachandran R. M., Gomes A.S.L., and Sauvain, E., *Nature*, 368, 436 (1994)
10. Sha, W.L., Liu C-H. and Alfano, *Opt. Lett.* 19, 1922 (1995)
11. Masood Siddique, Alfano R.R, Berger G.A. Kempe A. and Genack A.Z., *Opt. Lett.*, 21,450, 1996
12. Letokhov,v. S.*et al, "Non-resonant feedback in Lasers"*, Pergamon Press Ltd, (1970)
13. Markushev V NI, Zolin V F ,Briskina Ch. 1986 Sov: .1. Quantum *Electron.* 16 28
14. Gouedard C., Husson D., Sauteret C., Auzel F and Migus A, *J. Opt. Soc. Am. B* 10 2358, 1993
15. Cao, H., *Waves in random media*, 13, R1, (2003)
16. Auzel F and Goidner P, *J. Alloys Compounds* 300, 2000
17. Wiersma D S. and Lagendijk A, *Phys. Rev. E* 54 4256,

18. Berger, G.A., Kempe M and Genack A.Z., *Phys. Rev.E,* 56, 6118,1997

19. K. M. Yoo, Feng Liu and R. R. Alfano, Optics Letters, 16, 1068, (1991)

20. Wei Cai, M. Xu, Melvin Lax and R. R. Alfano, Optics Letters, 27, 731, (2002)Cai

21. Koichi Furutsu, Yokio Yamada, Phys. Rev. E, Vol. 50, 3634, (1994)

# Chapter 2
# BACKGROUND

## 2.1 Overview

This chapter highlights the basic concepts concerning light scattering[1-4] and optical amplification in active gain media[5, 6] in order to understand the results of light propagation in scattering media and the processes involved in interaction of radiation with optically active media. The disordered scattering media usually consists of a homogeneous host material that contains scattering particles of some arbitrary density distributed randomly throughout the host. The optical active properties of the disordered material can be either absorptive in nature or have positive gain when excited at appropriate wavelengths. The optical activity can come from either adding absorption or gain in the host material or by adding scattering particles that can be absorptive or emissive when excited at the wavelength of interest. Other kind of turbid media are continuously scattering such as tissues.

## 2.2 Scattering processes

The interaction of incident light with disordered media effects the incident light by changing its intensity, phase coherence, direction, polarization and temporal profile. The process of light interacting with condensed matter is known as light scattering. The interaction of light with condensed matter resulting in scattering is divided into the following basic processes:

**2.2.1 Elastic scattering:** Light can be scattered elastically (i.e. with no change in wavelength or color) after a scattering interaction with a particle. Light

scattered after an elastic scattering event from molecules or a scattering particle much smaller than the wavelength in the atmosphere is termed as Rayleigh Scattering. The scattering large particles or from arbitrary sized particles as termed as Mie Scattering.

**2.2.2 Inelastic Scattering:** Laser light can be scattered inelastically from molecules or particles. In this instance, the wavelength of the scattered light is shifted, and the change in wavelength is dependent on the molecule or a scattering particle, which scattered the light. This process is termed as Raman and Brillouin Scattering.

**2.2.3 Scattering from optically active materials:** A specific molecule, a cluster of molecules or optically active scattering particle in the scattering medium can absorb light traveling through a medium. In the case of a molecule, the absorbed energy can be re-radiated at the same or another wavelength. This process by which the absorbed light is remitted is known as fluorescence. Under well-defined conditions, this fluorescent light can induce stimulated emission and laser action in an excited medium. The process where laser light can be absorbed, but not radiated optically, is called absorption.

## 2.3 Scattering from single particles

Elastic scattering of radiation is defined as an incident plane wave, of wavelength

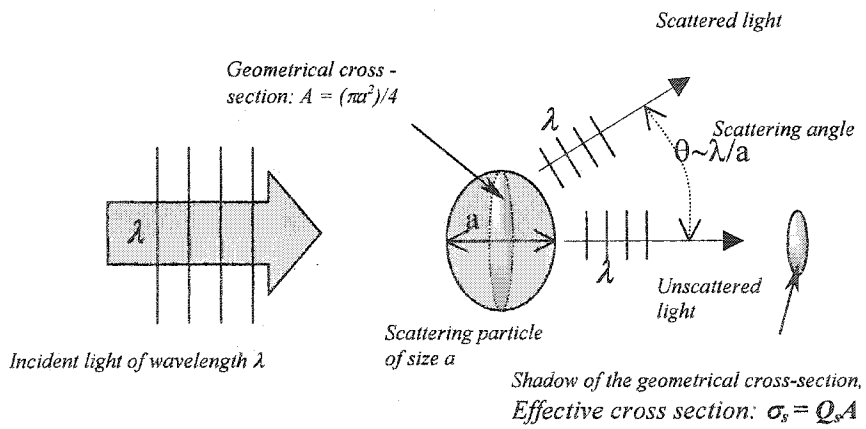


Figure 2.1 *Scattering of light from a particle*

$\lambda$, interacting with a single particle, of size d, condensed matter and resulting in a scattered component traveling at an angle $\theta$ and an unscattered component traveling in the same direction as that of the incident pulse as shown in figure 1.1. The direction and intensity of scattered radiation depends on the size and dielectric constants of the scattering particle and the wavelength, $\lambda_i$ of the incident radiation. For example, scattering efficiency of small particles is proportional to $\lambda_i^{-4}$. This wavelength dependence gives the sunlit sky a blue color since shorter wavelength of blue light gets scattered more in all directions whereas the reddish longer wavelength light scatter to a lower degree therefore one sees more blue color scattered from the atmosphere. At sundown when the sun is the level of the horizon, the sunlight coming straight towards the viewer has larger reddish component since the blue light gets preferentially scattered out, giving the sunset its orange, amber and reddish hues and tones.

The pattern of intensity of light scattered in all directions is given by the phase function $p(\theta)$. The measure of anisotropy, called the g factor, is linked to the phase function by:

$$g = \int_0^{\pi} p(\theta)\cos(\theta)2\pi\sin(\theta)d\theta \qquad (2.1)$$

or $$g = \int_{-1}^{1} p(\cos\theta)\cos(\theta)d(\cos(\theta)) = \langle\cos\theta\rangle \qquad (2.2)$$

where

$$\int_0^{\pi} p(\theta)2\pi\sin(\theta)d\theta = \int_{-1}^{1} p(\cos\theta)d(\cos(\theta)) = 1 \qquad (2.3)$$

The anisotropy factor, $g$, is a measure of the directionality of the scattered light where the average cosine reflects the difference between the amount of light scattered in the forward and back direction and it has a value between 1 and –1.

### 2.3.1 Dependence of scattering on particle size

The pattern of scattering from a spherical scattering particle can be classified into three general groups depending of the relative size of the particle as compared with the wavelength of the incident light. The dielectric constant of the scattering particle may have a wavelength dependent complex component and thus exhibit absorption or gain.

When the particle is much larger than the wavelength, a >> λ, the particle behaves with lens-like properties where the light is mainly scattered in the forward direction. For a particle size much larger than the incident wavelength, the scattered intensity at a scattering angle, $\theta$, of the scattered light is small, varying approximately as $\theta \approx \frac{\lambda}{a}$ where $a$ is the size parameter of the particle.

In the case where the particle is of the order of the size of the scattering particle, a ~λ, interference effects dominate the scattering pattern and the scattering intensity is heavily dependent on the scattering angle.

In the case of the wavelength of incident light being much larger than the size of the scattering particle, λ >> a, the scattering is produced by the instantaneous field amplitude of the incident electromagnetic radiation and the scattering assumes the pattern of an externally driven Lorentzian dipole. The scattering is at large angle θ. These various cases are illustrated in figure 2.2 where the relative index of refraction (poystyrene/water), $m$ = 1.8, is for a polystyrene particle in water ($n$ = 1.33) and wavelength (in air), λ = 0.62 μ (laser line of a CPM dye laser), are used to calculate the

scattering patterns of the perpendicular and parallell polarized scattered light using Mie theory. The solid lines and dashed lines represent the parallel polarized and the perpendicularly polarized with respect to the polarization of the incident light intensity of the scattered light. The value of the average cosine, $g$, as a function of 0.62 μ wavelength and three sizes of polystyrene particles of is shown in figure 2.3. A brief description of the Mie Scattering theory, sufficient to calculate the scattering parameters such the cross sections, average cosines and the angle dependent scattering pattern, is given in Appendix A. The computer program to numerically calculate the scattering parameters such as the scattering amplitude function pattern, the scattering, extinction cross-sections and the anisotropy factor is given in Appendix B

. The scattering categories are as follows:

*i)* Isotropic: where the wavelength is much larger than the scattering particle, $d << \lambda$ i.e. scattering intensity is uniformly distributed over all angles. The isotropic scattering is usually called **Rayleigh scattering**. The scattering cross section of the particle in isotropic scattering is given by

$$\sigma_s = \frac{8}{3}\pi k^4 |\alpha|^2 \qquad (2.4)$$

and

$$I_{scatter} = \frac{\left(1+\cos^2(\theta)\right)k^4|\alpha|^2}{2r^2} I_{incident} \approx \lambda^{-4} \qquad (2.5)$$

where $\alpha$ is the polarizability of the particle material k is the wave vector, $k = 2\pi/\lambda$. For the case where the polarizability is isotropic i.e. for natural incident light, $I_{scatter}$ is the

scattered intensity at an angle θ from the particle as shown in figure 2.2c for a particle with radius $r = 0.01\mu$.

*ii)* Anisotropic: When the wavelength is of the same order as the particle size, $\lambda \approx d$. The scattering intensity and the phase function is best given by Mie theory for arbitrarily sized scatterers as shown in figure 2.2b

*iii)* Forwardly scattered: $\theta \approx \frac{\lambda}{a}$, where the wavelength is much larger than the particle size such that most of the scattered intensity lies in the forward direction as shown in figure 2.2a.

**2.4 Radiative transport in disordered media**

The transport of radiation in a medium containing a dense random distribution of scattering particles, such that the light propagating through scatters off multiple scattering particles, can be described statistically assuming the light has scattered enough that no phase correlation or coherence exists and the electrical fields can be treated as scalar. The equation governing the transport is the optical equivalent of the Boltzmann transport equation known as the Radiative Transfer Theory (RTE). The RTE is used to describe the propagation of light where a local gradient of light may exist.

The RTE equation is given by;

$$\frac{dI(\vec{r},\vec{s},t)}{dl} = -\mu_T I(\vec{r},\vec{s},t) + \frac{\mu_T}{4\pi}\int p(s,s')I(\vec{r},\vec{s},t)d\Omega + S(\vec{r},\vec{s},t) \qquad (2.5)$$

where $\frac{d}{dl} \equiv \frac{\partial}{c\partial t} + \vec{s}.\nabla$, the specific intensity, $I(r,s,t)$, is the number of photons traveling at $\vec{r}$ in $\vec{s}$ direction per unit area per unit time, $\mu_T = \mu_a + \mu_s$ is the total

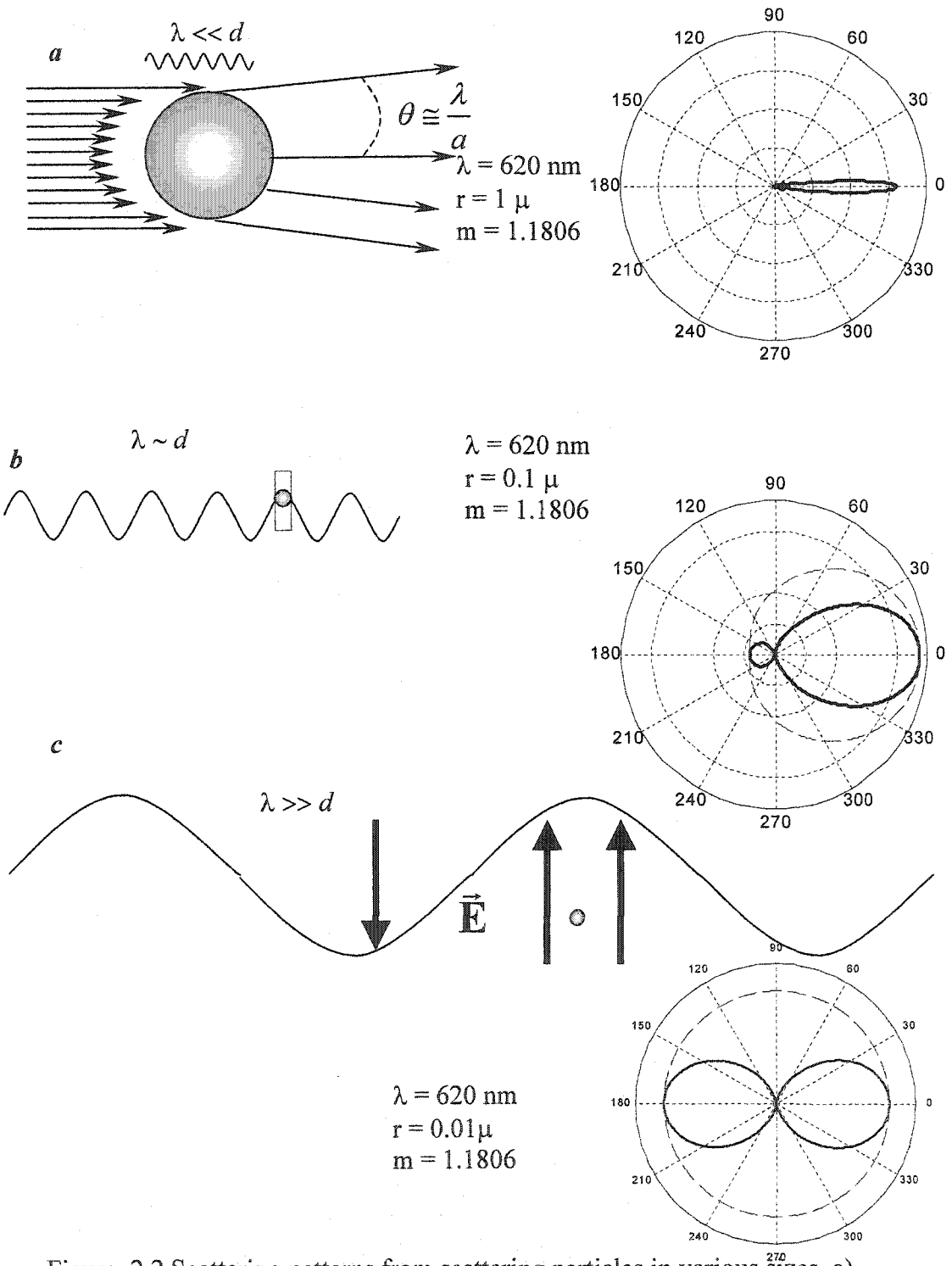


Figure. 2.2 Scattering patterns from scattering particles in various sizes. a) particles size d >> λ, *b*) d ≈λ, *c*) d << λ. Solid lines are parallel polarized and dashed line are perpendicularly polarized scattered light.

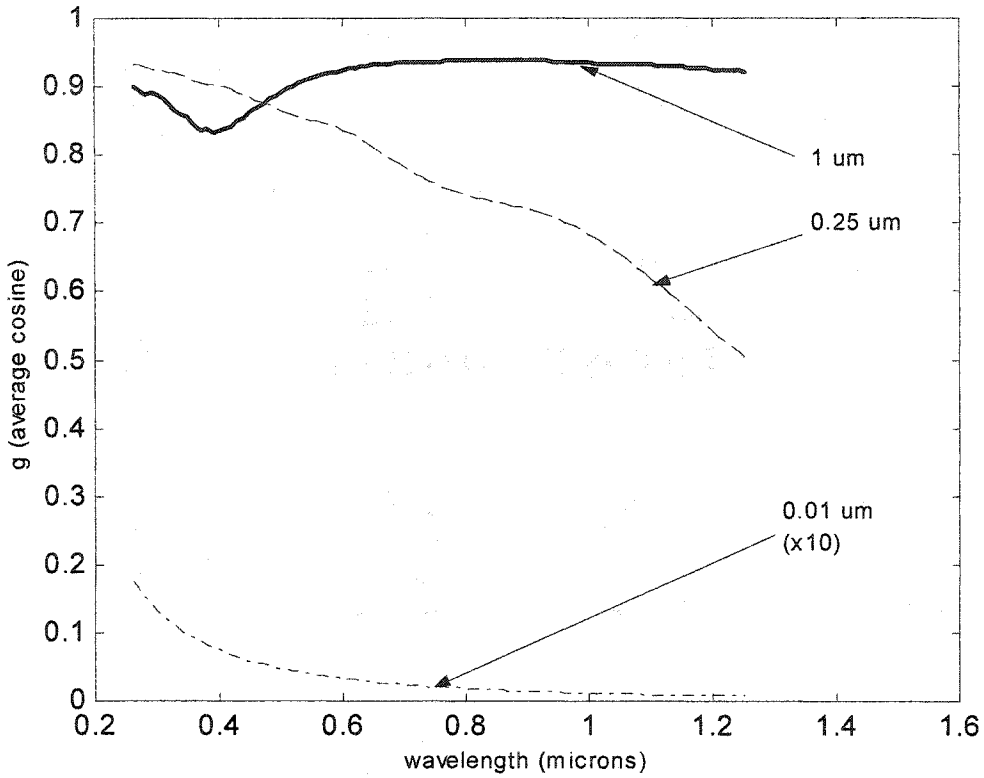


**Figure 2.3**. Variation of the average cosine, *g*, for an incident wavelengths of varying from 0.25μ to 1.2μfor polystyrene spheres of radii 1μ, .1μ and .01μ. The profile for the particles size .01μ was multiplied by a factor of 10 for clarity

scattering coefficient where $\mu_a$ and $\mu_s$ are the absorption and scattering coefficients respectively.

The coefficients are related to the particle density and the cross-section as by

$$\mu_a = \rho\sigma_a \qquad (2.6)$$

and $$\mu_s = \rho\sigma_s \qquad (2.7)$$

where ρ is the scatterer density, σ is the appropriate cross-section (subscripts, *a:* absorption, *s:* scattering) and $S(\vec{r},\vec{s},t)$ accounts for any source of additional light in the medium.

## 2.5 Diffusion Theory

The transport of photons down a photon concentration gradient can be modeled in a more practical way by using the diffusion theory model derived from Fick's laws of diffusion. The use of diffusion theory is appropriate in media more dominated by scattering than absorption such that each photon undergoes many scattering events before terminating with absorption or by exiting from the medium. The basic equations arebased on equation of continuity, which relates the changes in density of the diffusing substance to its flow, and "constitutive" relation which specifies how the flow is determined by the density distribution.

The Fick's first law relates the photon flux, J ($cm^{-2}s^{-1}$), to the change in optical intensity, I, by

$$J = -D(\partial I/\partial x) \qquad (2.8)$$

where D ($cm^2s^{-1}$) is the diffusivity constant for the medium given by $D = c/3\mu_s(1-g)$.

Fick's second law relates the accumulation of optical concentration within a volume to the local curvature of concentration gradient such that

$$\partial I/\partial t = D(\partial^2 I/\partial^2 x). \tag{2.9}$$

The general 3-D diffusion equation thus becomes;

$$\partial I(\vec{r},t)/\partial t = D\nabla^2 I(\vec{r},t) \tag{2.10}$$

The general diffusion equation, taking absorption and source terms into account is given by:

$$\frac{\partial I(\vec{r},t)}{\partial t} = \nabla(D\nabla I(\vec{r},t)) - c\mu_a I(\vec{r},t) + q^{(0)}(\vec{r},t) \tag{2.11}$$

where $q^{(0)}$ is the zeroth moment of any source present in the volume under consideration.

The diffusion equation can be considered as a first order linear approximation of the Boltzman transport equation under conditions that the volume under consideration is not near a strong source where the gradients are strongly nonlinear and in the absence of strong absorption, which tends to prevent a photon from engaging in a random walk.

The key characteristic parameters of diffusive light in a medium with ρ scattering particle density and $\sigma_s$ and $\sigma_a$ as the scattering and absorption cross sections respectively. The value for $\sigma_s$ and $\sigma_t$ are calculated using the Mie theory and given in Appendix A and Appendix B.

The key length parameters, $l_a$, $l_s$, $l_t$, $L$ and $\overline{z}$, that characterize the diffuse propagation in scattering media are given below.

*1.* $l_s$, the scattering mean free path length represent the average path length a photon travels before encountering a scattering eve. It is related to the particle density ρ

and the scattering cross-section, $\sigma_s$ (calculated from the Mie theory), as shown in Fig 2.4, by

$$l_s = 1/\rho\,\sigma_s \qquad (2.12)$$

*2.* $l_t$: the transport mean free path length represent the average length a photon takes after numerous scattering interaction before its direction gets randomized. The direction cannot be correlated with the direction of the incident light. The transport mean free path length depends on the particle size and dielectric constants, the incident wavelength, $\lambda$ and the average cosine, $g$. The light scattering becomes isotropic, i.e uniformly isotropic after traveling a distance of, $l_t$, which may entail one or multiple scattering interactions as shown in Figure 2.4. The transport mean free path, $l_t$, is related to the scattering cross section, particle density and average cosine, $g$, as:

$$l_t = \langle l_s\,(1+\cos\theta + \cos^2\theta + \cos^3\theta \ldots + \cos^n\theta)\rangle = l_s/(1-\langle \cos\theta \rangle) \qquad (2.13)$$

$$= l_s\left\langle \frac{1-\cos^n\theta}{1-\cos\theta} \right\rangle = l_s \frac{1}{1-\langle\cos\theta\rangle} = l_s \frac{1}{1-g} \qquad for\ \cos\theta << 1 \qquad (2.14)$$

as shown in Figure 2.4

*3.* **Absorption length,** $l_a$: The absorption length is the distance, $l_a$, travelled by the incident light over which the intensity is reduced by a factor of $e^{-1}$ due to absorption. The absorption arises from imaginary part, $k$, of the index of refraction, $N = n + ik$, of the material under consideration. It is related to the absorption cross-section, $\sigma_a$, of the scattering particle by:

$$l_a = \frac{1}{\rho_a \sigma_a} \qquad (2.14a)$$

where $\rho_a$ is the density of scatterers with absorption cross-section $\sigma_a$.

*4.* **Diffusion Probability:**

In a semi-infinite medium with diffusivity D, the probability of finding a photon at a distance z at a time t, after injection of a short optical pulse, is given by:

$$P(t) = \frac{1}{(4\pi Dt)^{3/2}} e^{-\frac{z^2}{4Dt}}. \tag{2.15}$$

The key parameters of a diffuse pulse traveling through a scattering media are the peak time, $t_{peak}$ and average time, $t_{ave}$.

*5.* $t_{peak}$: The peak of the broadened pulse as given in equation 2.15 is given by setting the derivative of P(t) to zero as given below,

$$\frac{\partial}{\partial t} P(t) = \frac{\partial}{\partial t}\left( \frac{t^{-\frac{3}{2}}}{(4\pi D)^{\frac{3}{2}}} e^{-\frac{z^2}{4Dt}} \right) = 0 \tag{2.16}$$

$$= \frac{-3t^{-\frac{5}{2}}}{2(4\pi D)^{\frac{3}{2}}} e^{-\frac{z^2}{4Dt}} + \frac{t^{-\frac{3}{2}}}{(4\pi D)^{\frac{3}{2}}} e^{-\frac{z^2}{4Dt}} \left( \frac{z^2}{4D} t^{-2} \right) = 0$$

$$= \frac{t^{-\frac{7}{2}}}{(4\pi D)^{\frac{3}{2}}} e^{-\frac{z^2}{4Dt}} \left[ \frac{-3t}{2} + \frac{z^2}{4D} \right] \Rightarrow \left[ \frac{-3t}{2} + \frac{z^2}{4D} \right] = 0$$

which gives the peak time as,

$$t_{peak} = \frac{2}{3} \frac{3z^2}{4l_t} = \frac{z^2}{2cl_t} \tag{2.17}$$

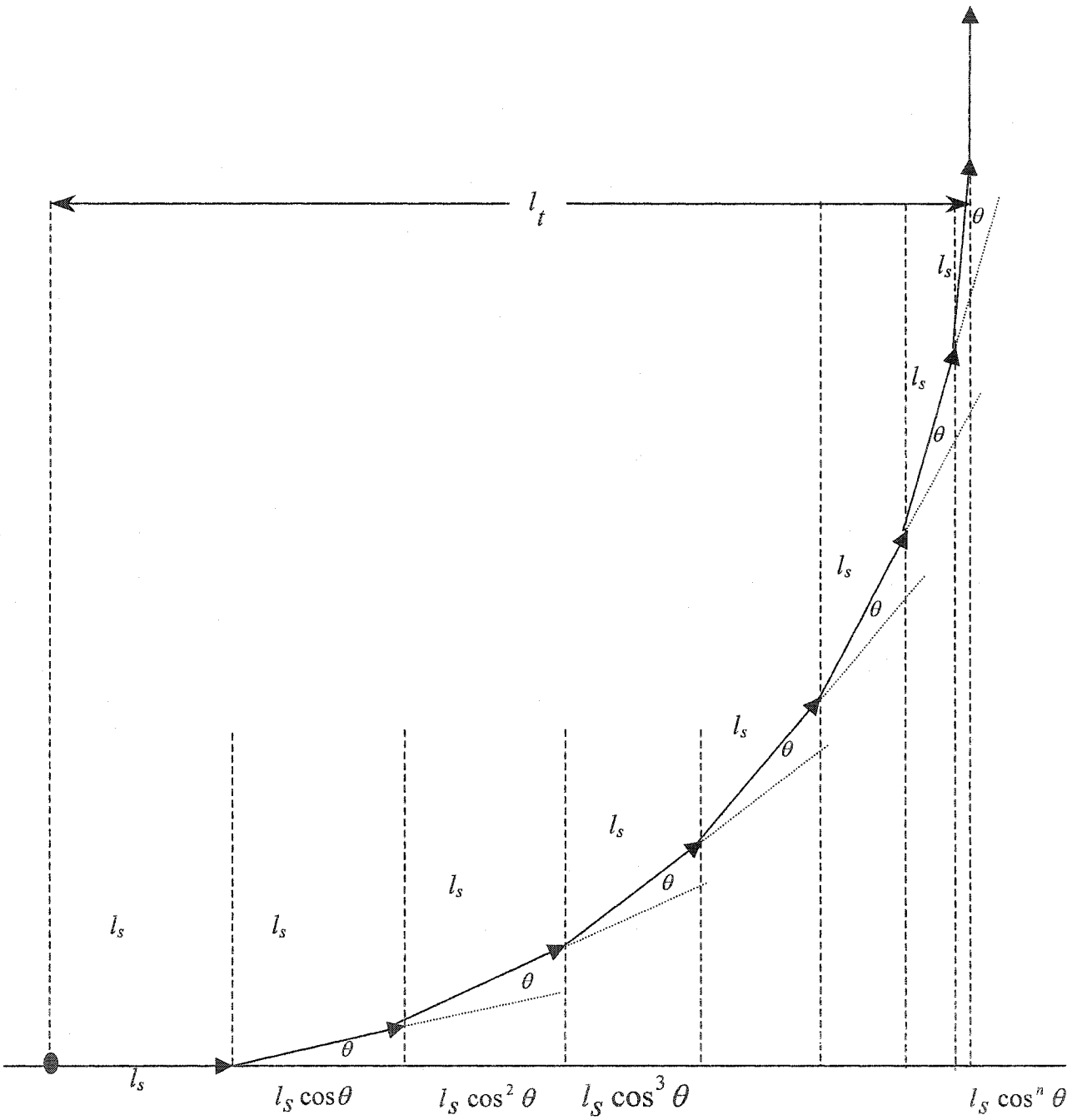


**Fig. 2.4** Relationship between mean free scattering distance, $l_s$,, and transport mean free path, $l_t$, related by:
$l_t = \langle l_s (1+\cos^1\theta + \cos^2\theta + \cos^3\theta \ldots + \cos^n\theta)\rangle = l_s/(1-\langle \cos\theta \rangle) = l_s/(1-g)$

Average time, $\bar{t}$

The average time a photon takes to travel a distance z from equation 2.15 is given by:

$$\bar{t} = \frac{\int_0^\infty tP(t)dt}{\int_0^\infty P(t)dt} \tag{2.18}$$

let $b = (z^2/4D)$, $a = (4\pi D)^{-3/2}$, $x = bt^{-1}$ and $dt = -bx^{-2}dx$, then equation 2.15 can be written as;

$$P(t) = ab^{-\frac{3}{2}}x^{\frac{3}{2}}e^{-x} \tag{2.19}$$

and

$$\int_0^\infty P(t) = ab^{-\frac{3}{2}}\int_0^\infty x^{\frac{3}{2}}e^{-x}\left(-bx^{-2}\right)dx = -ab^{-\frac{1}{2}}\int_0^\infty x^{-\frac{1}{2}}e^{-x}dx = -ab^{-\frac{1}{2}}\Gamma\left(\frac{1}{2}\right)$$

$$= ab^{-\frac{1}{2}}\frac{1}{2}\Gamma\left(-\frac{1}{2}\right) \tag{2.20}$$

and

$$\int_0^\infty tP(t) = ab^{-\frac{3}{2}}\int_0^\infty x^{\frac{3}{2}}\left(bx^{-1}\right)e^{-x}\left(-bx^{-2}\right)dx$$

$$= ab^{\frac{1}{2}}\int_0^\infty x^{-\frac{3}{2}}e^{-x}dx = -ab^{\frac{1}{2}}\Gamma\left(-\frac{1}{2}\right) \tag{2.21}$$

where the following properties of the gama function were made use of

$$\Gamma(n) = \int_0^\infty x^{n-1}e^{-x}dx \tag{2.22}$$

and

$$\Gamma(n+1) = n\Gamma(n) \tag{2.23}$$

substituting 2.20 and 2.21 in 2.18 gives the average time as,

$$\bar{t} = \left| \frac{ab^{\frac{1}{2}}\Gamma\left(-\frac{1}{2}\right)}{2ab^{-\frac{1}{2}}\Gamma\left(-\frac{1}{2}\right)} \right| = 2b = \frac{2z^2}{4D}$$

$$\bar{t} == \frac{3z^2}{2cl_t} \tag{2.24}$$

a graphical depiction of the average time and peak time is given in figure 2.5

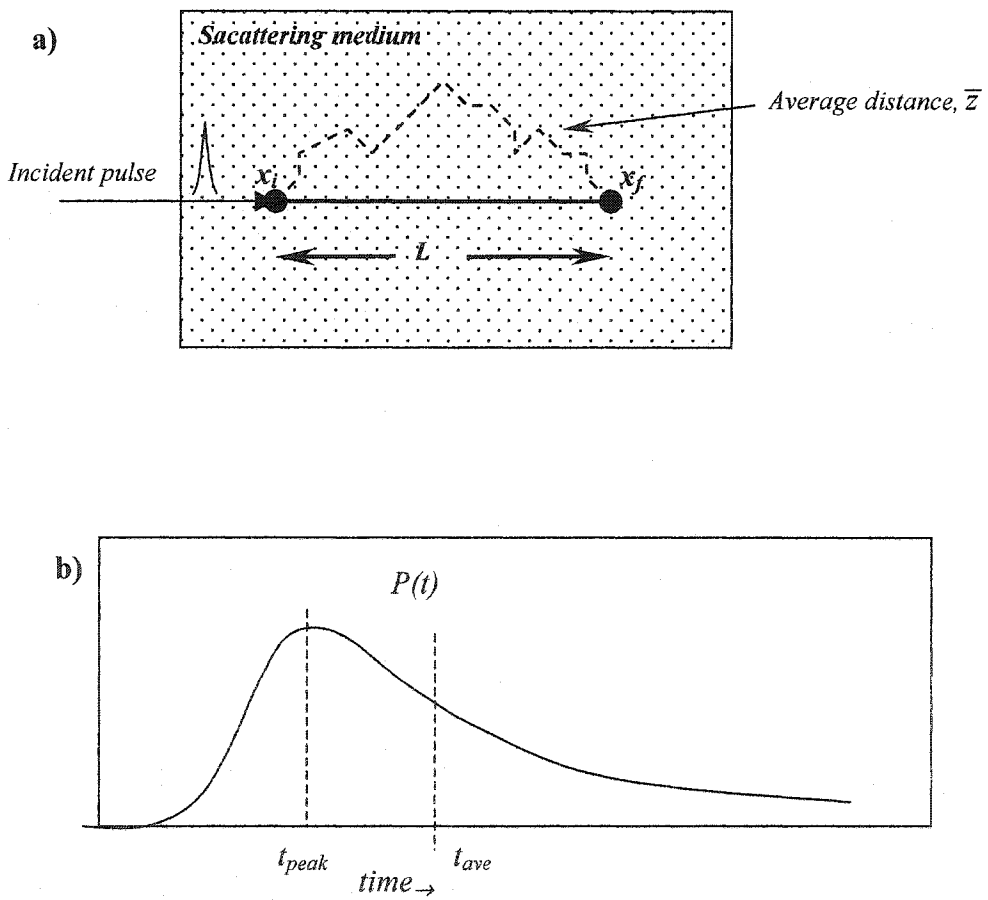


**Figure 2.5.** a) average distance, $\bar{z}$, traveled by a photon between points $x_i$ and $x_f$. b) average time $t_{ave}$ and peak time $t_{peak}$ given by the diffuse intensity $P(t)$

**6. Absorption length $L_a$ in presence of absorptive medium**

$$L = \sqrt{l_t l_a / 3} \qquad \text{for} \qquad l_a >> l_t. \qquad (2.25)$$

**7. The diffusion constant, D:**

$$D = \frac{c l_t}{3} \qquad (2.26)$$

**8. The average path length from scattering**

Average distance traveled by a photon for a linear length L between the initial point, $x_i$, and the final point, $x_f$, as $L = |x_f - x_i|$ is given by

$$\overline{z} = \frac{\overline{t}}{c} = \frac{L^2}{2l_t} \qquad (2.27)$$

The average path length , $\overline{z} > L$ , where L is the ballistic distance e.g. if L = 1 cm and $l_t$ = 1 mm, then the average path length traveled by a photon, $\overline{z}$ = 10 L. The increase in traversed path over linear path length plays an important role in increasing the gain as the radiation travels a longer distance in the gain material.

**8 Ballistic transport**

In a scattering medium, an incident ultrashort coherent optical pulse travelling through a the medium loses energy continuously due to scattering. The instantaneous intensity of this coherent component is given by

$$I_{ballisitc} = f \exp\{-z(1/l_s + 1/l_a)\} \qquad (2.28)$$

where z is the distance traversed in the direction of the incident pulse and f is a factor depending on the collection efficiency of experimental setup.

## 9. Temporal profile of diffuse component in a slab geometry

The intensity of an ultrashort optical pulse propagating in the $\hat{z}$ direction through a scattering medium bounded between z = 0 and z = d is given by,

$$I_z(t) = \frac{D}{\pi z^2} \sum_{m=1}^{\infty} m(\pi z/d)^2 \sin(m\pi z/d) \exp(-Dt(m\pi/d)^2) \exp(-vt/l_a) \quad (2.29)$$

where $z = z+z_0$; $z_0 = .7l_t$

The point $z_0$ , called the extrapolation length, is used to satisfy the following boundary conditions at the interface between media,

*a)* the normal component of the current $-D\hat{n}\cdot\nabla\rho$ is continuous,

*b)* the density is continuous is at all points of the surface.

The boundary at $z = 0$ does not satisfy the diffusion equation condition for the Fick's second law. The appropriate condition is that the normal component is zero on the boundary. An incident wave of intensity, *I*, fails this condition. If the escape of photons is possible across the boundary (as in majority of the cases for experiments with light diffusion), the situation becomes more complicated and the Fick's laws are no longer valid. An appropriate boundary condition can be obtained by using the Milne[5] problem, where the density can be assumed to be zero near the boundary at $z_0$ which satifies the boundary condition for the partial differential equation for diffusion using methods of images. The Milne problem satisfies the boundary condition,

$$I_d(\vec{r}) - \frac{0.7104}{\rho\sigma_t W_0} \frac{\partial}{\partial n} I_d(\vec{r}) = 0 \quad (2.30)$$

where $I_d$ is the diffusive component of the scattered light intensity. The approximated extrapolation length is given by

$$z_0 \approx \frac{2}{3\rho\sigma_t} \tag{2.31}$$

where $W_0 = \sigma_s/(\sigma_s+\sigma_a)$ is the albedo of the particle, and $\sigma_t$ is the transport cross section.

## 2.6 Optical Gain in Active Media

This section described the fundamental optical processes that are invovled in obtaining optical gain in excited gain media to obtain the laser action. The basic processes such as the absorption and stimulated emission cross sections and lifetimes of variuos energy levels for the gain media under considereation are described.

The laser is an optical resonator where the energy supplied by a pump source is converted into coherent light upon emission. The basic function of the laser design is to maximize this energy conversion and to control the coherence properties of the emitted light. All lasers consist of three main parts:

1. Pump / Energy source
2. Laser medium to supply optical gain/amplification
3. Optical Cavity or Resonator

The laser consists of other parts such as saturable absorbers, prisms, wave plates, polarizes etc. as well, which are added to control or enhance the spectral and time-dependent properties of the laser output. In this section, the description if lasers is limited to define the fundamental requirements to generate laser output and gain medium is assumed to be organic dyes dissolved in a fluid solvent such as methanol, ehtanol or water to compare with the experimental results described later in the chapter. Th de concentrations typically range from $10^{-5}$ to $10^{-3}$ Molar. The interaction between the dye and the solvent effects the wavelength and the efficiency of optical amplification.

The process by which the energy is supplied to the laser gain medium is called the pumping mechanism. In case of organic dyes, the pump sources is usually optical in nature where the laser medium is excited by either a flash lamp or another laser. The dye molecules absorb the pump light and release this energy by three processes;

*i)* Non-radiative and thermal relaxation

*ii)* Spontaneous emission

*iii)* Stimulated emission

The non-radiative energy is released in form of thermal heating and other relaxation processes such as translational and rotational.

The optical emission consists of the other two process. The spontaneous emission is the the process by which the dye molecule lowers its its energy by spontaneously emitting a photon. The direction and the phase of the emitted photon is incoherent or random. The seond optical process, stimulated emission, is the process by which other photons present in the system interact with the excited molecule. Under stimulated emission interaction, the excited dye molecule looses its energy by emitting a photon with the same wavelength, phase and direction as the photon it is interacting with. The emitted photon is thus coherent since its energy adds to the energy of the stimulating photon coherently. Stimulated emission is the gain process by which the emitted optical energy of the system is amplified coherently.

A basic functional laser incorporates coupled dynamics of three fundamental process.

a) Rate of excitation of the dye molecules by the pump source.

b) Rate of stimulated emission by excited dye molecules.

a) Rate of energy loss from the cavity.

A first-order model which incorporates the three fundamental processes of laser dynamics is called the Rate-Equation Model. The rate-equation model is useful in calculating first order values of the threshold pumping rate, energy conversion efficiency and in describing the evolution of lasing process.

The active gain media being considered in this research are mainly Xanthene class of organic dyes with homogeneously broadened emission spectra. In active dye material, the excitation light is absorbed leaving the dye molecule in an excited state. The excited molecule can then relax emitting radiation, a process commonly known as fluorescence. Under well-defined condition, the fluorescence can produce stimulated emission and laser action. The gain properties of a material used in lasers to produce optical amplification depend on characteristic properties of material; absorption and emission spectra, wavelength dependent absorption and emission cross sections, radiative lifetimes and density of the excited molecules/species in an amplifying system. The physical properties of commonly used organic laser dyes and the key principles involved in optical amplification of spontaneous and stimulated emission dynamics are presented in the next section.

### 2.6.1 Photophysics of organic laser dyes

The optical properties of optically active materials depend on the complex energy level distributions specific to that material. The energy levels of dye molecules form bands around the states of the dye as shown in the figure 2.5a. The band structure results from the vibrational and rotational degrees of freedom associated with the binding of the atoms that make up the dye molecule. The lowest band has been designated as $|S_0\rangle$. The

configuration of the electrons in the $|S_0\rangle$ band is such that their total quantum-mechanical spin adds up to zero, called the singlet state. When the dye molecule absorbs a photon, its energy state is raised by exciting the outer most electrons into a new orbit. This new charge distribution, called the Frank-Condon State, is not in equilibrium and atoms quickly redistributes its positions to minimize their total binding potential and dissipate excess energy. This redistribution is a fast process and the dye molecules relax to their equilibrium state of either the lowest state or the equilibrium of the state $|S_1\rangle$. There are five processes by which the dye molecule might leave the ground state of $|S_1\rangle$ as shown in figure 2.5a. The main two processes are the spontaneous or stimulated emission by which the molecule emits a photon and relaxes to the Frank-Condon State of $|S_0\rangle$ and then relaxes to the ground state within a few picoseconds. The rate of excited-state absorption depends on the number of molecules in the ground state of $|S_{1,G}\rangle$. Table 2.1 lists the cross sections of the state-to-state transitions for Rhodamine 6G. and the lifetimes of the state-to-state transitions is given in Table 2.2.

The absorption and emission spectra for rhodamine 640 dye in Methanol is shown in figure 2.5b. The absorption peak wavelength is 570 nm and the emission peak wavelength is 616 nm.

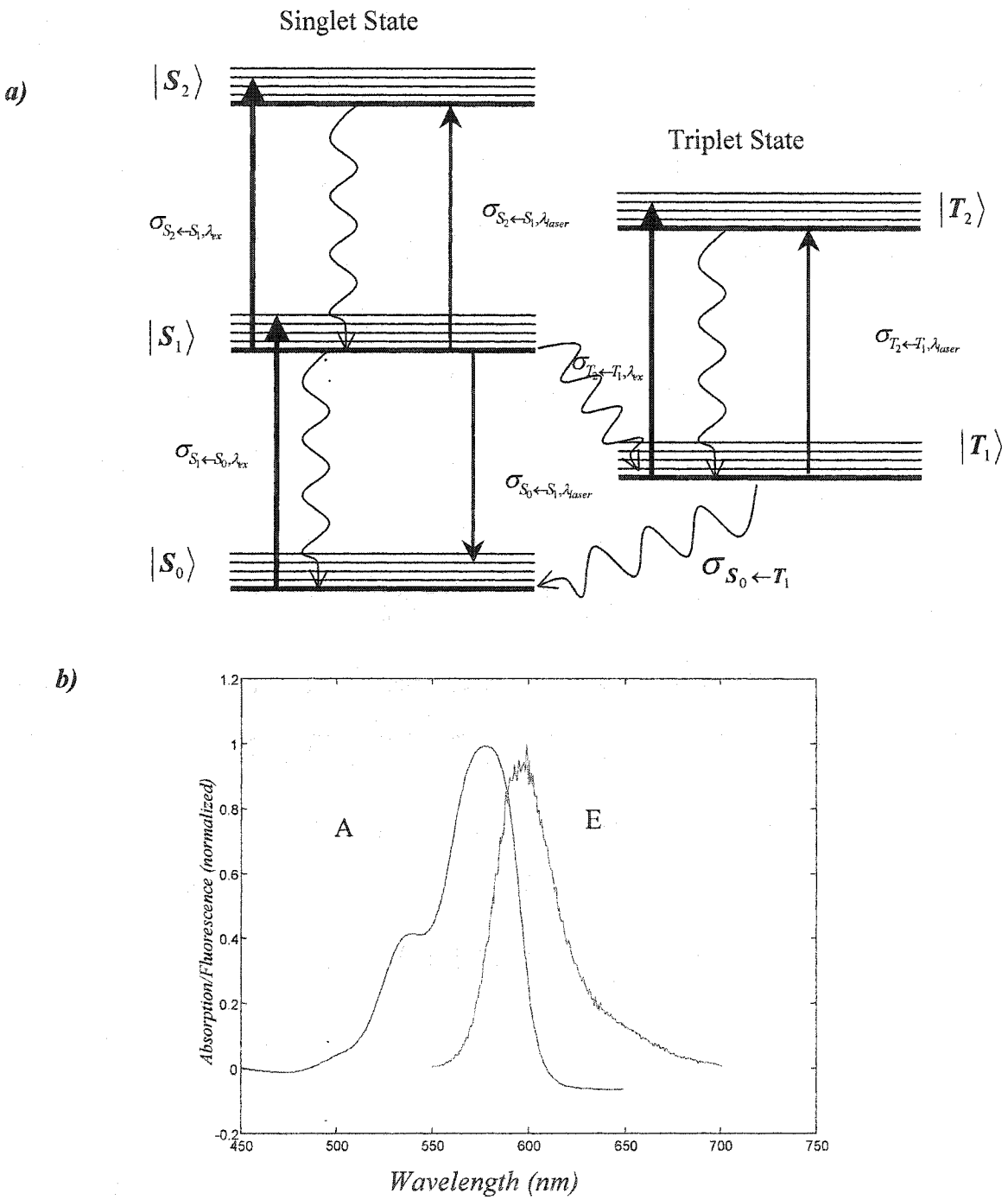


**Figure 2.6.** a) Generalized energy level diagram for a typical Xanthene class of organic laser dye. b) absorption and emission spectrum of Rhodamine 640 dye in Methanol. A: *absorption*, E: *emission*

**Table 2.1**

Intraband Dcay lifetimes for Rhodamine 6G

| | |
|---|---|
| $\|S_1\rangle \rightarrow \|S_0\rangle$ | $\tau_{s_0 \leftarrow s1} = \tau_1 = 3.7 \times 10^{-9}$ sec |
| $\|S_2\rangle \rightarrow \|S_1\rangle$ | $\tau_{s_1 \leftarrow s_2} \prec\prec 1ps$ (Fast) |
| $\|S_1\rangle \rightarrow \|T_1\rangle$ | $\tau_{T \leftarrow s} = \tau_1 = 5 \times 10^{-8}$ sec |
| $\|T_2\rangle \rightarrow \|T_1\rangle$ | $\tau_{T_2 \leftarrow T_1} \prec\prec 1$ ps (Fast) |
| $\|T_1\rangle \rightarrow \|S_0\rangle$ | $\tau_{s \leftarrow T} = 5 \times 10^{-8}$ sec |
| $\|S_1\rangle \rightarrow \|S_0\rangle$ **(Rhodamine 640/methanol)** | $\tau_{s_0 \leftarrow s_1} = \tau_1 = 4.7 \times 10^{-9}$ sec |

**Table 2.2**

Cross Sections for Rhodamine 6G ($\lambda_{excitation}$= 530 nm, $\lambda_{emission}$= 580 nm )

| | |
|---|---|
| $\sigma_{s_1 \leftarrow s_0}(\lambda_{excitation})$ | $3.8 \times 10^{-16}$ cm$^2$ |
| $\sigma_{s_1 \leftarrow s_0}(\lambda_{emission})$ | $1 \times 10^{-19}$ cm$^2$ |
| $\sigma_{s0 \leftarrow s1}(\lambda_{emission})$ | $1.2 \times 10^{-16}$ cm$^2$ |
| $\sigma_{s_2 \leftarrow s1}(\lambda_{excitation})$ | $4 \times 10^{-17}$ cm$^2$ |
| $\sigma_{s_2 \leftarrow s_1}(\lambda_{emission})$ | $1 \times 10^{-17}$ cm$^2$ |
| $\sigma_{T_2 \leftarrow T_1}(\lambda_{excitation})$ | $1 \times 10^{-17}$ cm$^2$ |
| $\sigma_{T_2 \leftarrow T_1}(\lambda_{emission})$ | $1 \times 10^{-17}$ cm$^2$ |
| $\sigma_{s_1 \leftarrow s_0}(\lambda)$ **(Rhodamine 640)** | **$4 \times 10^{-16}$ cm$^2$** |

### 2.6.2 Spontaneous Emission and Stimulated Emission

The key factor in generating optical gain in excited dye molecules is the density of the dye molecules. The excited dye molecule emits photons by two competing processes. The forst process is spontaneous emission, by which the molecules emits an incoherent photon. The rate at which the spontaneous photon is emitted depends on the number density of dye molecules in excited state and the Einstein-A coefficient between levels $|E_2\rangle$ and $|E_1\rangle$, $A_{12}$, the spontaneous emission rate given by the relationship,

$$R_{|E_2\rangle\rightarrow|E_1\rangle} = R_{sp} = A_{12}V_g\rho_2 = \frac{1}{T_{12}}V_g\rho_2 \tag{2.34}$$

where $R_{sp}$ is the rate of spontaneous emission, $V_g$ is the volume of the excited gain medium and $\rho_2$ is the density of excited dye molecules. $T_{12}$ is the lifetime of the upper level or the gain lifetime. For Rhodamine 640 the lifetime $T_{12}$ is 4.9 ns.

The rate of stimulated emission is proportional to the number density $\rho_2$ of excited dye molecules in upper state, the flux of optical power , $U_L(\omega_{12})$,circulating in the medium at the transition frequency $\omega_{12}$ and the emission cross section, $\sigma_{st}$. The rate of stimulated emission, $R_{st}$, is given by;

$$R_{st} = \frac{\sigma_{st}(\omega_{12})cU_L}{\hbar\omega_{12}}V_g\rho_2 \tag{2.35}$$

### 2.6.2a Stimulated Absorption and Relaxation to the Ground State

Stimulated absorption is the reverse of stimulated emission where a dye molecule in the lower state $|E_1\rangle$ absorbs from the phtons in the lasing mode and raises its energy back to $|E_2\rangle$ thus lowering the optoical energy in the laser cavity. The rate of stimulated

absorption, $R_{st,a}$ is like stimulated emission except that it is proportional to the number of dye molecules in the lower state $|E_1\rangle$, i.e $N_1 = V_g.\rho_1$

$$R_{st,a} = \frac{\sigma_{st}(\omega_{12})cU_L}{\hbar\omega_{12}} V_g \rho_1 \tag{2.36}$$

The second process by which the the dye molecule in lower state $|E_1\rangle$ may lose its energy is by incoherently returning to the ground state $|E_0\rangle$. The rate of recovery to the ground state, $R_{10}$, is proportional to the effective Eisnstein A-Coefficient, $A_{01}$ between the levels $|E_1\rangle$ and $|E_0\rangle$.

$$R_{10} = A_{01} V_g \rho_1 = \frac{1}{T_{01}} V_g \rho_1 \tag{2.37}$$

Usually this time, $T_{01}$ is very short, of the order of 1 ps and the density of molecules, $\rho_1$, in state $|E_1\rangle$, is approximated to be $\rho_1 \sim 0$.

### 2.5.2*b* Cross-sections and Amplification Coefficients

Te net growth or decay with distance caused by atomic transitions for a wave carrying power P, through an optically active atomic medium can be written in terms of the cross sections given above as:

$$\frac{dP}{dz} = -\lim_{\Delta z \to 0}\left(\frac{\Delta P_{abs}}{\Delta z}\right) = -(N_1\sigma_{12} - N_2\sigma_{21})P \tag{2.38}$$

Where $\sigma_{21}$ and $\sigma_{12}$ are the stimulated emission and absorption cross sections respectively. The relationship between the upwards and downwards transition cross sections $\sigma_{12}$ and $\sigma_{21}$ on a degenerate transition is given by

$$g_1 \sigma_{12} = g_2 \sigma_{21} \tag{2.39}$$

so the above relationship can be rewritten in terms of intiensity I, and population difference as:

$$\frac{1}{I}\frac{dI}{dz} = -\Delta N_{12}\sigma_{21} = -\left[\left(\frac{g_2}{g_1}\right)N_1 - N_2\right]\sigma_{21} \tag{2.40}$$

The growth or decay rate for a wave passing through a medium may also be written using Beer's Law as

$$I(z) = I(z_0)\exp[-\alpha_m(z - z_0)], \tag{2.41}$$

where $\alpha_m$ is the amplification or the extinction coefficient. This equation can be written in terms of the differential equation as:

$$\frac{1}{I}\frac{dI}{dz} = \alpha_m(\omega), \tag{2.42}$$

which gives a useful relatinaship between the coefficient $\alpha_m$ and the $|E_1\rangle \rightarrow |E_2\rangle$ transition interms of population difference and the cross sections as

$$\alpha_m(\omega) = \Delta N_{12}\sigma_{21}(\omega) \tag{2.43}$$

To calculate the gain or loss per unit length, one needs to know the atomic density and the transition cross section.

**2.5.2c Calculation of Stimulated Emission Cross Section**

Stimulated Emission is the key process by which laser action and optical amplification takes place. The efficiency of stimulated emission is characterized by the stimulated emission cross section, $\sigma_{st}$,. The stimulated emission cross section at a frequency $\upsilon$ is given by the relation:

$$\sigma_{se}(\upsilon) = \frac{\lambda_0^2}{8\pi n^2 \tau_s} g(\upsilon, \upsilon_0) \qquad (2.44)$$

where $\lambda_0$ is te wavelength of the peak of the emission line, n is te index of refraction of thehost medium, $\tau_s$ is the spontaneous emission radiative lifetime, $g(\upsilon,\upsilon_0)$ is the normalied lineshape function obtained from the emission spectrum, $\upsilon_0$ is the center frequency and $\upsilon$ is the frequency in the units of Hz. The normalized line function is obtained from the fluorescence spectrum from the relation:

$$g(\upsilon, \upsilon_0) = I_n(\upsilon, \upsilon_0) / \Delta\upsilon_{eff} \qquad (2.45)$$

where $I_n(\upsilon,\upsilon_0)$ is the fluorescence intensity distributoin function, in untis of photon emission rate per unit frequency, normalized with respect to the peak value given as:

$$I_n(\upsilon, \upsilon_0) = I(\upsilon, \upsilon_0) / I(\upsilon_0) \qquad (2.46)$$

and $\Delta\upsilon_{eff}$ is the effective width (FWHM) of the emission spectrum. The cross section is thus given by

$$\sigma_{se}(\upsilon) = \frac{\lambda_0^2}{8\pi n^2 \tau_s} \frac{I_n(\upsilon, \upsilon_0)}{\Delta\upsilon_{eff}} \qquad (2.47)$$

The absorption and the fluorescence emission spectrum is shown in figure 2.5b. The radiative lifetime $\tau_s \equiv \tau_{s2\to s1} \cong 4.9$ ns and the index of refraction of methanol n = 1.33. The stimulated emission cross section , $\sigma_{st}$(620 nm), was calculated as;

$\sigma_{st} = 4\text{x}10^{-16}$ cm$^2$

References

1. C. F. Bohren and D. R. Huffman, "*Absorption and scattering of light by small particles*", Wiley-Interscience, 1983

2. Ishimaru, Akira, "*Wave propagation and scattering in Random Media*", IEEE Press, (1997)

3. H. C. van de Hulst, "*Light scattering by small particles*", Dover, 1981

4. S.Chandrasekhar, "*Radiative transfer*", Dover 1960

5. Siegman, Anthony, *"Lasers"*, University Science Books, (1986)

6. Duarte F.J., Hillman, L.W., "*Dye laser Principles*", Academic Press, 1990

7. Milne, E. A. , Philos. Trans. Roy. Soc. (London), A, 223, 201 (1922)

# CHAPTER 3

# TIME RESOLVED STUDIES OF STIMULATED EMISSION FROM DYE ACTIVE COLLOIDAL AND SANDY SOLUTIONS

## 3.1 Introduction

Optical amplification using stimulated emission has been an area of great interest even before the proposal for the operation of the first laser/maser by Charles Townes[1] et al in the 1950's. These non-laser models were based on using the stimulated emission effect to obtain optical gain in an open cavity configuration as opposed to the resonant cavity used by Townes et al. V. A. Fabrikant and his students had filed a patent application on amplifying electromagnetic radiation from Ultraviolet through the radio spectrum in 1951 in the then Soviet Union. Robert E. Dicke[2], in 1954, proposed the concept of the "optical bomb" in which a short excitation pulse would produce an inverted population, which would then generate an intense burst of spontaneous emission. In 1956 he filed a patent on using a pair of parallel mirrors forming a Fabry-Perot interferometer, as a resonant cavity. Maiman[3] demonstrated first laser action in ruby medium. Lasing action in disordered media has been an area of great interest since it was first proposed by Letokhov[4] and demonstrated[5,] in the 1960's when theory and practical demonstration of lasers were being newly developed. The emission of intense optical and X-ray pulses had been noticed in the emission from interstellar excited dust as a naturally occuring laser-like emission but was not fully understood. Light scattering has been considered to be the undesirable loss mechanism in conventioanl lasers where an excited optical gain medium is placed in a resonant cavity to establish oscillation conditions in

order to enhance the optical gain and establish frequency stabilization and coherence at the emission wavelengths. The presence of scattering is deterimental to the lasing action since it increases the input threshold and destroys the coherence and frequency selection in the laser cavity.

Lasing action in disordered media represents the process of light amplification by stimulated emission where either the feedback is supplied by the scattering induced by the presence of the disordered media or the disordered media acts as the gain-enhancement factor in the lasing process.

In this chapter the temproal evolution of optical amplification in colloidal suspensions is explored by comparing ultrafast emission measurements on a time scale comparable with the residence time of the pump photons in the medium and much shorter than the excited-state lifetime. A Monte Carlo simulation of photon migration and level occupation is performed to model the optical amplification phenomenon in colloidal media since the conventional models for light amplification in excited media do not match the experimental results. The 10-ps excitation pulse used in these experiments was an order of magnitude shorter than in previous measurements[6]. The temporal profile of emission was measured with a resolution of 10 ps in a series of turbid samples of Titania particles suspended in solutions of Rhodamine 640 perchlorate in which lasing was observed by Lawandy[6] and Alfano's group soon afterwards[8-13] in 1994.

In conventional resonator-type lasers, the presence of any scattering media in the gain medium is highly undesirable as it increases the input threshold and destroys any temporal and spatial coherence and severely degrades the frequency stability. Ever since the demonstration of laser emission by Townes and establishment of operating principles

for obtaining lasing threshold, the conventional wisdom dictates that any losses due to scattering in the gain media should be eliminated or minimized for efficient and effective lasing conditions. This chapter deals with the emission dynamics of laser materials where the scattering was enhanced by adding scattering particles to the laser media. Letokhov *et al* first proposed the idea of optical gain in scattering clouds containing uniform gain in the 1960's as a model of a nonresonant feedback laser action. His group demonstrated the principles of incoherent feedback by using scattering media as an incoherent reflector replacing a cavity mirror. The work was further developed by the experimental investigations of the alterations in spectral profiles of emission of crushed laser crystals under varying excitation intensity by Markushev[5] and others[15-30]. They demonstrated the dependence of emission lineshape as a function of incident intensity and the particle shape. Gouedard[21] analyzed the shift in emission lifetime in excited powder aggregates of laser powders in 1993 by measuring the temporal and spectral coherence from the contrast of near-field speckle pattern.

The laser-like emission from colloidal scattering gain media was first termed as random lasers after demonstration of laser-like behavior of emission spectrum by Lawandy[6,14] et al. Soon afterwards[8-13] Alfano's group demonstrated of drastic spectral and lifetime shortening under excitation by ultrashort intense pulses in 1994. Since the demonstration of laser-like emission in 1994, there has been a flurry of theoretical and experimental activity to investigate the lasing action in disordered media in different materials and configuration to better understand the transient dynamics of emission radiation.

The lasing process in scattering media was subdivided into two categories based on incoherent and coherent feedback. Cao[31-40] *et al* demonstrated the evolution of multiple laser lines in densely packed powder aggregates of ZnO particles. They have termed this process as coherent feedback random lasers. In extremely dense packing of lasing particles, when the transport mean free path length was of the order of the wavelength, the emission is effected by coherent interference of radiative emission from within the scattering particles.

This chapter is divided into mainly four sections. The threshold characteristics of a laser are described in Section 1 for later comparison with the emission characteristics random lasers. The description of the experiment and results are presented in section 2. In section 3 a Monte Carlo simulation, based on photon dwell time, is presented. Section 4, deals with the analysis of the results and compares the various models currently under consideration in literature and a superradiance model of laser action in neat and colloidal medium is presented.

**3.2 Elements of laser action in resonant cavities.**

Laser action produced in conventional lasers by placing an excited gain medium in a resonant cavity such that at the input power threshold the optical gain in the gain medium equals the loss in the cavity and a sustainable oscillation condition is established. In this chapter, the Rhodamine 640 is used as the optical gain medium which is a sub-class of Xanthene class of organic. Then a general description of the gain processes and the emission properties of a conventional laser is presented to later compare with the emission properties of the laser-like emission from the optically active disordered media.

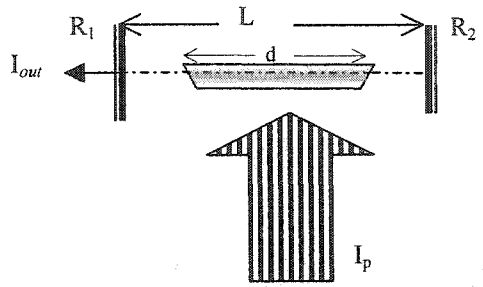


Figure 3.1 Basic configuration of a laser oscillator. It consists of two mirror of reflectivity $R_1$ and $R_2$, L distance apart, gain medium of length d, pumped at intensity $I_p$ by an external energy source.

### 3.2.1 Laser Oscillation Threshold

The basic configuration for a laser oscilator cavity consists of a laser gain medium placed between two parallel mirrors L distance apart as shown in Figure 3.1. The gain medium is externally excited by a pump source of intnesity $I_p$, and the oscillator has an optical output of intensity $I_{out}$. The basic requirement for reaching laser oscillating threshold to maintain a steady-state laser oscillation is that the round trip gain, including all losses, must be unity with a phase shift of integer multiples of $2\pi$. The oscillation condition is maintained only if the circulating power in the cavity is neither grows or decays.

The round-trip gain, $g_{rt}$, in the cavity is thus written in terms of the losses as;

$$g_{rt} = r_1 r_2 \exp\left( \alpha_m(\omega) p_m - \alpha_0 p - i\left( \frac{\omega p}{c} + \Delta k_m(\omega) p_m \right) \right) = \exp(-iq2\pi) \qquad (3.1)$$

where $r_1$ and $r_2$ are the reflectivities of the mirrors, $\alpha_m$ is the gain coefficient of the laser medium cavity, $\alpha_0$ is the intra-cavity losses, $\Delta k$ is the phase shift, p is the cavity length perimeter p = 2L and $p_m$ is the gain medium length parameter 2d, where d is the length of the gain medium under excitation. From the threshold gain equation above, the amplitude condition is,

$$r_1 r_2 \exp(\alpha_m(\omega)p_m - \alpha_0 p) = 1 \qquad (3.1a)$$

And the phase shift condition that the round-trip phase shift in the cavity be an integer, q, multiple of $2\pi$,

$$\frac{\omega p}{c} + \Delta k_m(\omega)p_m = q2\pi \qquad (3.2)$$

The gain coefficient required to reach the threshold in the laser cavity in terms of losses form the mirror transmissions and internal losses in the cavity will be,

$$\alpha_m(\omega)p_m = \alpha_0 p + \ln\left(\frac{1}{R_1 R_2}\right) = \alpha_c \qquad (3.3)$$

where $R_1 = r_1^2$, $R_2 = r_2^2$ and $\alpha_c$ is the sum of all forms of lossy processes in the cavity..

Assuming a general Lorenztian lineshape for the atomic transition of the laser gain coefficient as,

$$\alpha_m(\omega) = \frac{3}{4\pi}\frac{\gamma_{rad}\lambda^2}{\Delta\omega_a}\frac{\Delta N}{1+[2(\omega-\omega_a)/\Delta\omega_a]^2} \qquad (3.4)$$

where $\omega_a$ is the midband frequency of the Lorenztian line-shape and $\Delta\omega_a$ is the FWHM (full-width-half-maximum) bandwidth around $\omega_a$. The inversion density required to reach threshold and to maintain a steady state oscillation in the cavity mode located at the midband $\omega = \omega_a$, is given by,

$$\Delta N = \Delta N_{th} \equiv \frac{2\pi}{3}\frac{\Delta\omega_a}{\gamma_{rad}}\frac{1}{\lambda^2}\frac{\alpha_c}{p_m} \tag{3.5}$$

Which can be written in terms of the more familiar transition cross section, $\sigma_{st}$ as

$$\Delta N_{th} = \frac{\alpha_c}{\sigma_{st} p_m} \tag{3.6}$$

### 3.2.2 Threshold Pump power

A more important and practical parameter for laser threshold is the input power required to achieve the threshold inversion density. The requirement for the pump power threshold is to achieve upper level population density $N_{2,th}$ that is enough to maintain the threshold inversion $\Delta N_{th}$ taking into account the population accumulation at the lower laser level and its rate of emptying out. Assuming an efficiency factor of $\eta_p$ for the pump power to which ends up in population $N_2$ at the upper laser level as,

$$N_2 = \frac{R_p}{\gamma_2} = \frac{\eta_p P_p}{\gamma_2 \hbar \omega_p V_g} \tag{3.7}$$

Where $P_p/V$ is the pumping power per unit volume and $\gamma_2$ is the total decay rate of upper level. Combining the expressions for upper level population $N_2$ and the threshold inversion density, the pump power density required for a given laser system is given by,

$$\frac{P_{p,th}}{V} = \frac{1}{\eta_p}\frac{N_{2,th}}{\Delta N_{th}}\frac{\omega_p}{\omega_a}\frac{\gamma_2}{\gamma_{rad}}\frac{4\pi^2}{3}\frac{\hbar\Delta\omega_a}{\lambda^3}\frac{c\alpha_c}{2L} \tag{3.8}$$

where $\alpha_c$ is the total cavity losses, $\lambda$ is the laser wavelength, $\omega_a$ and $\omega_p$ are the midband of the absorption lineshape and pump frequencies respectively.

### 3.2.3 The laser threshold region

The key feature of interest in the context of lasing in random media is the discontinuous change in power that occurs in laser oscillator. The laser oscillation occurs suddenl as soon as the oscillation conditions are met and there is a sudden jump in the output power from a random gaussian noise to a coherent steady state oscillation of much higher intensity.

To obtain a steady state oscillation condition, the upper level population, $N_{ss}$, has to be raised to the threshold inversion value $N_{th}$. This inversion threshold value is given by:

$$N_{th} = \frac{\gamma_c}{\gamma_{rad}} p \qquad (3.9)$$

where $\gamma_c$ and $\gamma_{rad}$ are the cavity and spontaneous decay rates respectively and p is the cavity mode number. The cavity decay rate is given by the

$$\gamma_c = \frac{\alpha_0 d + \ln(1/\ R_{tot})}{T} \qquad (3.10)$$

where T is the cavity round trip time and $R_{tot}$ is the total reflectivity of the output coupling mirrors and the cavity mode number for a medium gain linewidth of $\Delta\omega_a$ centered at $\omega_a$ is given by,

$$p = \frac{4\pi^2 V_c}{\lambda^3} \frac{\Delta\omega_a}{\omega_a} \qquad (3.11)$$

The below threshold upper-level population remains proportional to the pumping rate i.e $N_2 \sim R_p\tau_2$ until the upper-level population reaches $N_{th}$ at the threshold pumping rate

$R_{th}$.The pumpiing rate $R_p$ is usually written as normalized to the threshold pumping rate as ,

$$r = \frac{R_p}{R_{th}} \tag{3.12}$$

The steady state values of the number of photons in the cavity , $n_{ss}$ , and the upper level population, Nss, below the threshold pumping rate is given by,

$$\left.\begin{aligned} n_{ss} &\approx \frac{r}{1-r} \\ N_{ss} &\approx r \times N_{th} \end{aligned}\right\} \qquad r < 1 \tag{3.13}$$

and above threshold,

$$\left.\begin{aligned} n_{ss} &\approx (r-1)\gamma_{rad}\frac{p}{\gamma_2} \\ N_{ss} &\approx N_{th} \end{aligned}\right\} \qquad r > 1 \tag{3.14}$$

The main feature of the threshold conditions is that the cavity photon number, p, jumps sharply from below threshold to above threshold as shown in figure 3.2

### 3.3 Experimental measurements

The 10-ps excitation pulse used in these experiments was an order of magnitude shorter than in previous measurements. The temporal profile of emission was measured with a resolution of 10 ps in a series of samples of titania particles suspended in solutions of Rhodamine 640 perchlorate in which lasing was observed by Lawandy[6]. Suspensions are particularly useful because they allow one to change the transport mean free path $l_t$ independently, in which the direction of propagation at the pump frequency is randomized, and the small-signal absorption length at the pump wavelength $l_a$ by varying the density of scatterers and the dye concentration, respectively.

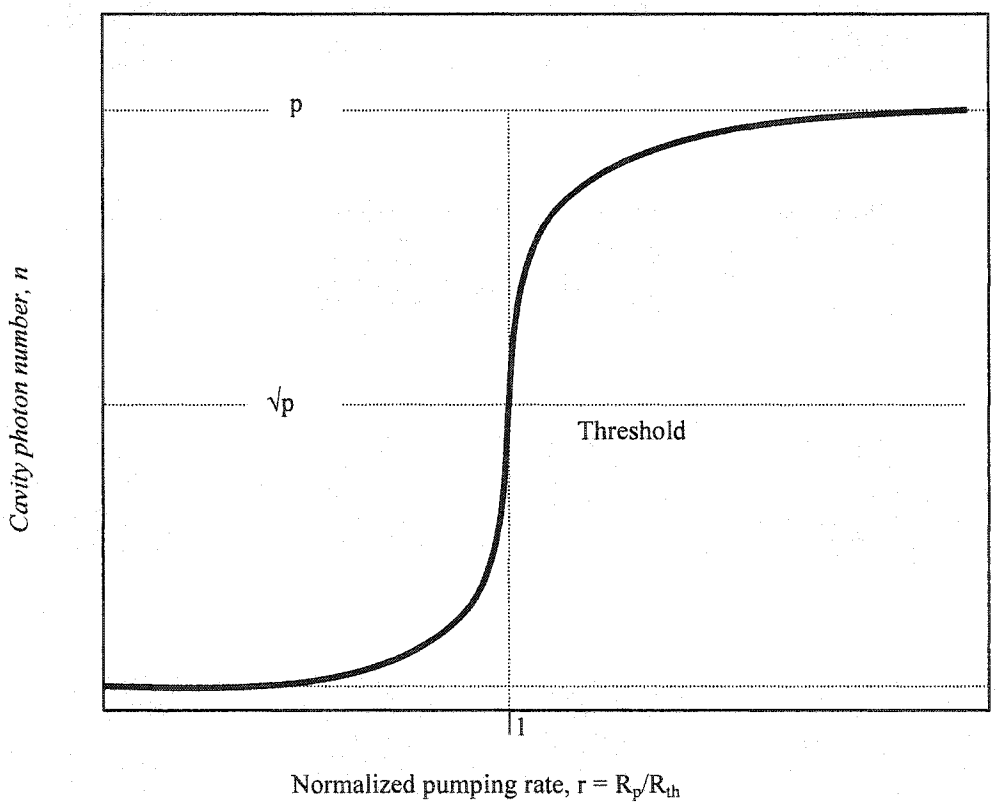


Figure 3.2, Output power characteristics of laser oscillator for pumping rate below and above threshold

### 3.3.1 Colloidal Media

The colloid samples were produced by mixing DuPont R960 powder of Alumina-coated Titania particles with an average diameter of 0.25 um with Rhodamine perchlorate dye in methanol solution. The dye concentrations varied between $10^{-4}$ M and 2.5 x $10^{-3}$ M, corresponding to absorption lengths la between 1400 and 50 ,um. The density of scatterers was varied between 5 x $10^{9}$ and 5 x $10^{11}$ $cm^{-3}$. The highest concentration studied had a volume fraction of 0.4%. The values of $l_t$ that correspond to these concentrations were measured to be between 16 um and 1.6 mm for the emitted light and 10μ and 1 mm for the pump light.

### 3.3.2 Sandy Pastes

Rhodamine 640 perchlorate dye in methanol solution of $10^{-3}$ M concentration was used as the optically active medium in all measurements. Two classes of disordered host media were prepared: (1) discretely disordered dilute colloidal solutions, (2) densely packed powders. The discretely scattering dilute colloidal samples were made by adding $TiO_2$ particles coated with $Al_2O_3$ (average diameter 0.25um) to the active dye host solution in varying densities. The wet, densely packed powders in the active dye host were prepared by adding powdered $Al_2O_3$ (5, 0.3, and 0.03μ diameter) and $TiO_2$ (0.25um diameter), in a cuvette of the host dye and allowing them to settle until maximum packing density was reached at the bottom. Two kinds of these sandy densely packed powder samples were prepared: (1) wet powders which were obtained by adding the powders to the dye host in a cuvette and (2) a dried paste, which was obtained by mixing the powders with dye solution and allowing them to dry.

For temporal measurements, the samples were excited by a 10-ps pulse at 527 nm, obtained from a frequency-doubled single shot Nd-glass laser. The pump pulse intensity was varied from 450 uJ to about 1 uJ by inserting neutral density filters in the path of the excitation pulse. The pulse was focused to a spot size of 0.5 mm onto the slightly off-axis (approximately 5 deg) sample surface. The portion of the pulse transmitted through the beam splitter was collected by an energy meter to monitor the pulse energy. The backscattered light from the front surface of the sample surface was collimated and the pump pulse then filtered out by longpass filters to cut off wavelengths shorter than 540 nm. The collimated light was then focused onto the slit of the streak camera along with a small portion of pump pulse (reference pulse) timed to arrive about 50 ps earlier than the signal light. The streak camera was a Hamamatsu C979 with a SIT tube (C1000) and a temporal analyzer to measure and record the signal with a temporal resolution of about 10 ps.

The absorption length for the neat dye solutions at $10^{-3}$M concentration was measured to be 140 μ. The transport mean-free-paths at the excitation wavelengths of the dilute colloidal dye solutions of titania particles, calculated using Mie theory, varied from approximately 1800 μ for a particle density of $5x10^{9}$ $cm^{-3}$ to 18μ for $5x10^{11}$ $cm^{-3}$ density. The volume content of titania in these solutions did not exceed 0.5%. The time-resolved stimulated emission from these colloidal dye solutions was measured in a wide range of samples for $l_t > l_a >$ d to $l_t < l_a$,d domains, where $l_t$ is the transport mean-free-path length, $l_a$ is the absorption length of the neat dye solution (both at the excitation wavelength), and d is the diameter of the spot size of the input pulse. The transport mean-free-paths in the case of densely packed powders are about 4μ in the case of $TiO_2$ powders.

In the neat $10^{-4}$ M dye solution a short pulse on the picosecond time scale was observed only for pulse energies above 25μJ. The threshold for lasing action is defined as the pump energy for the duration of the emitted pulse is 100 ps. As scatterers are added to the solution, laser action up to the highest energies available with our laser for scatterer densities of $5 \times 10^{9}$ and $5 \times 10^{11}$ cm. As the density of the scatterers is further increased, laser action reappears at higher thresholds than in neat dye solution. At higher dye concentrations action requires a higher incident power in the neat solution, but the addition of scatterers lowers the threshold for lasing action significantly below the value in the neat solution, and pulses with widths comparable with that of the incident pulse are observed.

An example of the change in the temporal and spectral emission profiles are shown in Fig. 3.3. The temporal narrowing of emission profiles is shown in Fig. 3.3(*i*) and fig. 3.3*(ii)* and the spectral narrowing is shown in Figures 3.3(*iii)* and 3.3*(iv)*. Table 3.1 gives the pulse width, uncorrected for the temporal resolution of the streak camera, as well as the threshold energy for lasing for a wide range of values of $l_t$ and $l_a$ In the weak-scattering regime in which the transport mean free path is much larger than the wavelength, one can therefore ignore wave interference in computing average transport within the medium. The energy flow of pump and emitted photons can then be modeled by a random walk of photons[4-13,48]. The neglect of wave coherence is in accord with the observation that local intensity fluctuations in reflection from powdered samples are small[5].

All samples of active densely packed wet powders exhibited stimulated emission as indicated by their ultrafast temporal profiles. Samples with smaller grain sizes of

$Al_2O_3$ (0.03μ) had higher thresholds than those with larger grain sizes. In the dried-paste form, an ultrafast time-resolved profile of the emissions could only be obtained from the alumina powders of 5μ and 0.3μ at a lowered threshold. In the samples where stimulated emission was observed, the duration of the emission was of the same order as the input pulse. The lasing thresholds for the range of samples tested are given in Table 3.2.

**TABLE 3.1**

Threshold pump energies and measured FWHM of emission for various particle densities and dye concentrations

| | DYE CONCENTRATIONS (MOL/L)/$L_A$ (μM) AT THE FOLLOWING THRESHOLD ENERGIES (μJ)/EMISSION FWHM (PS)[B] | | |
|---|---|---|---|
| Particle density ($cm^{-3}$)/l (μm) | $10^{-4}$M/(1400μ) | $10^{-3}$M/(140μ) | 2.5 x $10^{-3}$M/(50μ) |
| 0 | 25/(56ps) | 45/(30 ps) | 50/(30 ps) |
| 5 x $10^{9}$/1600 | NL | 35/(16 ps) | 15/(18 ps) |
| $10^{10}$/800 | NL | 25/(16 ps) | 10/(18 ps) |
| 5 x $10^{10}$/160 | 90/(80 ps) | 17/(26 ps) | 8/(18 ps) |
| $10^{11}$/80 | 50/(50 ps) | 15/(22 ps) | 12/(18 ps) |
| 5 x $10^{11}$/16 | 50/(24 ps) | 13/(20 ps) | 6/(20 ps) |

[a] The transport mean free path given is for the emitted light. The duration of the emitted pulse was the shortest obtained at pump energies upto 400 μJ. In most cases the shortest pulse width was reached well below this pump energy

[b] NL, Lasing was not observed for pump energies as high as 400 μJ.

**Table 3. 2**

Input Threshold intensity for sandy pastes

| POWDER MATERIAL | PARTICLE SIZE (DIAMETER) | THRESHOLD EENRGY | |
|---|---|---|---|
| | | WET/MUCKY | DRY PASTE |
| $Al_2O_3$ | 5 μ | 5 μJ | 10 μJ |
| $Al_2O_3$ | 0.3 μ | 7 μJ | 10 μJ |
| $Al_2O_3$ | 0.03 μ | 20 μJ | 100μJ |
| $TiO_2$ | 0.25 μ | 1.5 μJ | No laser action |

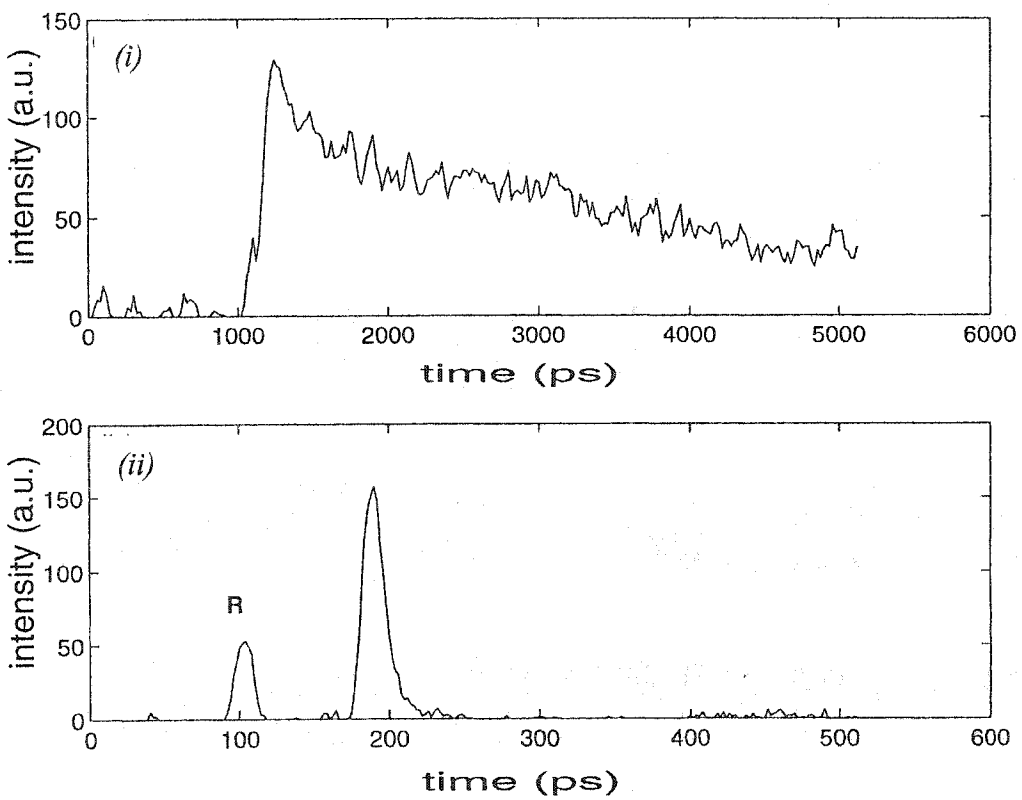


**Fig 3.3** Time resolved emission from colloid solution fo titania powder ($10^{10}$ $cm^{-3}$) in Rhodamine 640, ($10^{-3}$M). The earlier pulse marked R is a fixed pre-pulse pulse for temporal refence. ***(i)*** below threshold, for neat dye at 18μJ input ***(ii)*** above threshold at 16 μJ for scattering density of $10^{11}$ $cm^{-3}$

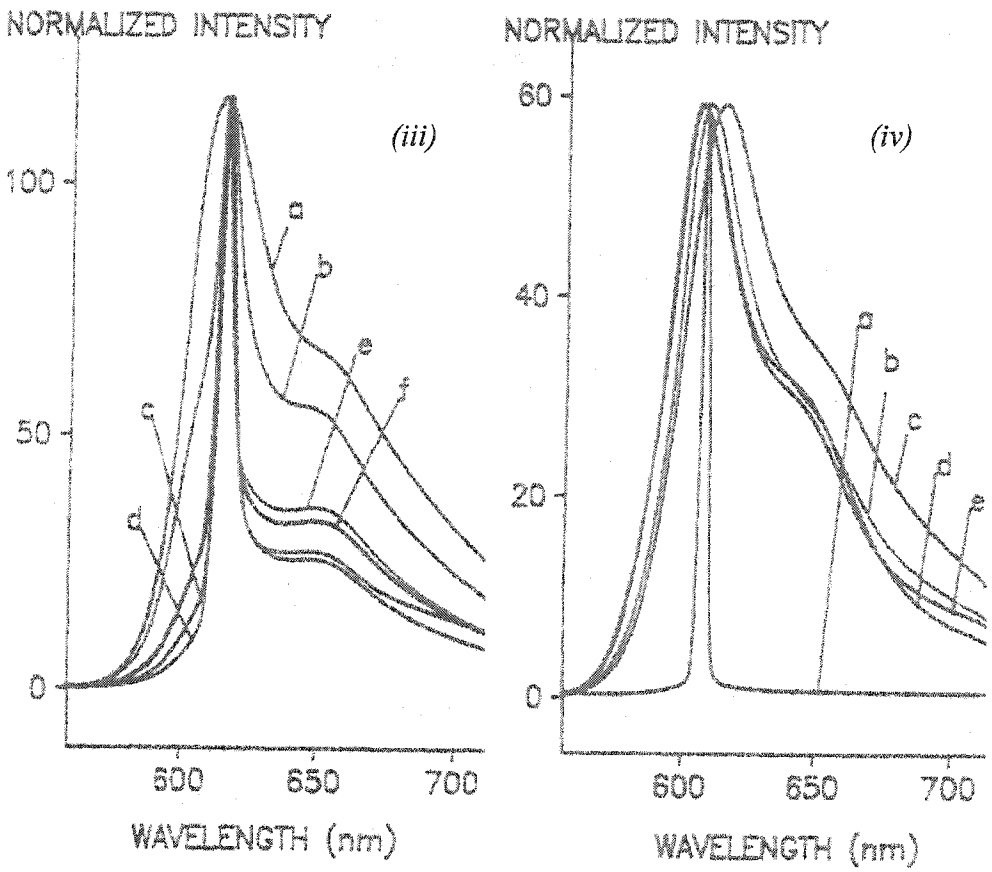


**Fig 3.3** Narrowing of spectral profile of emission from colloid solution for titania powder in Rhodamine 640, using 7ns, 530 nm incident pulses: ***(iii)*** Rhodamine 640 ($(2.5x10^{-2}M$) solution for fixed incident energy of 0.17 mJ, for titania densities of, a: 0 $cm^{-3}$.(neat dye), b: $5x10^{9}$ $cm^{-3}$., c: $5x10^{10}$ $cm^{-3}$, d: $5x10^{11}$ $cm^{-3}$ , e: $10^{12}$ $cm^{-3}$ , f: $2.5x10^{12}$ $cm^{-3}$. ***(iv)*** Rhodamine 640 solution of $5x10^{-4}$ M concentration at fixed incident energy of 0.10 mJ for titania densities of, a: neat solution, b: $5x10^{10}$ $cm^{-3}$, c: $5x10^{11}$ $cm^{-3}$, d: $10^{12}$ $cm^{-3}$, e: $2.5x10^{12}$ $cm^{-3}$ (reference 7)

### 3.4 Monte-Carlo Simulation

The Monte Carlo simulation allows us to study the dynamics of molecular excitation and deactivation and wave transport in the medium on the same footing and is equivalent to solving the coupled nonlinear photon diffusion and molecular rate equations when diffusion theory is applicable.

In the Monte-Carlo simulation the random walk of photons is computed with a temporal step size equal to the mean free time $\tau = l_t/v$, where v is the phase velocity in the solution. The values of $l_t$ at the incident and the emitted frequencies are taken to be the same. The incident beam is assumed to be random after penetrating a distance $l$ into sample. We further assume that the incident beam is a plane wave with incident intensity equal to fluence of the incident pulse divided by the equivalent area of the beam at the laser surface, which is taken to be $\pi\omega^2_0$, where $\omega_0$ is the beam waist. This model focuses exclusively on the evolution of sample along the longitudinal direction normal to surface. The average magnitude of the projection the displacement of diffusing photons along the longitudinal dimension during one mean free time $l_t/2$. After each mean free time, photons that are not absorbed and that do not pass through the sample surface have moved either to the right or to the left by with equal probability. The internal reflectivity of sample boundaries is 0.15. The sample thickness taken to be 1 mm, which is much larger than the intensity attenuation length $L_a = (l_t l_a/3)^{1/2}$ for the range of parameters considered.

The dye molecule is modeled as a four-level system. Because the relaxation times from the terminal levels 4→2, respectively, of the pumped and emitting transitions, are

generally on a subpicosecond time scale, as shown in Table 2.1, we assume that only ground state, level 1, and the emitting state, level 3, have significant population, $n_1 + n_3 = n$, where n is the density of dye molecles. and $n_i$ is the density of molecules in the *i*th level. The level populations and the emission and absorption photons are governed by rate equations that involve the cross sections for absorption of the pump radiation of the pump radiation and for emission as well as the level populations and the densities of pump and emitted photons.

In the Monte Carlo computation we keep track the density of incident and emitted photons and of the population density $n_3$ at points with depths in the medium that are multiples of *l/2* at time intervals that are multiples of $\tau$. The emission spectrum of Rhodamine 640 as shown in figure 2.5b is divided into 20 segments of equal area. The spatial and temporal evolution of the photon density of each of these segments of the spectrum is followed separately. We take threshold to be the pump energy at which the ratio of the total number of stimulated and spontaneously emitted photons is unity. At this point we find that the emission spectrum has narrowed to a few nanometers and the emission has a width of less than 100 ps. Thus the transition in temporal and spectral features of emission appears to occur at the same pump energies, and our criterion for the threshold in consistent with that used in this and previous experiments.[6]

The temporal profile of the total number of emitted photons at all frequencies is shown in Fig. 3.4 for a 10-ps incident pulse for incident power levels that correspond to excitation below, at, and above threshold in a sample with values of $l_t$ and $l_a$ similar to the experimentally measured profiles as shown in Fig. 3.5. At low pump energy the emerging photons are produced predominantly by spontaneous emission with the molecular

lifetime of 4 ns (table 2.1a) as shown in Fig. 3.4(a). At the threshold for laser action we find an emission pulse of width 40 ps, which reaches its peak 60 ps after the arrival of the leading edge of the pump pulse (Fig. 3.4(b)). Above threshold the emission shortens dramatically and reaches its peak value at earlier times.

At pump energies six times above threshold the peak of the pulse is delayed by 10 ps and its width narrows to 3 ps, which is shorter than the incident pulse (Fig. 3.4(d )). The emission spectrum narrows from the width of 40 nm associated with spontaneous emission below threshold to 7 nm above threshold. The temporal profiles in the experiment and in the simulations are similar. The principal difference is that the lasing thresholds found in the simulations are an order of magnitude lower than observed experimentally. This difference cannot be explained by absorption of the emitted light in the medium, which was omitted in the above calculations. We find that including the absorption typically raises the threshold by only 40%. However, the difference in the thresholds between experiment and our model may be due to the neglect of the transverse excitation profile. Because this omission results in a flat transverse gain profile, the emitted photons cannot escape the gain region by transverse diffusion. The difference between the experiments and the simulations should diminish when $l_t$ and $l_a$ become significantly smaller than the beam diameter.

In Fig. 3.6 the results of the computation of the threshold energy as functions of $l_t$ with $l_a$ held constant at 120 μm and as a function of $l_a$ with $l_t$ held constant at 30 μm are shown. In these calculations the actual spectral distribution of the spontaneous emission was represented by an effective cross section of $\sigma_e = 4.2 \times 10^{-16}$ cm$^2$. The threshold

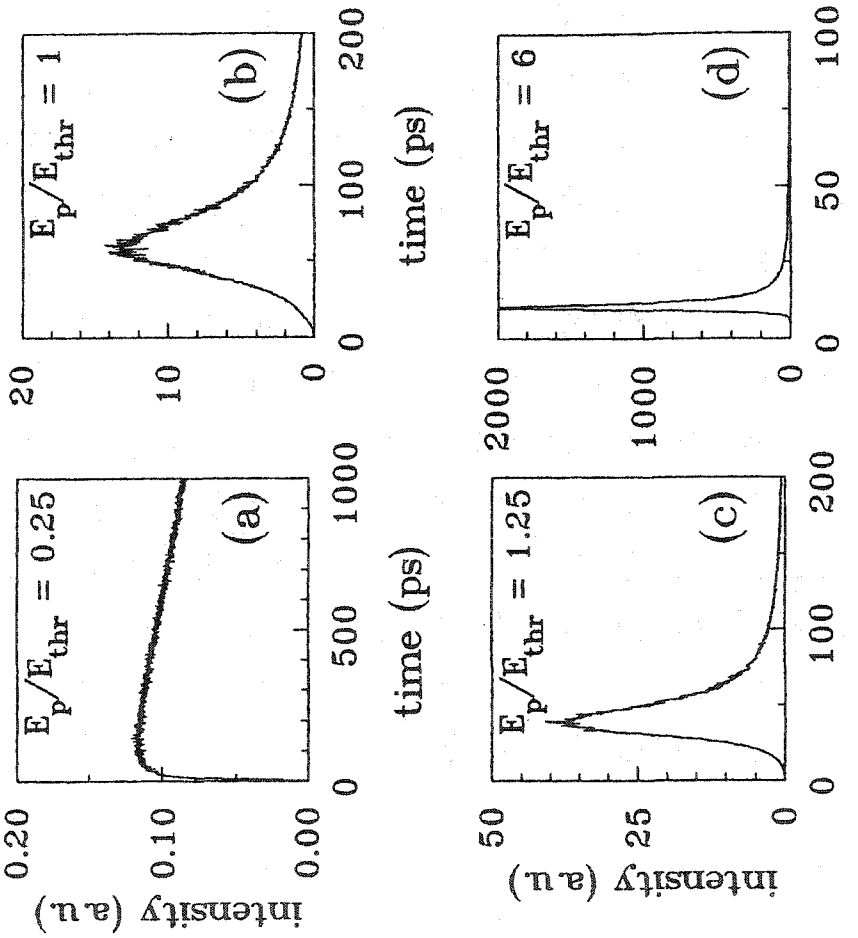


Figure 3.4 Monte-Carlo simulation for a 1 mm thick layered sample where , layer thickness = $l/2$ externally pumped at varying intensities: a) below threshold, spontaneous emission, b) at threshold, c) 23% above threshold and d) 6 times the threshold intenisty

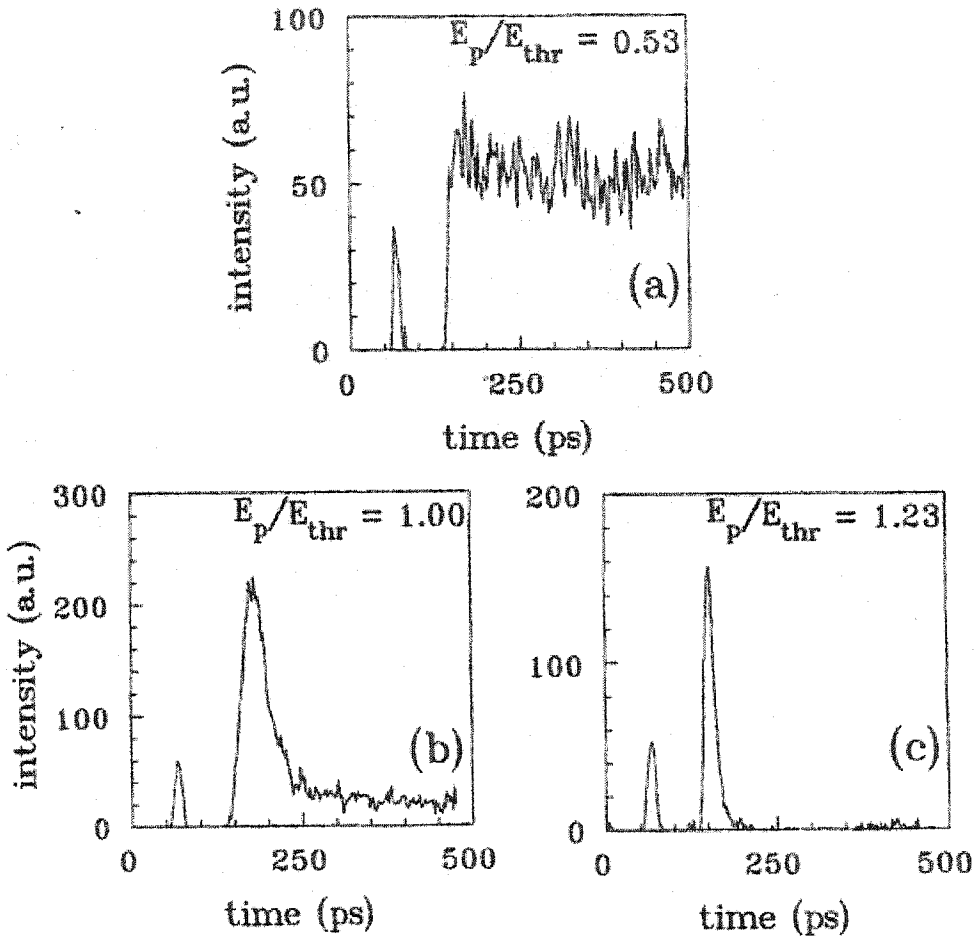


Figure 3.5 Experimental measured temporal profiles for a Rhodamine 640 in methanol/titania colloidal sample for pumping intensity: a) below threshold, b) near threshold and c) above threshold

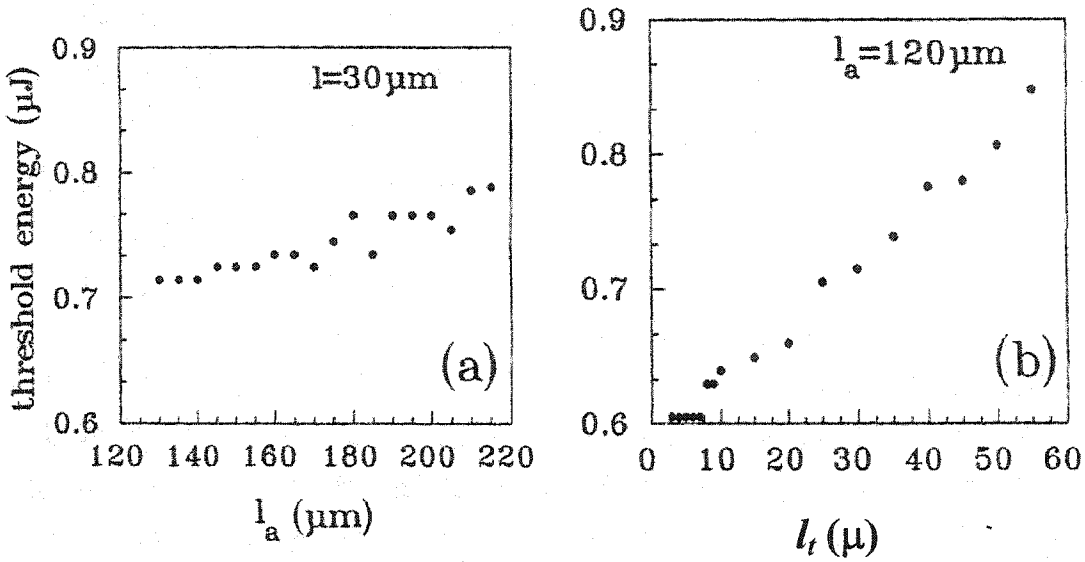


Fig. 3.6 calculated threshold pump energy versus a) $l_a$ for fixed $l_t = 30$ μ and b) $l_t$ for fixed $l_a = 120$ μ.

depends only weakly on $l_t$ and $l_a$. This can be anticipated by considering the limit in which bleaching of the pump transition is negligible.[4] In the absence of gain or loss for the emitted photons the average path length of photons that are spontaneously emitted in the excited region of depth $L_a$ is $\langle z \rangle = \frac{L_a^2}{l_t} \propto l_a$. The small-signal gain in the medium is inversely proportional to $l_a$. Thus the pump energy threshold, which depends on the gain-path length product, would be independent of $l_t$ and $l_a$.

In the present measurements, as well as in previous reports of lasing in random media, the lasing threshold is reached at the point at which the pump transition is bleached. Such bleaching increases the penetration of the pump and consequently leads to longer path lengths for emitted photons within the gain region, which results in a reduced threshold in these systems. This effect is taken into account in the present Monte Carlo simulation, which we find is in qualitative agreement with measurements of pulsed emission.

The threshold characterisitcs of a laser oscillator are compared with the characteristics of the mirrorless laser in table 3.3 below

**Table 3.3**

Comparison of the measured emission properties of disordered media with laser emission

| Laser Oscillator | Mirrorless lasers |
|---|---|
| • Sudden rise in power output in oscillating mode | • Sudden rise in power output at a cetain threshold level |
| • Clamping of upper level population and suppression of fluorescence | • Suppresion of fluorescence |
| • A sudden sharp spectral narrowing | • Sudden sharp spectral narrowing |
| • Sudden sharp spatial narrowing as opposed to isotropic fluorescence | • Spatial narrowing is unclear due to scattering of the emission pulse |
| • Change in statistical character of laser radiation frm random Gaussian noise | • Change in stastical nature of emission. The coherence nature is still unclear |

### 3.5 Models for laser action in disordered media

There are many theories currently under consideration in scientific literature to best model the experimentally observed laser action. The experimentally measured results match closely to the characteristics of conventional oscillator based lasers emission. The basic physics behind this kind of laser-like emission is not yet clear and many models cover some aspect of this process for certain conditions. Some of these

models proposed currently under consideration and focus of research are presented in this section.

### 3.5.1 Model of Scattering walls as reflectors

To explain the laser action in disordered media, a simple scattering walls feedback model, as shown in Fig. 3.7, is envisioned. The scatterers act as a feedback conduit inside the media by forming photon-confining walls around the directly pumped excited region. The directly pumped excited region is shaped like a thin disk whose diameter is the exciting pulse's spot size and the thickness $L_a$ is the absorption length, modified by the presence of scatterers, of the excitation wavelength, into the scattering medium given by diffusion theory is:

$$L_a = \sqrt{\frac{l_t l_a}{3}} \qquad \text{for } l_a > l_t \text{ and } L_a > l_a \tag{3.14}$$

for the case of $l_a > l_t$, $L_a > l_a$ . The photons are scattered/reflected back into the optically excited disk by the reflecting walls formed by the scattering media surrounding the active disk formed by the excitation pulse. The reflectivity of the surrounding scattering walls is dependent on the scatterer density. The excitation radiation is absorbed near the surface to a maximum depth of $l_a$ or less. When the flux of photons spontaneously emitted from the excited disk and scattered back from the surrounding wall of the host medium into the excited medium reaches a critical limit, the energy deposited in the medium by the pump pulse is extracted by the stimulated emission, which is dominated by the wavelengths with the highest gain. The amount of feedback is dictated by the reflectivity of the

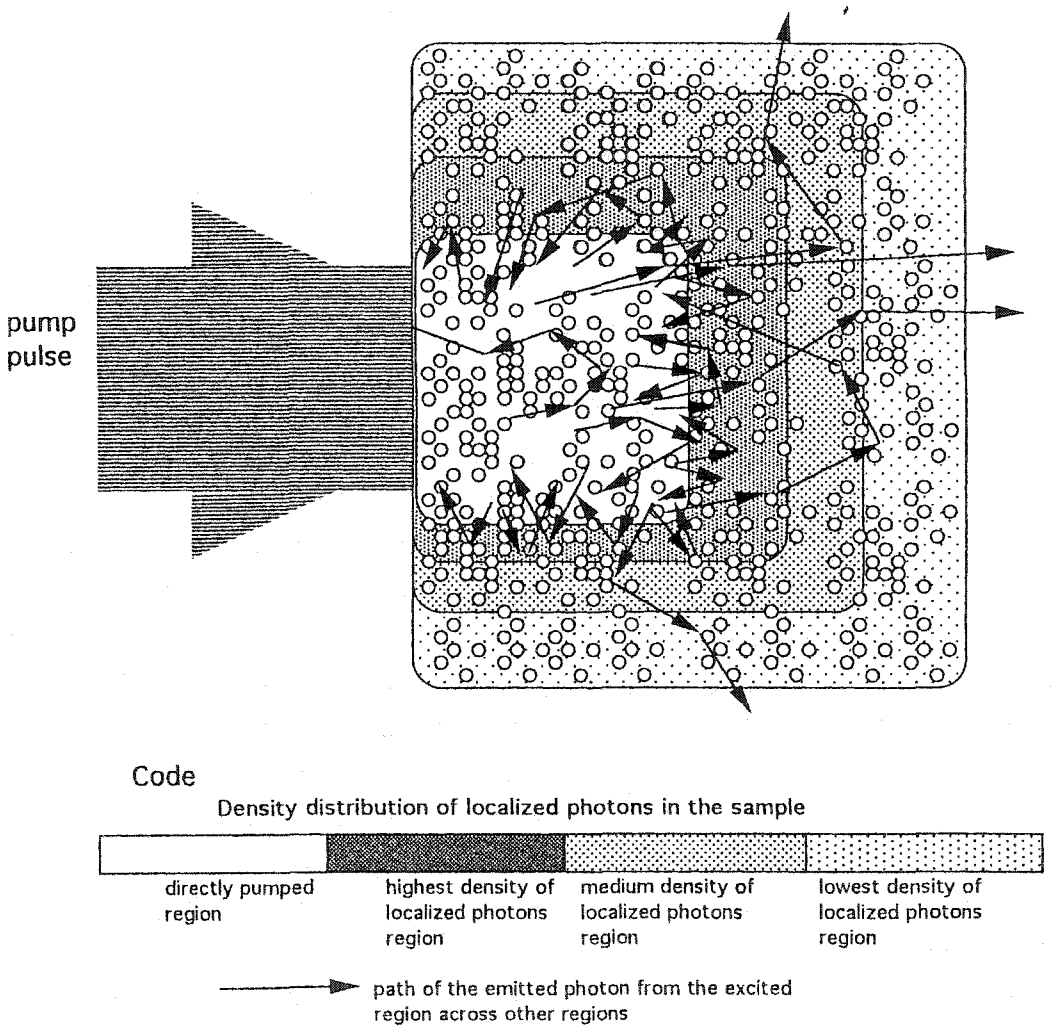


**Figure 3.7** Pictorial depiction of a reflecting walls model representing the effect of scattering media as scattering walls which act as a feedback mechanism to affect a laser like emission

scattering walls around the directly pumped region, where the confined photons reach density maximum. The reflectivity of these scattering walls is dependent on the transport mean-free-path at the emission wavelength, $l_t$. The transmission, T, of a slab medium of thickness L, is[52], $T(L) = \frac{(z_{0r} + z_p)}{(L + z_{0l} + z_{0r})}$, where $z_{0r,l}$ is the extrapolation length at the right and the left side of the slab and $z_p$ is the depth of the source function in the scattering medium. For L >> $l_t$, the transmission can be approximated by $T(L) \approx 1 - \frac{l_t}{L}$. A qualitative measure of the amount of feedback induced by these scattering walls back into the excited region can be considered as the effective reflectivity of the scattering medium given by,

$$R_{eff} = 1 - T(L) \sim 1 - \frac{l_t}{L} \qquad (3.15)$$

where L is the transverse dimension of the scattering region, $l_t$ is the transport mean-free-path and $R_{eff}$ is the effective reflectivity of the medium at the emission wavelength. The amount of energy extracted by stimulated emission is dependent on the feedback due to reflectivity. Higher reflectivity implies more feedback, thus lowering the required excitation intensity to reach lasing threshold. When the scatterer density is made progressively lower (increasing the $l_t$) the reflectivity of the scattering walls around the excited region decreases, which in turn in-creases the required input excitation intensity to reach the critical feedback level needed for laser action. To support this model, the effect of reflectivity of the scattering host on input threshold energy is presented in Table 3.4. The feedback reflectivity is shown to increase with a decrease in $l_t$ along with its corresponding decrease in input threshold energy. The dependence of lasing threshold on

scatterer threshold has clearly been established. The results indicate the dependence of scattering-feed back on scatterer density as depicted in Table 3.4. In the case of densely packed powders, as presented in Table 3.4, the $R_{eff}$ for $TiO_2$ is of the order of 0.9996, which is much higher than the dilute colloidal sample case. The threshold is accordingly lower. In this region, one has to keep in mind that in the case of densely packed powders, the value of the host dye concentration is altered because the volume content of the powders is more than 50%and photon localization effects may come into play to enhance the feedback effects.

**Table 3.4**

Effective Reflectivity of random laser medium

| $l_t(\mu)$ | **THRESHOLD ENERGY** $10^{-3}$**M: L$_A$= 140μ** | $R_{eff} \sim 1 - \frac{l_t}{L}$ |
|---|---|---|
| Neat dye | 45μJ | 0.00 |
| 1400 | 35 μJ | 0.86 |
| 700 | 25 μJ | 0.93 |
| 140 | 17 μJ | 0.986 |
| 70 | 15 μJ | 0.993 |
| 14 | 13 μJ | 0.9986 |

### 3.5.2 Generation of optical amplification in an amplifying diffusive scattering cloud

In an open optically active system of volume V, the number of modes of oscillation, N, is given by the Rayleigh-Jeans formula as

$$N= 4\pi(V\upsilon^2\Delta\upsilon)/c^3 \qquad (3.16)$$

where c is the velocity and $\upsilon$ is the frequency of light. In a Fabry-Perot type of oscillator, which consists of mainly two plane and parallel mirrors, the radiation losses are very high and only small number of modes, propagating normally to the mirrors have small radiation losses. That is why Fabry-Perot resonators are widely used for the generation of coherent emission.

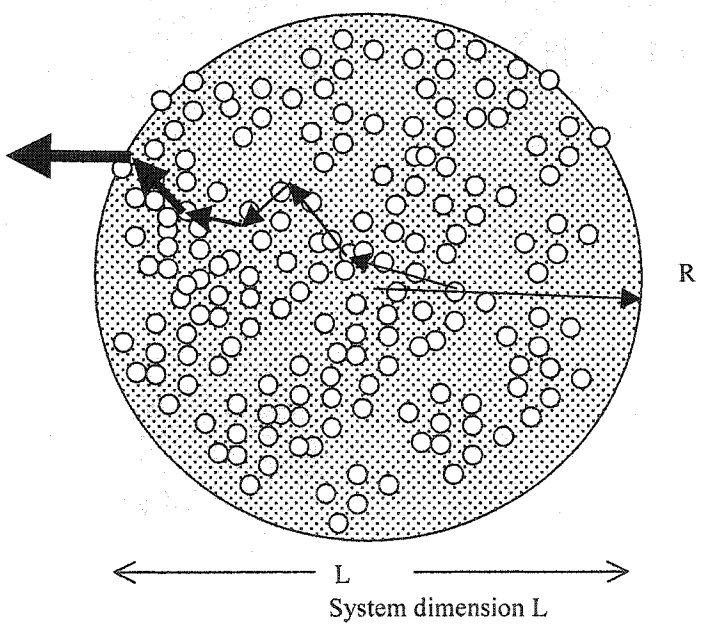


Figure 3.8 Model of a spherical system with randomly distributed scattering particles. The gain is uniform throughout the host medium. The radius of the sphere is R and for general purposes of the model, the overall dimension is L

A diffusive amplifying cloud is an ensemble of identical scattering particles with an average number of particles per unit volume $N_0$. The host medium has a complex permittivity $\varepsilon = \varepsilon_0 + i\varepsilon''_\omega$ where $\varepsilon''_\omega$ represents the wavelength dependant gain in the medium. The gain length in the excited medium $l_g$, is defined as the length over which the intensity is increased by a factor of $e$. The two main parameters used to describe a diffusion dominated propagation of the optical wave in a medium are the scattering length $l_s$ and the transport mean free path length, $l_t$. The scattering length is the average distance a photon has to travel before encountering a scattering event, it is related to the particle density $N_0$ and the scattering cross section of the scattering particles $\sigma_s$ as $l_s = \frac{1}{\sigma_s N_0}$ and $l_t = \frac{1}{N_0\sigma_s(1-\langle\cos\theta\rangle)}$ where $\langle\cos\theta\rangle$ is the average scattering in the forward direction as mentioned in section 2.4. The average distance a photon travels between two points in the medium is given by $\bar{z} = \frac{l_t^2}{z}$. Using this identity, one can use a define an amplification length, $l_{amp} = \sqrt{\frac{l_t l_g}{3}}$.

When the photon transport mean free path is much smaller than the typical dimension, L, of the scattering medium but much longer than the optical wavelength, the motion of the photon is considered to be diffusive where the photon travels an average path length $\bar{z} > L$ in the scattering medium. The diffusion equation for photon energy density $\phi(\vec{r},t)$ in the presence of uniform gain is

$$\frac{\partial\phi(\vec{r},t)}{\partial t} = D\nabla^2\phi(\vec{r},t) + \frac{v}{l_g}\phi(\vec{r},t) \qquad (3.17)$$

where the diffusion constant D is given by, $D = \frac{vl_t}{3}$.

The general solution to equation xx above is given by

$$\phi_\omega(\vec{r},t) = \sum_n a_n \Psi_n(\vec{r}) \exp\left[\left(DB_n^2 - \frac{v}{l_g}\right)t\right] \tag{3.18}$$

where $\Psi_n$ and $B_n$ are the eigenfunctions and eigenvalues of the following equation,

$$\nabla\Psi_n(\vec{r}) + B_n^2\Psi_n(\vec{r}) = 0 \tag{3.19}$$

with the boundary condition $\Psi_n = 0$ at an extrapolation length $d = \frac{2}{3}l_t$ as given in chapter 2. The solution of $\phi(\vec{r},t)$ in equation gives the threshold condition as,

$$DB^2 - \frac{v}{l_{g,\omega_0}} = 0 \tag{3.20}$$

where B is the lowest eigenvalue for $B_n$, $l_{g,\omega 0}$ is the gain length at the spectral maximum of the gain profile of the active host medium.

When the region occupied by the ensemble of scattering particle takes the form of a sphere of radius R,then

$$\Psi_n(\vec{r}) = \frac{1}{r}\sin\frac{n\pi r}{R} \qquad B_n = \frac{\pi n}{R} \qquad B = \frac{\pi}{R} \tag{3.21}$$

and for a cylinder of height H and radius R, the smallest eigenvalue B is given by,

$$B = \left[\left(\frac{2.4}{R}\right)^2 + \left(\frac{\pi}{H}\right)^2\right]^{\frac{1}{2}} \tag{3.22}$$

In general, the the lowest eigenvalue of $B_n$ is of the order of medium dimension 1/L which gives a general value for the threshold condition predicts a critical volume

$$V_{critical} \approx L^3 \approx \left(\frac{l_t l_g}{3}\right)^{3/2} \tag{3.23}$$

Upon examining the case of a spherical region of radius R, the above threshold condition indicates that once the volume of the excited region reaches the critical volume, $V_{critical}$, the photon density $\phi(t)$ increases exponentially with $t$.

In reality, gain saturation would set in quickly when the average distance traveled by a photon in excited medium, $\bar{z} = \frac{R^2}{2l_t}$, exceeds the gain length $l_g$, gain saturation condition is reached increasing the gain length thus resulting in a fluctuating intensity as a function of time. No such fluctuation was seen in the measured emission. There is no loss mechanism considered in the explanation so a critical element of lasing condition was not met, and the emission can be considered as a linear amplifier.

The diffusion model has a requirement that the smallest dimension of the optically active scattering medium be much greater than the transport mean free path. On the basis of measured temporal profiles, diffusion can be ruled out as being the only factor in the generation of ultrashort laser pulses from optically active scattering medium. Diffusion does not explain the dramatic lowering of incident power threshold and that the optically regions were of the order or even smaller than the transport mean free paths.

### 3.5.3 Oscillator-type Laser model

A model of feedback mechanism is based on a ring-type feedback resonator. The excited medium is modeled as a bounded disc with uniform gain. The probabilities, $R_{t1}$, $R_{t2}$ and the average path length $L_{path}$ of a photon returning to the same point in the excited gain medium after traveling outwards and inwards respectively were calculated using Monte-

Carlo simulations. The threshold gain $g_t$ was calculated using steady state lasing threshold equation as,

$$R_{t1}R_{t2}e^{g_t L_{path}} = 1 \tag{3.24}$$

where $L_{path} = \bar{z}$ . In these calculation, the round trip phase condition

$$kL_{pen} = 2\pi m \tag{3.25}$$

where k is the wave-vector and m is the integer, was ignored. The justification used was that the probability of a photon returning in a diffusive medium is low so only a return probability into the gain medium is considered and phase matching condition is not a strict requirement as interference effect on the feedback negligible. This mechanism was termed as incoherent feedback. The incoherent feedback was used to account for the lasing threshold and emission spectrum.

### 3.5.4 Powder Laser

In the 1980's Markushev[4] *et al* obtained intense emission from optically exciting pulverized laser crytals of $Na_5La_{1-x}Nd_x(MoO_4)_4$, and other $Nd^{3+}$-activated materials such as $La_2O_3$, $La_2O_2S$, $Na_5La(MoO_4)_4$ etc. The particle sizes were of the order of 10μ-100 μ. Various other materials such as Ti:Sapphire powders[15-20], $Pr^{3+}$ doped powders and LiF, were investigated. Various models[21-30] were proposed to explain the intense short emission pulses such as ASE, distributed feedback laser cavities and superradiance were considered but none of these models were considered to be satisfactory.

### 3.5.5 Random Lasers with coherent feedback

Laser-like emission has been reported from semiconductor powders, polycrystaline films, π-conjugated polymer films, organic dye-doped gel films, opal

crystals saturated with polymer and laser dye solutions. This kind of laser action was termed as random laser with coherent feedback[31-47]. The semiconductors powders (ZnO) were densely packed where the grain size was of the order of 100 nm.The transport mean free path, $l_{tr}$, was measured to be

$$l_{tr} \sim \lambda$$

The main feature of the measured spectral emission from these kind of densely packed samples was the presence of narrow (< 1Å) discrete spikes on top of the narrowed spectral emission profile narrowed when the input pump intensity crossed a threshold value.

The presence of these narrow spectral and spatial intense spikes was attributed to the presence of inter-particle scattering and contructive interference of backscattered light that in turn select the resonant frequencies. Light is trapped in these regions through multiple scattering and interference. The interference effect is frequency dependent so the light can be localized at discrete frequencies. Due to interference effects, it was speculated that multiple resonant cavities are formed from recurrent scattering events.

The temporal evolution of emission profile from the ZnO powders was measured[44] when pumped by short pulses of 10 ps. The decay time was seen to be less than 50 ps and a long decay time of over 167 ps from the spontaneous decay.

The emission from the multiply resonant emission was statistically analyzed by photon counting methods[33] and the emission was found to have photon distribution P(n) was measured to have Bose-Einstein distribution below threshold as,

$$P(n) = \frac{\langle n \rangle^n e^{-\langle n \rangle}}{n!} \qquad (3.26)$$

where $\langle n \rangle$ is trhe average photon number. Above the threshold, the photon distribution approaches Poisson distribution as,

$$P(n) = \frac{\langle n \rangle^n}{\left[1 + \langle n \rangle\right]^{n+1}} \tag{3.27}$$

The Poisson distribution is closer to the photon distribution from the traditional cavity resonators as opposed to the distribution measured for incoherent feedback lasers by Zacharakis[45].

The transition between the coherent and incoherent feedback mechanisms was measured by increasing the scatterer density in the Rhodamine 640/ Methanol solution. The emission spectrum started to shown spectral spikes of 0.2 nm bandwidth as the signature profile for coherent feedback when the scattering density was increased to $10^{12}$ $cm^{-3}$. The increase in optical scattering due to higher density of scattering particles increases the dwell time of light in the sattering medium. When the optical gain increases due to increase in the pumping intensity, lasing emission from the low loss modes due to resonant interference produces the discrete peaks in the emission spectrum.

The characteristic length scales for lasing in random media was measured by Ling[48] and theoretically predicted by John[49,50] and Genack[51] did not predict the mode spikes observed in the experimental measurements. The lasing threshold drops drastically when the transport mean free path aproaches the emission wavelength ($l_{tr} \sim \lambda$) and when the dimensions of the area of excitation , A, at the sample surface approached $l_{tr}$, the input threshold intesity became independent of the area size.

The coherent feedback in random lasers was investigated further by making micron sized agglomerated clusters of ZnO particles of sizes of diameter of the order of

10 nm[36]. The incident light was confined by strong localization and optical confinement for select wavelgnths. This micon sized laser medium required incident energy of 0.3 nJ which is much lower than any form of random lasers mentioned in the previous sections. This type of micron sized laser is different from what is traditionally termed as micro-lasers which consists of micron sized disks and spheres where the gain and lasing is attributed to the localization of emission radiation within the lasing particles due to morphological resonances and total internal reflections.

### 3.5.6 Mirrorless coherent emission from excited media

Some open-ended mirrorless optically active systems with high gain can exhibit laser like emissions. The open ended systems are modeled as coherently oscillating dipoles. These mirrorless laser-like phenomena are classified according to the size of the the active region, the density of active particles and the coherence of intial preparation. These systems can emit very bright and quasi-coherent beams out of each end of the laser medium as a result of strong amplification of the spontaneous radiation traveling through the longer dimension of the excited region. An example of a mirrorless system of length L and cross sectional area, $a$, is shown in figure 3.9. The emitted radiation emenating at

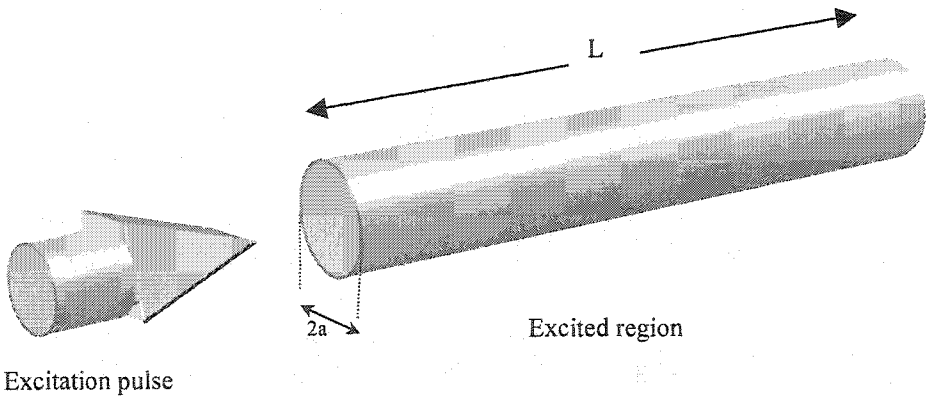


Figure 3.9. Graphical representation of an optically active medium with gain under excitation by an external pulse. The excited medium is a pencil shaped rod of length L and diameter 2a

the side end of the pencil-like medium travels through the length of the medium is called the end-fire mode. A naturally occuring phenomenon is the interstellar masers and X-ray lasers, where the spontaeous emission is highly amplified as it passes through the excited interstellar dust media. The models of mirrorless amplification are based on the concept of the macroscopic polarization, *p(t),* as a reuslt of individual atomic dipoles oscillating with some degree of coherence with each other depending on the intial exctation of the active medium. The directional and spatial coherence of the emitted radiation depends on the relative phases of the radiating atoms at the time of excitation.

The radiation emitted from mirrorless excited media prepared with varying degrees of initial coherence is classified in terms of the intensity and coherence of the emission as Superradiance, Superfluorescence or Amplified Spontaneous Emission (ASE).

These processes are briefly described in the following sections.

### 3.5.6a Dicke Superradiation

A system of excited medium, consisting of coherent array of dipole antennas, acting as a macroscopic coherent dipole was first considered analytically by R. Dicke[2]. The medium consists of a large number, typically of the orders of $10^6$ to $10^{10}$, of two-level atoms, all oscillating with very high degree of coherence between the individual oscillating dipoles. If such medium consists of N coherently oscillating atomic dipoles with $\mu_1$ oscillating moment each, then the macroscopic dipole moment within the vlume will be $N\mu_1$. The rate of the coherent radiative power of the emitted radiation will be proportional to the square of the macroscopic dipole as;

$$P_D \propto (N\mu_1)^2$$

where $P_D$ is power of the emitted coherent radiation. The usual incoherent form of spontaneous emission rate is proportional to the number of atoms N. The short burst of radiation, $T_D$, from the Dicke radiation will have a duration proportional to

$$T_D \approx \frac{1}{N} \qquad (3.28)$$

where as the spontaneously emitted radiation will have an exponential decay time $\tau$, independent of the number of atoms.

This type of emission from small volume and coherently prepared optically active media, first proposed by Dicke[2], has come to be known as Dicke-Superradiation. The atoms here are coupled together through their common overlapping radiation fields. The density of excited atoms in such a medium has to be such that the distance , $d$ ,between the excited atomic dipoles is $d < \lambda$ so that the individual atomic dipoles have overlapping radiation fields and the volume $V \sim \lambda^3$ so that the medium can act as a giant macropole as a whole.

**3.5.6b Incoherently prepared Dicke Superradiation**

As a general case of Dicke Superradiation, the excited atomic dipoles need not be coherent at the time of preparation but the atomic dipoles are randomly phased and the medium as a whole exhibits no macroscopic polarization.

As an example of an excited region, consider a prepared sample of length L and front surface area A, as shown in figure 3.9. The atoms in the upper-level will then begin to radiate spontaneously represented by the incoherent decay rate $\gamma_{rad}$ or at the decay lifetime of $\tau_{rad}$. If N atoms prepared in this incoherently excited medium were all contained in a volume, $V \approx \lambda_{em}^3$ where $\lambda_{em}$ is the emission wavelength, then all the atoms

would be coupled together through their overlapping radiation fields. When any of the atoms goes through a spontaneous emission event, the rest of the atoms will not continue radiating incoherently independently. Any small initial spontaneous emission from any atom will induce coherent oscillations in all the atoms and the system will exhibit a large and coherent macroscopic polarization. The time dependent instaneous energy $W_N(t)$ of such a system with N atomic dipoles is equal to instantaneous intensity $I_N(\hat{k},t)$ integrated over all solid angles as,

$$W_N(t)=\frac{N}{2}\left[\left(1+\frac{1}{N\mu}\right)\tanh\left(\frac{t-t_0}{2\tau_N}\right)-\frac{1}{N\mu}\right] \tag{3.29}$$

where the terms $\tau_N$ and $t_0$ are the pulse duration and delay time respectively. $\tau_N$ and $t_0$ are defined in terms of $\tau_{rad}$ and $N\mu$ as,

$$\frac{1}{\tau_N}\equiv(N\mu+1)\frac{1}{\tau_{rad}} \tag{3.30}$$

$$t_0\equiv\tau_N\ln(N\mu) \tag{3.31}$$

where the factor $\mu$ determins the interference effects arising from the finite shape and size of the collection of emitters depending on the geometry. For circular cylinders as shown in the figure 3.9, the value of $\mu$ can be approximated by,

$\mu = 3\lambda^2/8\pi A^2$ for $A >> (\lambda/2\pi)^2$ and $L < A/\lambda$ (3.32)

$\mu = 3\lambda/8L$ for $L >> (\lambda/2\pi)$ and $A << \lambda A$ (3.33)

The intensity of the the emission is found by differentiating $W_N$ and multiplying by $h\omega_0/2\pi$ as,

$$I_N(t)=\frac{\hbar\omega_0}{4\mu\tau_N}(N\mu+1)^2\,\mathrm{sec}\,h^2\left(\frac{t-t_0}{2\tau_N}\right) \tag{3.34}$$

The radiated intensity from a superradiating system consisting of N emitters is much larger than the incoherent intensity from the same N-emitter system,

$$I_{spontaneous} = \frac{N\hbar\omega_0}{\tau_1} \tag{3.35}$$

and a shortening of lifetime as shown in the figure 3.9 for a system where N~$10^9$, $10^7$ and $10^5$. This incoherently prepared system will evolve into a coherent superposition system in the same fashion as the coherently prepared system with the same radiative power proportional to $P_D \sim (N\mu_1)^2$. There is a random time delay associated with this system as the process is initiated by seeding through any randomly emitted spontaneous emission. The time delay will thus vary from shot to shot.

**3.5.6c Superfluorescence**

The Dicke superradiation is predicted only in systems with small volumes of the order of $\lambda^3$ with Fresnel number of the order $N_f \sim 1$ and inversion density is high so that the radiative coupling between the atoms becomes strong. Superfluorescence occurs in systems where sample length is small compared to the distance radiation can travel in one relaxation (dephasing) time and hence the propagation effects have to be taken into account. The sample length has to be short enough so that if the atoms were to cooperate coherently, they can communicate with each faster than the atoms can dephase. The superradiant lifetime $\tau_N$ can be related to the length L of the system for system $L > \lambda$. The superradiance lifetime $\tau_N$ can be related to the length of the system as,

$$\frac{1}{\tau_N} = \frac{3}{8\pi}\frac{\rho_N \lambda^2}{\tau_{rad}} L \tag{3.36}$$

where $\rho_N$ is the density of excited molecules and $N >> 1$.

The speed of light puts and upper limit on the distance light can travel in time $\tau_N$ which restrict the dimensions of the sample where coherent cooperation between the emitters can take place. The value of $\tau_N$ can be used to define the critical length $L_{cr}$ imposed by the requirement that light emitted from one end be able to reach the other end before the termination f the superradiant process ends:

$$L_{cr} = v\tau_N \tag{3.37}$$

where v is the speed of light in the host medium. A corresponding restriction on the decay rate $\tau_N$ will be imposed by the implication that

$$L_{cr} = \frac{8\pi}{3}\frac{v\tau_1}{\rho_N\lambda^2} \tag{3.38}$$

which gives the relationship between the density of excited molecules and the upper limit of the superradiant decay rate as,

$$\left(\frac{1}{\tau_N}\right)_{cr} = v\sqrt{\frac{3}{8\pi}\frac{\rho_N\lambda^2}{c\tau_{rad}}} \tag{3.39}$$

which establishes that the intensity and lifetime of the superfluorescent emission will follow the superradiant characteristics depend on the density of the excited molecules. The intensity of emitted radiation from a Superfluorescence phenomenon will be proportional to $(N\mu_1)^2$ as in the case of superradiant emission with a delay time less than the dephasing time of the lasing material. Superfluorescence emission is associated with a large-volume atomic collection that is prepared with no initial coherent polarization or oscillating dipole moment.

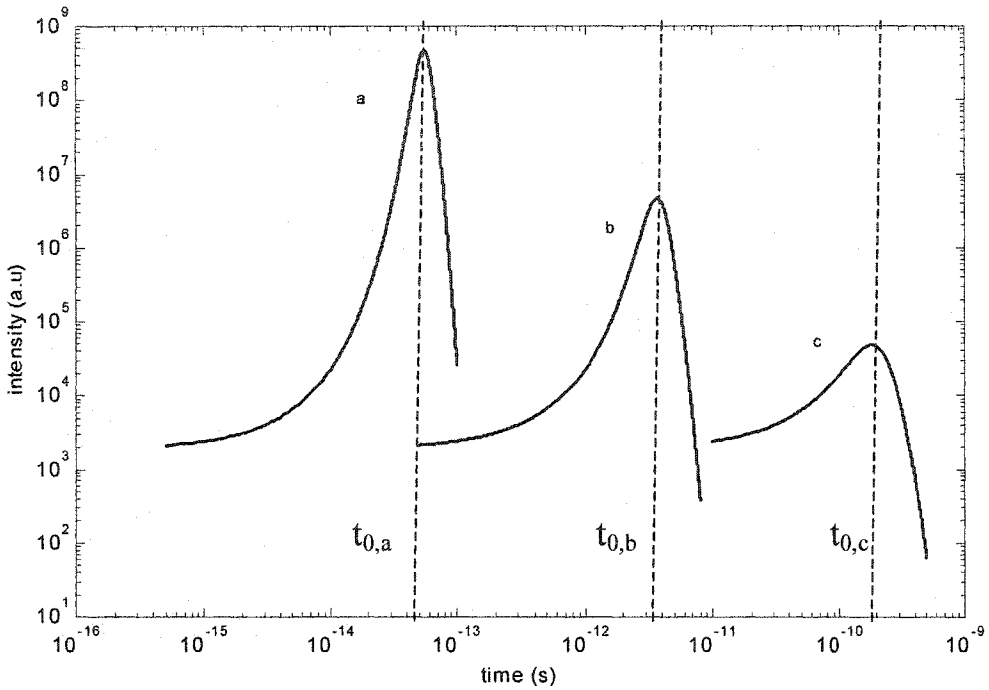


Figure3.10, time-dependent emission intensity of superradiant pulses as a function of number of cooperative atomic dipoles, a) $N = 10^9$, b) $N = 10^7$ and c) $N = 10^5$. The intensity is normalized to the incoherent intenisty, I(t)/N and the onset of superradiant emission occurs at time $t_{0,a}$., $t_{0,b}$ and $t_{0,c}$ respectively

### 3.5.6d Amplified Spontaneous Emission (ASE)

Amplified Spontaneous Emission is referred to any situation where spontaneous emission coming from a collection of atoms in excited state is linearly amplified in the direction with high gain. If the amplification is sufficiently large in a thin long cylindrical configuration, the output beam from each end of the collection will have high intensity and have moderately spatial coherence and directionality. The emitted radiation can become strong enough to induce saturation along the length of the gain medium and

extract major portion of the energy in the excited medium into the directional beams in the end-fire modes.

***i)* Characteristics of ASE emissions**

The amplified emission from an excited laser medium in the ASE domain are based on the rate equation regime as opposed to using the macroscopic polarization regime used for the superradiant and superfluorescence emission.

In an excited medium of dimension of length L and diameter 2a, as shown in figure 3.5 the spontaneous emission power, $P_{sp}$, radiating in all directions from a small unit volume is given by,

$$P_{sp} = N\gamma_{rad}\hbar\omega \tag{3.40}$$

Assuming L >> a, the contribution from a region of length *dz*, to the output amplified emission intensity *dI*, at the other end is given by

$$dI = \frac{\pi a^2 N\lambda_{rad}\hbar\omega}{4\pi L^2} e^{\alpha_m (L-z)} dz \tag{3.41}$$

where the gain medium has the stimulated emission cross section $\sigma_{st}$ and $\alpha_m = N\sigma_{st}$. Integrating the total spontaneous emission from the emtire sample , total ASE power is,

$$I \approx \frac{a^2 N\lambda_{rad}\hbar\omega}{4L^2} e^{2\alpha_m z} \int e^{-2\alpha_m z}$$

$$\approx \frac{a^2 N\lambda_{rad}\hbar\omega}{4\sigma_{st} L^2} e^{2\alpha_m L} \tag{3.42}$$

where the upper limit in the integral has been replaced by infinity under the assumption that the gain in the medium is large. The most of the emission intensity radiating from the end of the sample rod in the first gain length $(\alpha_m)^{-1}$ therefore the solid angle, $\theta$, of the end-fire mode as seen from the other end is

$$\theta \sim \frac{\pi a^2}{L^2} \tag{3.43}$$

The rate of stimulated emission induced by a wave of intensity I is given by,

$$W_{st} = \frac{\sigma_{st} I}{\hbar \omega} \tag{3.44}$$

The ratio of the stimulated emission transition rate due to ASE to the spontaneous emission transition rate at the output end of the sample rod can be written in the form,

$$\frac{W_{st}}{\gamma_{rad}} \approx \left(\frac{a}{2L}\right) e^{\alpha_m L} \tag{3.45}$$

therefore the stimulated gain is proportional to the aspect ratio $a/L$ and the gain coefficient $\alpha_m L$.

The emission lifetime from ASE is shortened when stimulated emission rate from the end of the rd length starts to exceed the purely spontaneous emission rate by a large ratio. When $\alpha_m L >> 2ln(2L/a)$ the presence of ASE will shorten the effective lifetime significantly.

The saturation effects in a homogeneous gain medium is given by

$$I_{sat} = \frac{\hbar \omega}{\sigma_{st} \tau_2} \tag{3.46}$$

where $\tau_2$ is the effective lifetime for the upper (excited) laser level. The ratio of ASE intensity to the saturation intensity at either end can be written as,

$$\frac{I(L)}{I_{sat}} \approx \left(\frac{a}{2L}\right)^2 \left(\frac{\tau_2}{\tau_{rad}}\right) e^{\alpha_m L} \tag{3.47}$$

When the gain coefficient $\alpha_m L$ becomes more than unity the ASE becomes large enough to produce high enough gain saturation and extracts significant power from the excited laser medium.

### *ii)* Mirrorless Laser Characterisitics

The characteristics of the various mirrorless laser-like process in excited media are tabulated below in table 3.5.

**Table 3.5**

**Comparative properties of mirrorless laser-like processes in excited gain media**

| Process | Intensity | Pulse width ($\tau_p$) | Volume dimension limit | Amplifying process |
|---|---|---|---|---|
| Superradiance | $\sim N^2$ | $\tau_p = \tau_N \sim 1/N^2$ | $V \sim \lambda^3$ | Radiative field overlap |
| Superfluorescence | $\sim N^2$ | $\tau_N \sim 1/N^2$ | $\lambda < L < v\tau_N$ | Coherent dipole coupling |
| ASE | $\frac{I(L)}{I_{sat}} \approx \left(\frac{a}{2L}\right)^2 \left(\frac{\tau_2}{\tau_{rad}}\right) e^{\alpha_m L}$ | $\tau_N < \tau_p < \tau_{rad}$ | $\alpha L \sim 1$* | Rate equation regime |

* $\alpha$ is the absorption coefficient from Beer's Law

### 3.6 Comparison with experimental data

The experimentally measured data is compared with the properties of mirrorless laser-like properties as described in section 3.2. The data is compared with the relative intensities and pulse duration of the of the emitted pulses as a function of the input energy and scattering particle density to ascertain the category of processes the emission falls into for the different experimental conditions.

The scattering length for each particle density, $\rho_d$, and the absorption length, $l_a$, for variuos dye concentrations is shown in table 3.1. The key property of the excited media under consideration is the density, $\rho_N$, and the number, N, of excited molecules in the medium. The calculated absorption and stimulated emission cross sections previously are;

Absorption cross-section $\sigma_a \sim 10^{-16}\ \mathbf{cm}^2$ (3.48)

Stimulated emission cross-section $\sigma_{st} \sim 6\mathbf{x}10^{-16}\ \mathbf{cm}^2$ (3.49)

The molecular density available for excitation is given by the the dye concentration as;

Concentration: $10^{-4}$M: $\rho_d \sim 6\mathbf{x}10^{16}\ \mathbf{cm}^{-3} \Rightarrow 10^4\ \mu^{-3}$ (3.50)

Concentration: $10^{-3}$M: $\rho_d \sim 6\mathbf{x}10^{17}\ \mathbf{cm}^{-3} \Rightarrow 10^5\ \mu^{-3}$ (3.51)

The actual number of excited molecular density depends on the absorption length;

$l_a = (\rho_d \sigma_a)^{-1}$ = *.16 cm or 1600μ* *($10^{-4}$M)* (3.52)

= *.016 cm or 160μ* *($10^{-3}$M)* (3.53)

where the number The number of excitation photons available per μJ,

**Number of photons for 532 nm ~** $5 \times 10^{12}\ (\mu J)^{-1}$ (3.54)

The beam width of the incident pulse at the sample surface was 0.5 mm

**Diameter, a= .5 mm , area A ~ .2 mm$^2$ = 2x10$^4$ μ$^2$** (3.55)

The total number of excited molecules per $l_a$ in an unsaturated medium is about 67% ( $e^{-1}$) of the incident number of photons per μJ of incident energy is about $10^{12}$ The total number of molecules in the excited volume, $\rho_d V = \rho_d \times A \times l_a$,

$$N = 6 \times 10^4 \times 2 \times 10^4 \times 1600 = 1.8 \times 10^{12} \quad (3.56)$$

As the incident energy increases, the excited region will get saturated and the region length will increase. What is more important here is that the density of excited molecules will not increase above $10^4$ $\mu^{-3}$ for $10^{-4}$M and$10^5$ $\mu^{-3}$ for $10^{-3}$ M concentration when fully saturated. The volume is given in the units of $\mu^3$ to get an order of magnitude figure for the feasibility of superradiant emission as the emission wavelength ($\lambda_e$ = 0.62) is of the order of 1μ. Under saturation conditions the excited molecular density will represent a weak superradiant regime, but due to longer absorption region due to absorption saturation, where the $L << v\tau_N$ as described for the superfluorescence emission, the excited sample is well suited for superfluorescence.

### 3.5.1 Emission characteristics of the random lasers

The onset of superfluorescent or superradiant can be measured by the increse in the power of emitted radiantion. The spontaneous emission intenisty is given by,

$$I_{sp} = Nh\nu_0/\tau_{rad} \quad (3.57)$$

Where $\tau_{rad}$ is the spontaneous decay lifetime of the medium and ν is the frequency of emitted wavelength. The superfluorecent emission power is a function of $N^2$ as described in the previous section.

The ratio of emitted power for different input power was measured for varying scatterer density. The power was calculated by integrating the temporal profiles over time as measured by the time-resolved measurement. The output power was calculated as

$$P_{l(fl)} = \frac{1}{\tau_{pulse}} \int_0^{\infty} I(t')dt' \qquad (3.58)$$

where the subscripts *l* and *fl* represent the power measured from profile when the emission was considered to be lasing (short pulsed) and when fluorescent (long pulse). The power was normalized to the input power for the profile under consideration. The ratio of the emitted power as taken where the fluorescnce power $P_{fl}$ was squared as $(P_{fl}/E_{in})^2$ to determine if the output power follows $N^2$ for superradiant or superfluorescent pulse. The ratio emitted power for $P_l$ and $(P_{fl})^2$ should not be more than 1 if all the emitted power is collected and accounted for. The experimental layout permits a lower collection efficieny as only the power emitted within the solid angle of collection in the backscattered direction is collected. The ratio calculated for the geometry used in the experiment gives a qualitative picture of the process involved as the fluorescent emision is isotropic and lasing emission is more directional in the backscatter direction. In case of neat dyes, the measured powers in the backscatter direction is misleading as the ASE power emitted under high input energies is much more directional as opposed to the situation where the emitted radiation has a chance of being scattered due to the presence of scatterers in the gain media. The ratio of the emitted powers is tabulated in Table 3.6. It can be seen that the emitted powers follows the $N^2$ law more closely and thus the emission process can be termed as superfluorescent.

The time-resolved intensities for various dye concentrations and particle densities are shown in figures 3.11 to 3.13. A time-delayed ASE pulse, with respect to the fluorescent emission, is shown in figure 3.11 for the low gain regime of $10^{-4}$M concentration. The relative intensities of the emission for varying dye concentrations and scatterer densities are displayed in figure 3.12 a-d. Figure 3.12a and b show profiles for a

scatterer density of zero and figure c and d show the profiles for scatterer density of $10^{11}$ $cm^{-3}$ in a dye concentration of $10^{-4}$ M. Figure 3.13 a to d show the drastic shortening of pulse durations for the neat dye concentration of $10^{-3}$M and scatterer density 0 (a and b) and of $10^{11}$ $cm^{-3}$ (c and d).

What is remarkable about the emission profiles is the drastic reduction in input energy to obtain the intense short pulsed output as the scatterer density is increased. Furthermore , no measureable delay was seen for short pulse emission when the dye concentration was increased to $10^{-3}$M. These measurements further enhance the

**Table 3.6**

Ratio of lasing output power to the square of fluorescent power normalized to the input energy

| Scatterer density ↓ / $\frac{P_l}{E_{in,l}} \Big/ \left(\frac{P_{fl}}{E_{in,fl}}\right)^2$ | | |
|---|---|---|
| **Dye concentration→** | **$10^{-4}$M** | **$10^{-3}$M** |
| **Neat*** | **28** | **133** |
| **$10^{10}$ $cm^{-3}$** | **NL** | **5.6** |
| **$10^{11}$ cm-3** | **2.5** | **5.9** |

**The power output ratio for neat dye is high because of the preferential directionality of emission as opposed to the isotropic spontaneous emission.*

model of reflective walls mentioned earlier where the scatterers not only enable the emission but also to increase the absorption density

### 3.7 Conclusion

In this chapter, the time-resolved emission profiles of lasing action in random media were measured. The random-laser media consisted of a Rhodamine/methanol solution hosting Titania particles as scatterers. The emission intensity and lifetime were measured as a function of varying input intensity, dye concentration and scatterer density. The measurements were taken over a wide range of $l_t$ and $l_a$ to firmly establish the lasing threshold dependence on scatterer density. Two models for the observed emission were proposed, 1) model of scattering-reflecting wallsf, and 2) Super-fluorescence. Emission intensity and lifetime measurements. Other models currently under research in the literature were compared.

The field of laser action in active disordered media is still in its evolution period. The underlying fundamental principles have yet to be established. Different proposed models address different aspects of the process and no demonstrably coherent theory has yet been established. Further research is needed to fully understand the processes involved and utilize in practical applications.

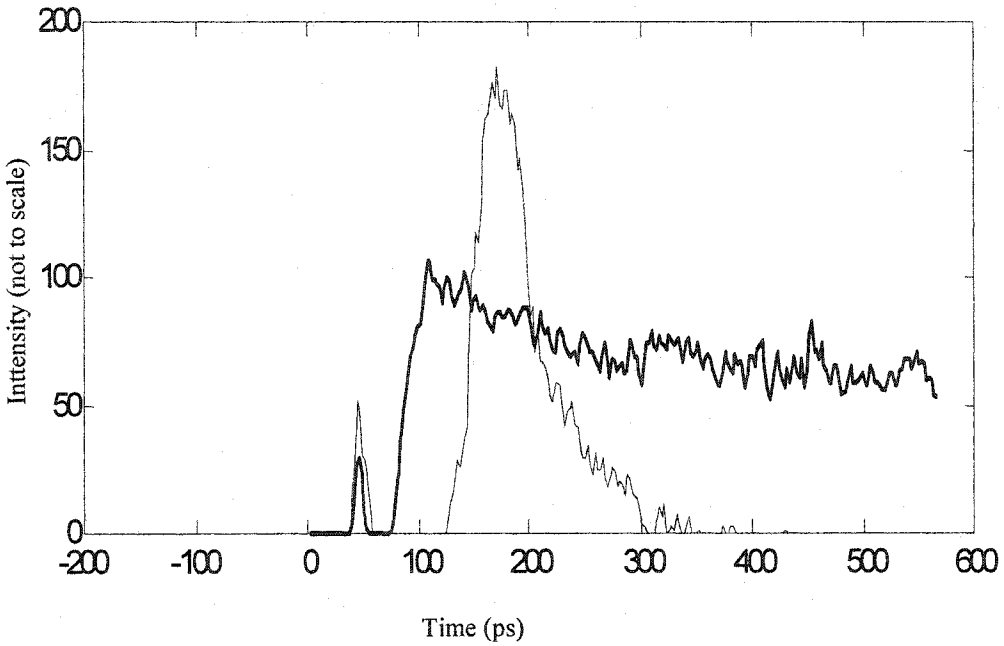


Figure 3.11 Time delay between the ASE emission for dye concentration of $10^{-4}$M and scatterer density of $10^{11}$ $cm^{-3}$. The long pulse is the fluorescent emission at an input energy 7.6 μJ and the short pulse is the ASE enhanced pulse for an input energy of 430 μJ.

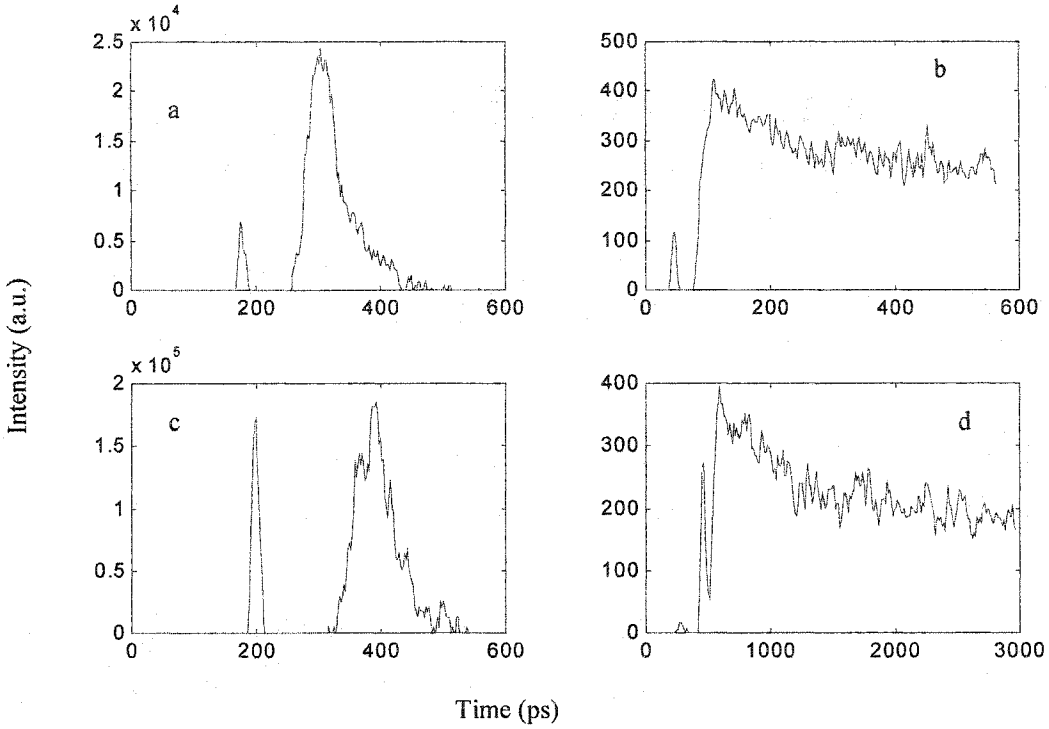


Figure 3.12 Relative intensities of emission for dye concentration of $10^{-4}$.for varying input energies. a) neat dye, 430μJ b) neat dye,8 μJ, c) scatterer density $10^{11}$ $cm^{-3}$,229 μJ d) scatterer density b) $10^{11}$ $cm^{-3}$,38 μJ

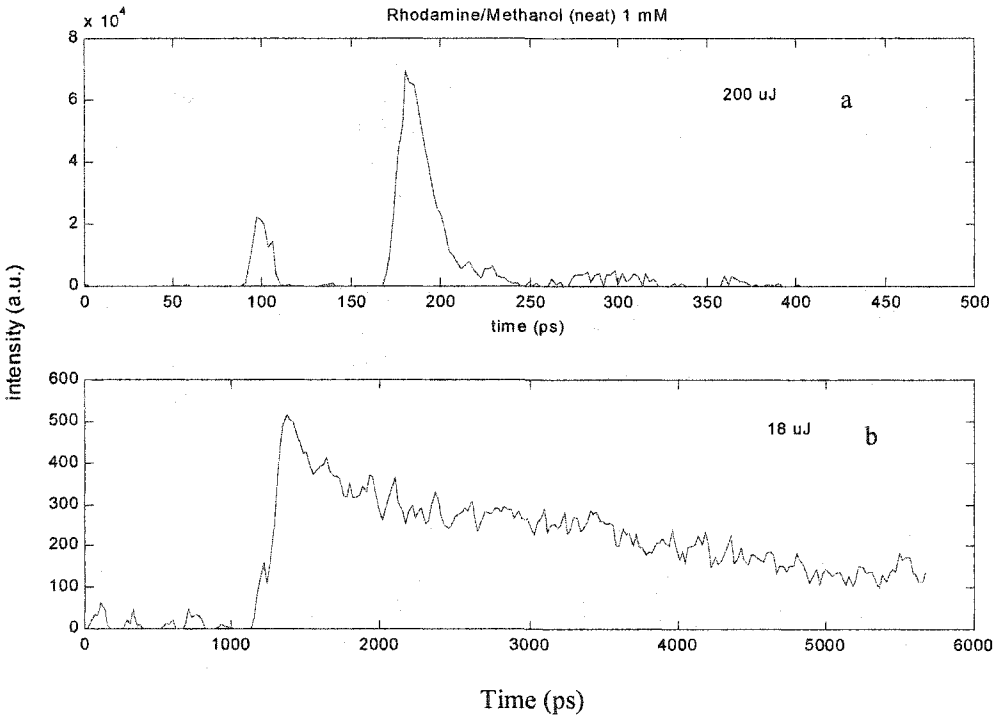


Figure 3.13, relative intensities of time resolved emission for neat dye at $10^{-3}$M concentration. a) short pulse emission at input energy 200 μJ, b) fluorescent emission at 18 μJ

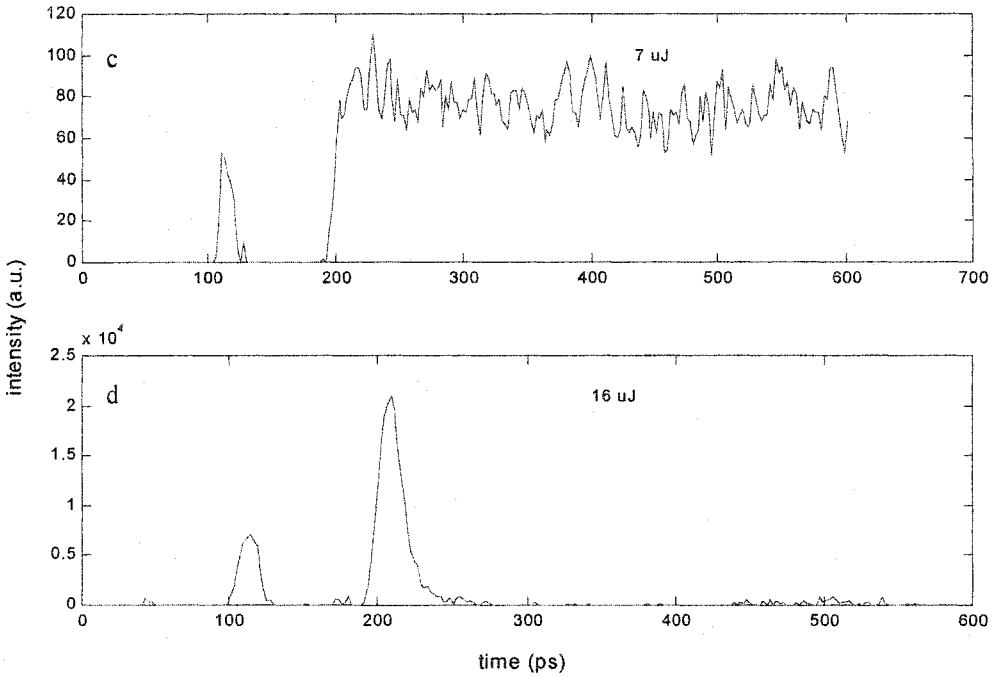


Figure 3.13 , relative intensities of time resolved emission for neat dye at $10^{-3}$M concentration.and scatterer density of $10^{11}cm^{-3}$ c) fluorescence emission at input energy 7 μJ, d) laser emission at 16 μJ

**References**


1. A. L. Schawlow and C. H. Townes, "Infrared and optical masers," Phys. Rev.112,1940-1949 (1958).
2. R. H. Dicke, Phys. Rev. 93, 99 (1954)
3. Maiman, T.H.,*Nature,* Vol. 187, No. 4736, pp. 493-494. 1960
4. R.V. Ambartsumyan, P.G. Kryukov and V.C. Letokhov, Sov. Phys. JETP 26 ( 1968 ) 835.,V.M. Markushev, V.F. Zolin and Ch.M. Briskina, Sov. J. QuantumElectron. 16 (1986) 281;
5. N.E. Ter-Gabrielyan, V.M. Markushev, V.M. Belan, Ch.M. Briskina, O.V. Dimitrova, V.F. Zolin and A.V. Lavrov, Sov. J.Quantum Electron. 21 ( 1991 ) 840, and references therein.
6 N.M. Lawandy, R.M. Balachandaran, A.S.L. Gomes and E. Sauvian, Nature 368 (1994) 436.
7. W. Sha, C.H. Liu and R.R. Alfano, Optics Lett. 19 (1994).
8. M. Siddique, Li Yang, Q.Z. Wang and R.R. Alfano, Opt. Soc. Am. Annual Meeting, Dallas, Texas, October 1994;
9. M. Siddique, Q.Z. Wang and R.R. Alfano, Opt. Soc. Am., Annual Meeting, Dallas, TX, October 1994;
10. W. Sha, C.H. Liu and R.R. Alfano, Opt. Soc. Am., AnnualMeeting, Dallas, TX, October 1994.
11. Masood Siddique, R. R. Alfano, G.A.Berger, M. Kempe and A. Z. Genack, *Opt. Lett. 21, 450, 1996*
12. Masood Siddique, Q.Z.Wang, R. R. Alfano, *J. Biomedical Opt.* 1, 442, 1996

13. M. Balachandran and N.M. Lawandy, Opt. Soc. Am.,Annual Meeting, Dallas, TX, October 1994.

14. Noginov M. A., Caulfield H J. Noginova N E and Venkateswarlu P, *Opt. Commun.* 118, 430 1995

16. Noginov M. A., Egarievwe S U, Noginova N E., Caulfield H. and Wang J C, *Opt. Mater.* 12 127, 1999

17. Noginov M. A, Egarievwe S U. Noginova N E, Wang J C and Caulfield H J, *J. Opt. Soc. Am.* B, 15, 2854, 1998

18. Noginov M A, Noginova N E, Egarievwe S U., Caulfield H J, Cochrane C., Wang J C., Kokta M R, and Paitz J, *Opt. Mater,:* 10 ,297, 1998

19. Noginov M A, Noginova N E, Egarievwe S U., Caulfield H J., Venkateswarlu P., Thompson T, Mahdi M and Ostrumov V, *J. Opt. Soc. Am.* B 13 2024, 1996

20. Noginov M A., Noginova N E, Egarievwe S U, Caulfield H J., Venkateswarlu P., Williams A and Mirov S B, *J. Opt. Soc. Am..* B 14, 2153, 1997

21. Gouedard C., Husson D., Sauteret C., Auzel F and Migus A, *J. Opt.* Soc. Am. B 10 2358, 1993

22. Briskina Ch M., Markushev V M, and Ter-G Gabrielyan N E, *Quantum Electron.* 26 23, 1996

23. Auzel F and Goidner P, *J. Alloys Compounds* 300, 2000

24. Zyuzin A Yu, *Europhys. Let.* 26 5 7, 1994

25. Zyuzin A Yu, *Phys. Rev:* E 51 5274, 1995

26. Zyuzin A Yu, JETP 86 445, 1998

27. Wiersma D S. and Lagendijk A, *Phys. Rev. E* 54 4256, 1997

28. Zolin V F, *J. Alloys Compounds* 300 214, 2000

29. Markhushev V, Ter-Gariclyan N E. Briskina Ch NI. Belan V R and Zolin V F 1991) Sov. J. *Quantum Electron.* 20 773

30. Markushev V NI, Zolin V F tilts! Briskina Ch. 1986 Sov: .1. Quantum *Electron.* 16 281

31. Cao H. Jiang X. Ling Y. Xu J *Y* and Soukoulis C M 2003 *Preprint* cond-mat/0301461

32. Cao H. Ling Y., Xu J Y and Burin A L, 2002 *Phys. Rev: E,* 66 R25601

33. Cao H., Ling Y., Xu J Y., Cao C Q and Kumar P, 2001 *Phys. Rev Lett.* 86 4524

34. Cao H., Xu J Y., Chang S-H and Ho S T, 2000 *Phys. Rev.* E 61 1985

35. Cao H., Xu J Y. Chang S-H., Ho S T, Seelig F W., Liu X and Chang R P H *Phys.Rev. Lett.* 84 5584, 2000

36. Cao H. Xu J Y, Seelig E W and Chang R P H *Appl. Phys. Lett.* 76 2997, 2000

37. Cao H., Zhao Y G, Liu X., Seelig E W and Chang R P H, *Appl. Phys. Lett.* 75 1213, 1999

38. Cao H., Zhao Y G., Ong H C and Chang R P H *Phys. Rev.* B 59 15107, 1999

39. Cao H., Zhao Y G., Ong H C., Ho ST., Dai J Y, Wu J Y and Chang R. P.H., *Appl. Phys. Lett.* 73 3656, 1998

40. Cao H., Zhao Y G., Ong H C, Ho S T., Seelig E. Q., Wang Q H., and Chang R.P.H., Phys. Rev. Lett. 82 2278, 1999

41. Frolov S V., Vardeny Z V., Yoshino K. Zakhidov A A, and Baughman R H, *Phys. Rev.* **B 59** R5284, 1999

42. Frolov S V., Vardeny Z V, Yoshino K. Zakhidov A A, and Baughman R H, Opt. *Commun.* 162 241, 1996

43. Yoshino K, Tatsuhara S., Kawagishi Y and Ozaki M, *Appl Phys. Lett.* 74 2590, 1999

44. Soukoulis C. M, Jiang X., Xu J Y and Cao H *Phys, Rev.* B 65 R041103, 2002

45. Zacharakis G., Heliotis G., Filippidis G., Anglos D and Papazoglou T G, *Appl. Opt.*, 38 6087, 1999

46. Zacharakis G, Papadogiannis N A., Filippidis G and Papazoglou T G, *Opt. Lett.* 25 923, 2000

47. Zacharakis G., Papadogiannis N A and Papazoglou T. G., *Appl. Phys. Lett.* 81 2511, 2002

48. A.Z. Genack and J.M. Drake, Nature 368 (1994) 400.

49. Ling Y., Cao H., Burin A L., Ratner M A., Liu X and Chang R P H., *Phys. Rev.* A 64 063808, 2001

50. John S., *Phys. Today*, 44, 32, 1991

51. John S and Pang G, *Phys. Rev.* A 54 3642, 1996

52. A. A Lisyansky, J.H. Li, N. Garcia. T.D. Cheung and A. Z. Genack, *"Photonic Band Gaps and Localization"*, Ed. C. M. Soukoulis, Plenum Press, New York, 1993

# CHAPTER 4

# MIRRORLESS LASER ACTION FROM OPTICALLY PUMPED DYE-TREATED ANIMAL TISSUES

## 4.1 Introduction

Dyes have been extensively used in biomedical tissues for diagnostic purposes in imaging and for therapeutic purposes in photoradiation therapy. They also make ideal tunable sources in a wide variety of laser systems[1]. Previously, as cited in chapter 2 and 3, Lawandy[2] et al., and others[3-7] have observed mirrorless laser action using optically excited dyes in discretely scattering dielectric particle suspensions using submicron size scattering particles. Laser action in discretely scattering media was first demonstrated by Letokhov and coworkers[8] in the mid 1960's where they used scattering media as an incoherent feedback source. Lasing action in discrete optically particles obtained by pulverizing laser crystals was demonstrated by Markushev[9.10] and others[11,12] in the 1980's and 1990's using optically active scatterers made of Nd doped crystallite powders of sizes ranging from approximately 1μ to 200μ. More recently Cao[12] et al. have used micorscopic clusters of ZnO nanometer scale sizes of the order of $\sim<$ 200nm.

The prior work has concentrated on using discrete dielectric particle scatterers to obtain mirrorless laser action in disordered media. The exact mechanism of these processes is still being researched and several mechanisms have been proposed. The field is still open to further investigation but the lasing dependence on the size, scattering parameters and particle density have clearly been established. The small sized particles can give rise to localization[13-16] while interaction with continuously disordered

heterogeneous active the large sized particles can support morphological resonance modes.

This chapter deals with the question as to whether such mirrorless laser action would take place in continuously heterogeneous optically active disordered media random. A class of such heterogeneous scattering media of great interest is the biomedical tissues. The particle sizes in such heterogeneous media range from 0.1μ to 10μ where the larger dimensions come from the cell membranes which defines the boundaries of the self contained cell structure, and the smaller sized particles are nuclei, mitochondria and other structures imbedded in the cell and tissues. The optical interaction with biomedical tissues is of great importance in the field of medical applications such as diagnosis, tomography, surgery and phototherapy. The presence and feasibility of mirrorless laser action in optically excited animal tissues treated with an optically active dye was investigated by measuring the temporal and spectral emission profiles.

The scattering mechanism in active animal tissues is different from the scattering system proposed by Letokhov[8] and from that of the highly scattering systems demonstrated previously[2-12]. Optical scattering in biomedical tissues arises mainly due to the larger cell size and a whole range of scattering particle sizes embedded in the cellular structure. A graphical description of the differences between the homogeneous and heterogeneous systems is given in figure 4.1. In a homogeneously disordered system, the incident optical radiation travels through a host medium of a fixed index of refraction while it scatters off particles of fixed index of refraction and size as shown in figure 4.1a.

The incident optical wave traveling through a heterogeneously continuous medium on the other hand, can have a tortuous path due to a host medium which has varying index of refraction as well as scattering off entities of varying sizes, indices of refraction embedded in larger cellular structures as shown in figure 4.2b. The optically active medium in the tissues is the Rhodamine 640 dye solution in Methanol which is located inside the cells so that the laser action might take place from scattering photons inside the cells as well as from the localization and microcavities formed due to intercellular scattering. Such heterogeneous continuously disordered active systems do not fall in either of the categories of scattering media investigated previously to understand the gain mechanisms in disordered systems.

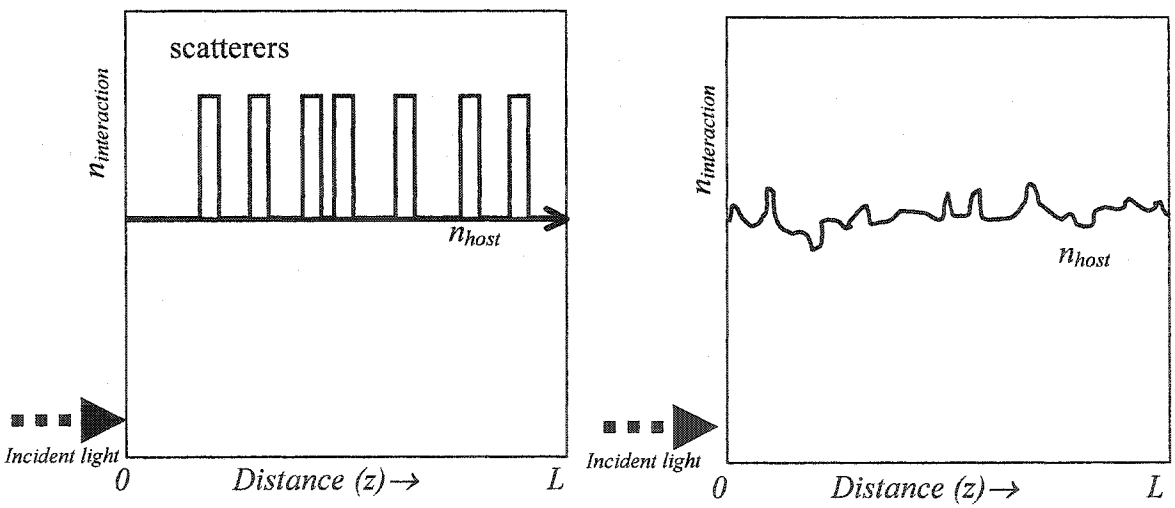


Fig. 4.1. Differences between the indices of refractions of homogeneous and heterogeneous disordered media. *a*) a homogeneous medium where the incident wave travels through homogeneous medium, it interacts with randomly distributed particles of the same size and index of refraction. *b*) a heterogeneously disordered system where the incident wave travels through a medium of changing index of refraction while encountering discrete particles of varying sizes and index of refractions

The underlying excitation and emission process that can occur in scattering active tissue media is pictorially shown in Fig. 4.2. The scattering in tissues is different from the discrete scattering whether it is in crystallite powders, powdered suspensions or intralipid suspensions. In scattering suspensions the photons scatter from discrete scattering particles propagating in the optically excited host medium where the optical gain is related to the beam diameter, the absorption

length of the dye and scattering mean free path lengths of the scatterers as explained in chapters 2 and 3. The output is amplified medium and the gain occurs in the region between the particles. The scattering in a continuously disordered heterogeneous tissue medium takes place inside and outside the embedded scatterers, ranging from 0.1μ to 10μ in size. The multilayered structure of the cells and the walls and the varying refraction indices of the plasma and other materials within the tissues take part in scattering. The variations of the refraction index in a tissue medium give rise to meandering photon paths even in the absence of any discrete scattering particles, making it a continuously disordered system. The active dye medium is absorbed within the cellular structure, making it a truly continuously disordered heterogeneous active scattering structure. The optical excitation of the lasing dye and gain due to scattering in such a medium becomes different from the discretely scattering suspension mentioned above. The dye is located inside the cell structure and the scattering takes place from the structures inside and outside the 10 nm size of the cell due to easy transportation of methanol molecules through cell membranes. The large size of the cell causes the scattering to be in the forward direction mostly.

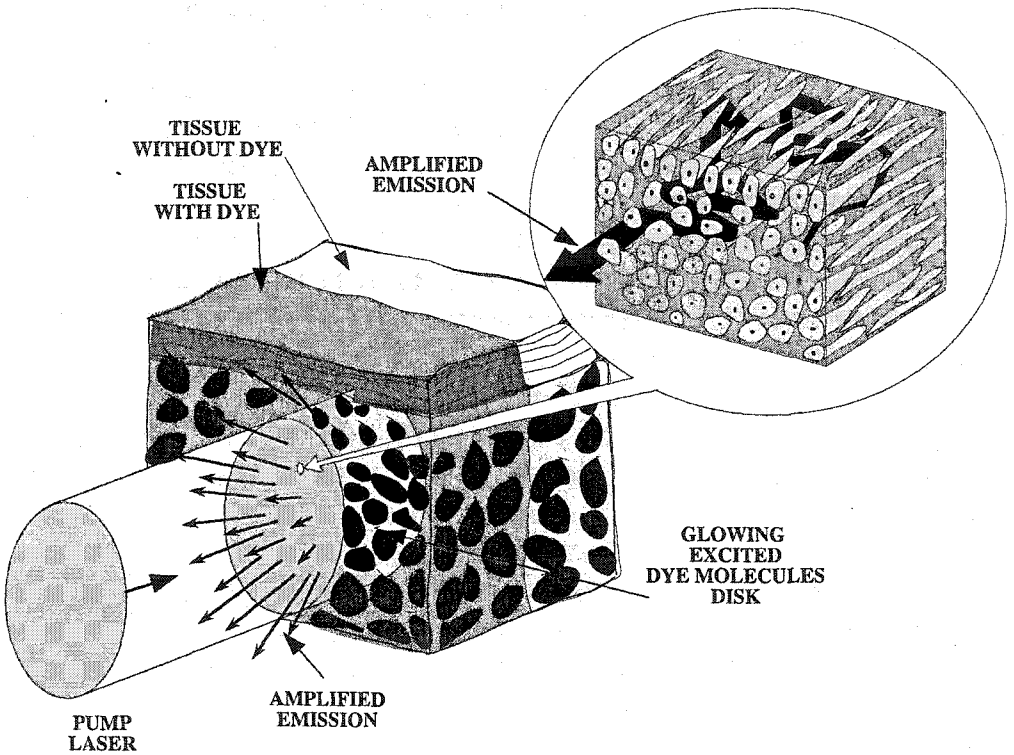


Fig. 4.2, Pictorial model of amplifying paths in a dye-stained tissue

The transport and scattering mean free path lengths, $l_t$, and $l_s$ in tissues such as chicken tissue or fatty tissues is of the order of $l_t$ = 0.5 mm in fats and $l_t$, = 3 mm for tissue making it different from any of the discretely scattering (homogeneously scattering) media mentioned above where $l_t$, and $l_s$ are of the order of 100μ or less. A comparison of the scattering parameters of biomedical tissues of interest is given in table 1. The scattering parameters in bio-medical tissues have been measured at different wavelengths. The scattering parameters of interest here are the fat and chicken tissues measured at 625 nm.

The lasing effect in a biological tissue is expected come from several factors, such as resonance effects within the cells, localization, feedback from longer paths of scattering photons

and microcavity formation due to intercellular scatterings. These basic differences in the tissue structures from discretely scattering structures make it necessary to understand the intensity dependent nonlinear photodynamics of animal tissues so that phototherapy and optical imaging of tissues can be carried out more effectively.

**4.2 Methods**

In the experiment a frequency doubled Nd:YAG laser producing 2 ns pulses and a mode locked Nd:Glass laser producing 10 ps pulses, both at 530 nm wavelength were used for excitation. of lenses into a spectrometer after the exciting radiation had been filtered by two longpass filters which cut off radiation of wavelengths below 540 nm. For temporal profile measurements of the emission, the tissues were excited by a 10 ps pulse

**Table 4.1**

**Approximate tranport mean-free-path lengths**

**and absorption lengths for various tissue types**

| TISSUE TYPE | Transport mean-free-path length $l_t$ *(mm)* | Absorption length $l_a$ *(mm)* |
|---|---|---|
| Chicken breast | 2.5 | 60 ±30 |
| Chicken fat | 0.6 | 155 |
| Pork breast | 1.2 | 70 |
| Pork fat | 0.35 | 300 |
| Benign human breast | 2.6 | 30 |
| Fatty human breast | 0.7 | 155 |
| Intralipid solution (1%) | 0.6 | 195 |
| Whole milk | 1.0 | 250 |

of 530 nm radiation and the time evolution of the emission intensity was recorded by a streak camera system. The experimental layout for temporal measurements is shown in figure 4.3. The spectral measurenet setup is similar where the streak canera is replaced by the spectrometer. The samples investigated were chicken tissues and pig fat, sliced into 1 $cm^3$ pieces.

The samples were treated with a solution of Rhodamine 640 dye in methanol of $10^{-3}$M concentration. The dye solution was uniformly absorbed in the samples as shown in fluorescence slide of a 10μ thin cross-section in figure 4.4. The cross-sectional and transverse sectional pictures are shown in figure 4.5a and figure 4.5b respectively where the cross sectional cellular size is shown to be around 10μ and the transverse length in a muscular structure is of the order of 100μ. The transport mean free path for the chicken tissue and pig fat was measured to be 2.5 mm and 0.35 mm respectively. The extinction length for Rhodamine 640 for a concentration of $10^{-3}$M is 140μ which is much lower than the intrinsic absorption length of the chicken tissue (~60 mm) and pig fat (~300 mm) and the intrinsic transport mean free paths for the two tissues . The samples were placed in open-top cuvettes and were excited by laser pulses on the exposed top. The tissues were sliced to remove the dried surface and to expose the fresh area where dye was still uniformly distributed in the tissue.

**4.3 Results and Discussion**

The spectrum and the temporal profiles of emitted radiation were measured as a function of excitation pulse intensity. At lower input intensity a broad bandwidth fluorescence

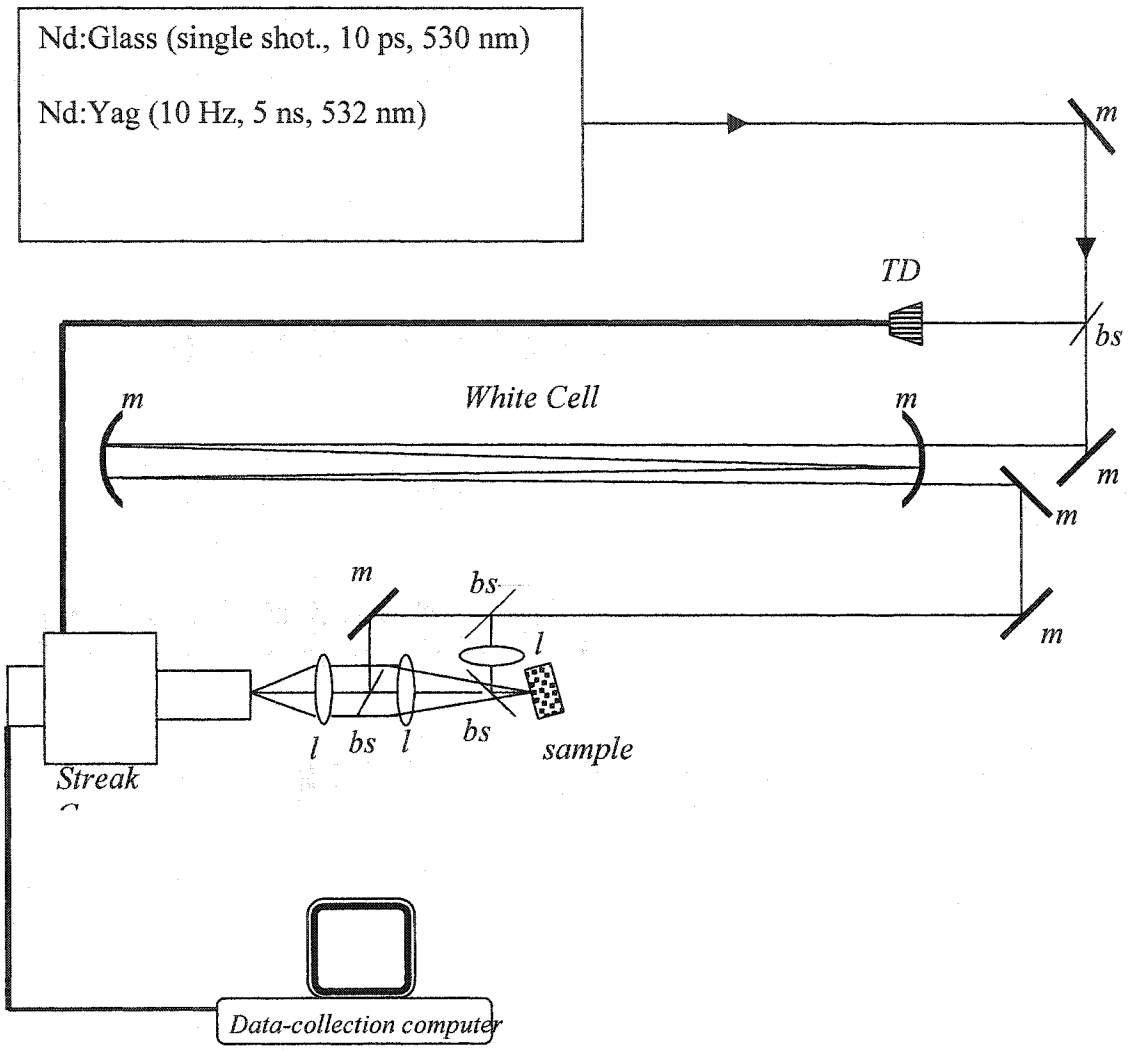


**Figure 4.3** Experimental Layout for temporal and spectral measurement. Nd:Glass laser was used for temporal measurements with a streak camera, and Nd:Yag laser (7 ns pulse) for spectral measurements with a spectrometer.

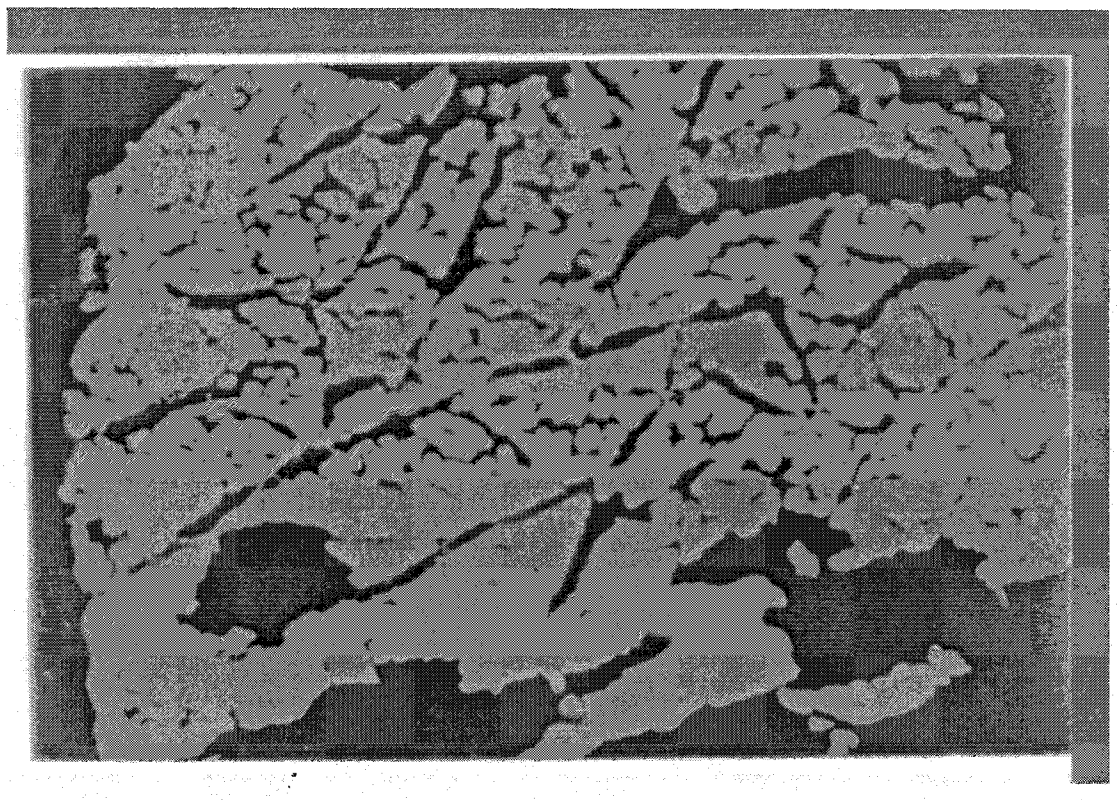

Figure 4.4 Fluorescence image of a 10μ this slice of a chicken tissue treated with a rhodamine640/Methanol solution. The dye is seen to be absorbed uniformly in the tissue

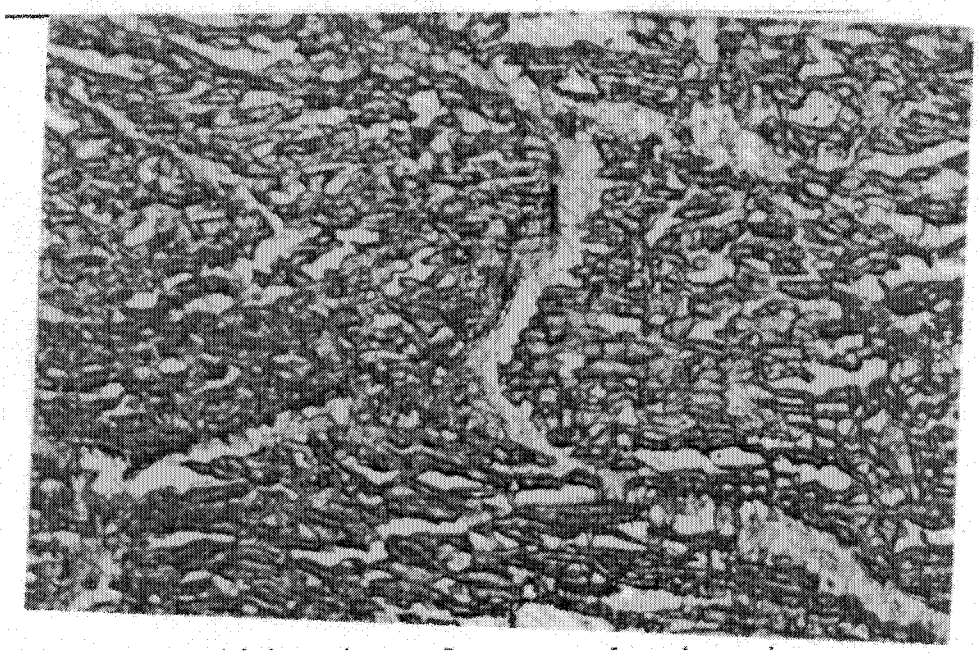

Figure 4.5a Iimage of a 10μ this slice of a chicken tissue sliced along the longitudinally in the direction of muscle fibers.

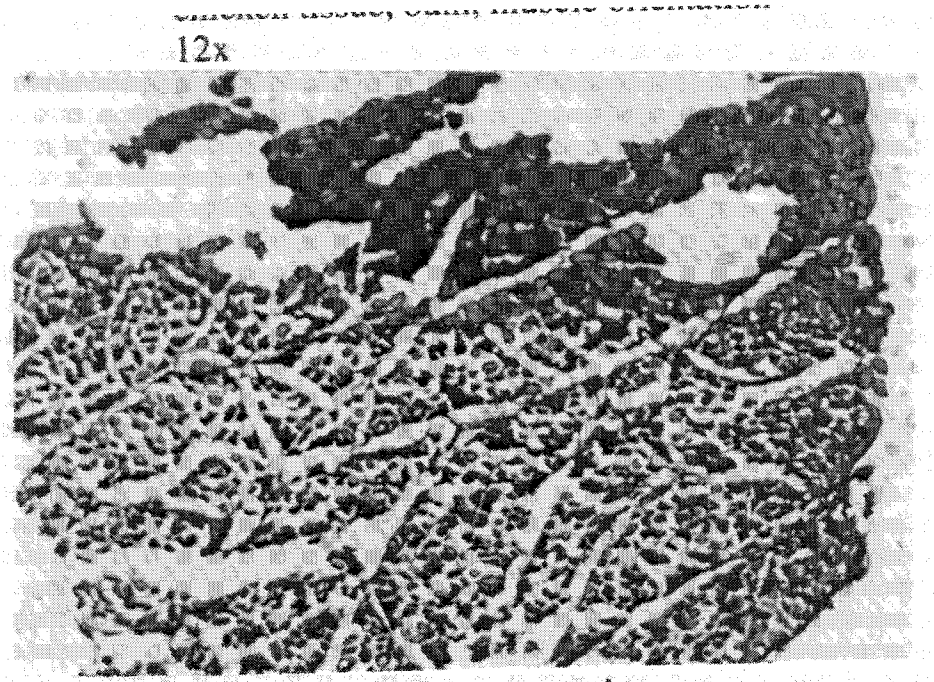


Figure 4.5b Iimage of a 10μ thin slice of a chicken tissue along the cross-section of the muscle fiber.

The beams were focused onto the biomedical sample surface to a spot size of 1 mm diameter to photoexcite the samples. For spectral measurements, the emitted radiation was collected by a series

emission spectrum was observed which narrowed upon increasing the intensity of the incident radiation The narrowing of the spectrum indicated the onset of laser action. On exciting the freshly exposed tissue, a narrowing of the emission spectrum was readily observed when the input intensity was above a threshold value. The results of these measurements are displayed in Figs. 4.6 and 4.7 for chicken and pig fat tissues, respectively. The bandwidth of the fluorescence at low input intensity was measured to be about 30 nm which narrowed to less than 9 nm when the input intensity was increased beyond the threshold energy of 20 mJ/pulse. Typical intensity dependent temporal profiles are plotted in Figures. 4.8 and 4.9. A long decay time, characteristic of spontaneous emission of the dye, of more than 4 ns was observed which shortened to a duration of about 50 ps when the input intensity was increased beyond the laser-action-energy threshold.

The scattering from various structures may trap the radiation to be amplified for many passes, setting up localized microcavities. At low input pulse intesity, the depth of excited region in the tissues is less than the intrinsic transport length, $l_t$ of the tissues. The emission from this excited region does not have enough gain length to amplify therefore output emission has typical temporal and spectral values for flourescence of the dye of 30 nm and 4 ns respectively. When the input pulse intensity is increased and approaches saturation intensity, the excited region increases in due to increase in absorption length in

the dye stained tissue. The increase in the excited region increases the average path length, $l$, of an emitted photon traveling the excited region by

$$l = \frac{1}{3}\sqrt{l_g l_t} \qquad (4.1)$$

where $l_g$ and $l_t$ are the gain length and the transport length respectively. The spontaneous emission from this excited gain medium in the tissues is selectively amplified as the stimulated emission due to increase in the path length and feedback from within the irradiated tissue volume. When the incident intensity is increased the gain length and the gain volume increases which leads to narrower spectral width and shorter temporal duration. More accurate models are needed to simulate the increase in the saturation volume of the tissues. Calculation[14,15] using the power fourier transform methods have been used to acertain typical path lengths in excited tissues to cause resonator-like feedbacks to support lasing modes in the microcavities created in this region.

The possibility of individual cells acting like a resonant cavity at lasing wavelngth can be discounted due the lack of high Q values needed. Individual cells are scattering sources and therefore unlikely to support resonances due to high Q values due to lack of any resonant symmetry. The cells can however trap emitted radiation long enough such the scattering due to the imbedded microstructures within the cell walls such as the mitochondria and nuclei can enhance the amplification processes and the escaping radiation encounters higher gain per pass as it travels through multiple cells as compared with the gain associated with an excited region without any trapping and scattering regions. The multiply scattered light can act as a feedback source to form longer cavity lengths to simulate condition like lasing microcavities. Typical path lengths of upto 100 μ

were seen in normal tissue and pathlengths containing no minimum have been reported in normal and cancerous human colon tissues[15]. Experimental measurements using rat tissues[16] also confirm the results.

The toxicity of Rhodamine dye solutions has not been studied in detail. Other solvents such as ethanol have lesser toxicity than the methanol. The Flourescein dye in PBS have been used to show lasing in colloidal media using latex microspheres as scattering sources. The emission peaks of the lasing radiation can also get affected by host tissues through binding and may not be the same for different tissues.

The tissue lasing process can be used to identify structural changes such as disease tissue or superficial lesion due to sharper spectral peaks and thus brighter emitted radiation from localized regions. This amplified emission results in the narrowing of the spectrum as well as shortening of the temporal profile resulting in a mirrorless laser action. This work may help provide additional insights for the theorists to obtain the mechanisms of optical interaction in discrete as well as continuously disordered actiue heterogeneous scattering media. The observation of stimulated emission of dyes in biomedical tissue can affect optical imaging and phototherapeutic treatment for tumors in humans.

**References**


1. F. Duarte, Dye laser principles (Academic Press, Boston, MA,1990).
2. N.M. Lawandy, R.M. Balachandaran, A.S.L. Gomes and E. Sauvian, Nature 368 (1994) 436.
3. W. Sha, C.H. Liu and R.R. Alfano, Optics Lett. 19 (1994).
4. Masood Siddique, R.R. Alfano, G.A. Gerber, M. Kempe and A.Z. Genack, *Opt. Lett.*, 21, 450 (1996)
5. M. Siddique, Li Yang, Q.Z. Wang and R.R. Alfano, Opt. Soc. Am. Annual Meeting, Dallas, Texas, October 1994;
6. M. Siddique, Q.Z. Wang and R.R. Alfano, Opt. Soc. Am., Annual Meeting, Dallas, TX, October 1994;
7. W. Sha, C.H. Liu and R.R. Alfano, Opt. Soc. Am., AnnualMeeting, Dallas, TX, October 1994.
8. R.V. Ambartsumyan, P.G. Kryukov and V.C. Letokhov, Sov. Phys. JETP 26 ( 1968 ) 835.
9. V.M. Markushev, V.F. Zolin and Ch.M. Briskina, Sov. J. QuantumElectron. 16 (1986) 281;
10. N.E. Ter-Gabrielyan, V.M. Markushev, V.M. Belan, Ch.M. Briskina, O.V. Dimitrova, V.F. Zolin and A.V. Lavrov, Sov. J.Quantum Electron. 21 ( 1991 ) 840, and references therein.

11. Gouedard C., Husson D., Sauteret C., Auzel F and Migus A, *J. Opt. Soc. Am. B* 10 2358, 1993

12. Cao, H., *Waves in random media*, 13, R1, (2003)

13. Pradhan and N. Kumar, Phys. Rev. B 50 ( 1994 ) .

14. )Randal C. Polson and Z. Valy Vardeny, App. Phys. Lett. V85, 1289 (2004)

15. Randal C. Polson G. Levina and Z. Valy Vardeny, App. Phys. Lett. V76, 3858 (2000) Lihong Wang, Da Liu, Nancy He, Steven L. Jacques and Sharon L. Thomsen, Applied Optics, V35,1775 (1996

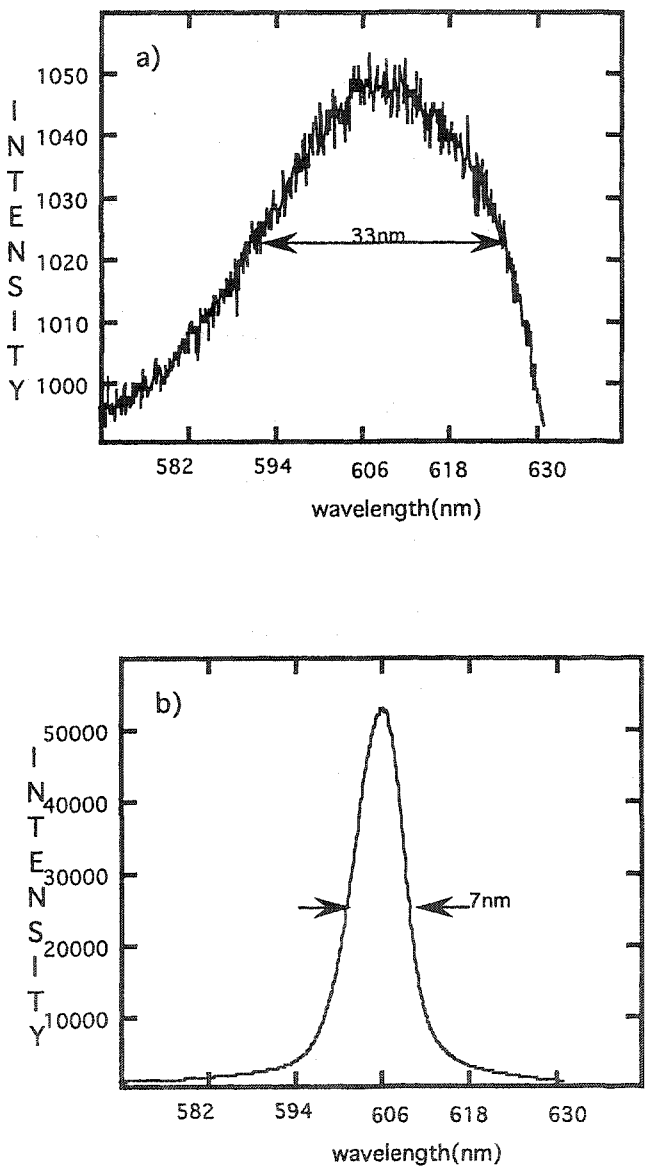


Fig. 4.6. The emission spectra from chicken tissue treated with rhodamine 640 dye ( 10 - 3M concentration ) . ( a) Fluorescence emission of 30 nm bandwidth at an input energy of 0.2 rnJ/pulse. (b) Narrowing of the output emission spectrum to 9 nm due to increased intensity, at 15 mJ/pulse.

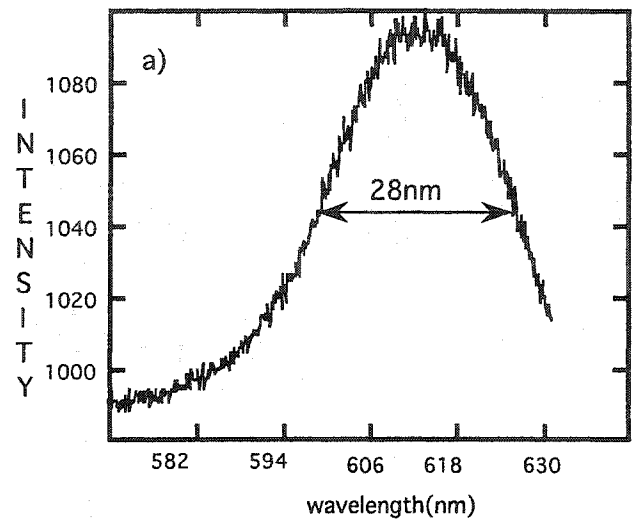


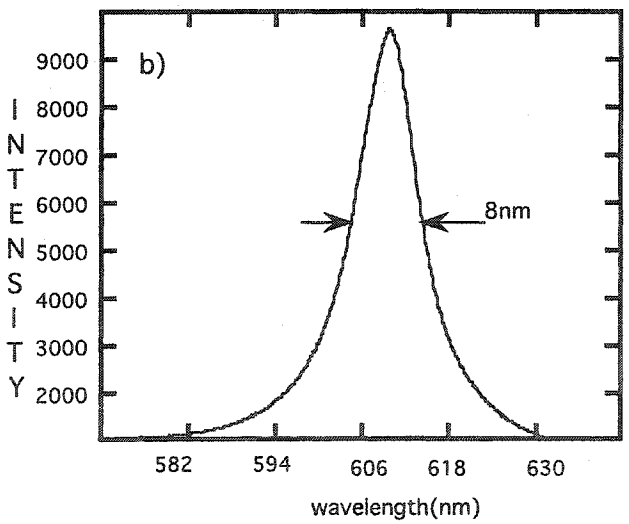


Fig. 4.7.The emission spectrum from pig fat, treated with Rhodamine 640 dye (10-3M) as a function of excitation intensity. (a) Fluorescence emission, of 28 nm, from low input intensity at 0.2 mJ/pulse.(b) Narrowing of the emission spectrum to 8 nm due to increasedexcitation pulse energy at 18 mJ/pulse

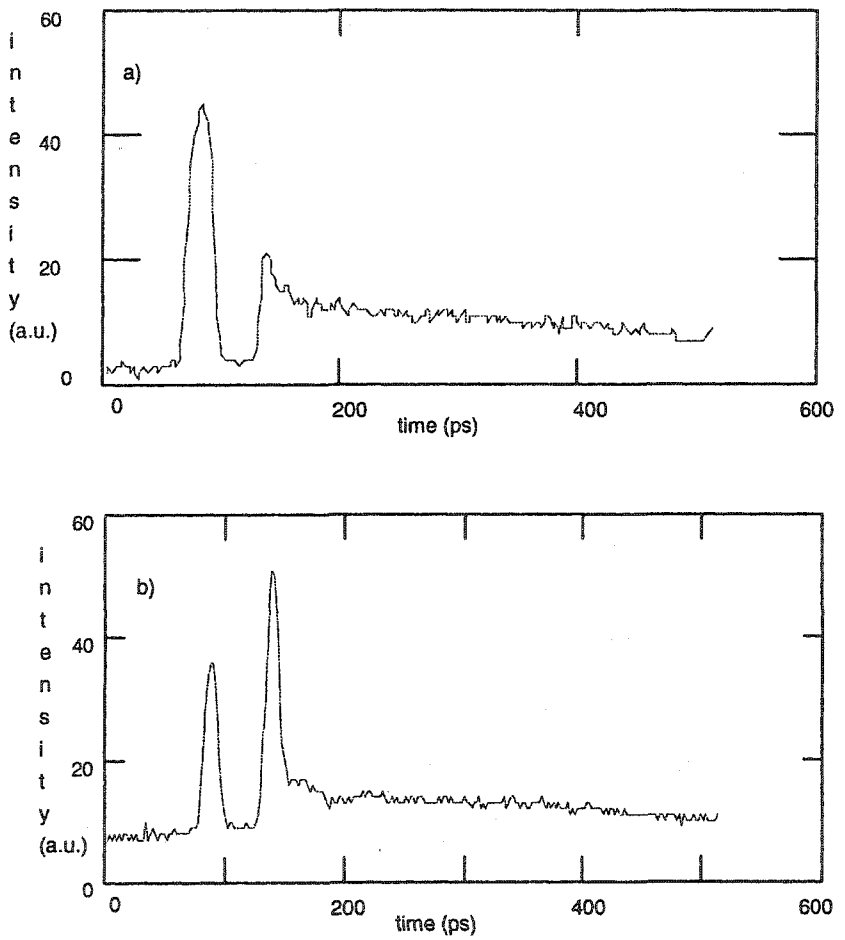


Fig.4.8. Time resolved emission profile of chicken tissue treated with rhodamine 640 ( $10^{-3}$M); the first pulse in both (a) and (b) is the 10 ps pre-pulse from the exciting source. ( a ) Long duration emission (greater than 4 ns) due to spontaneous emission at low intensity excitation (50 μJ ) . ( b ) Pulse shortening ( less than 50 ps ) due to increased input excitation intensity (300 μJ/pulse).

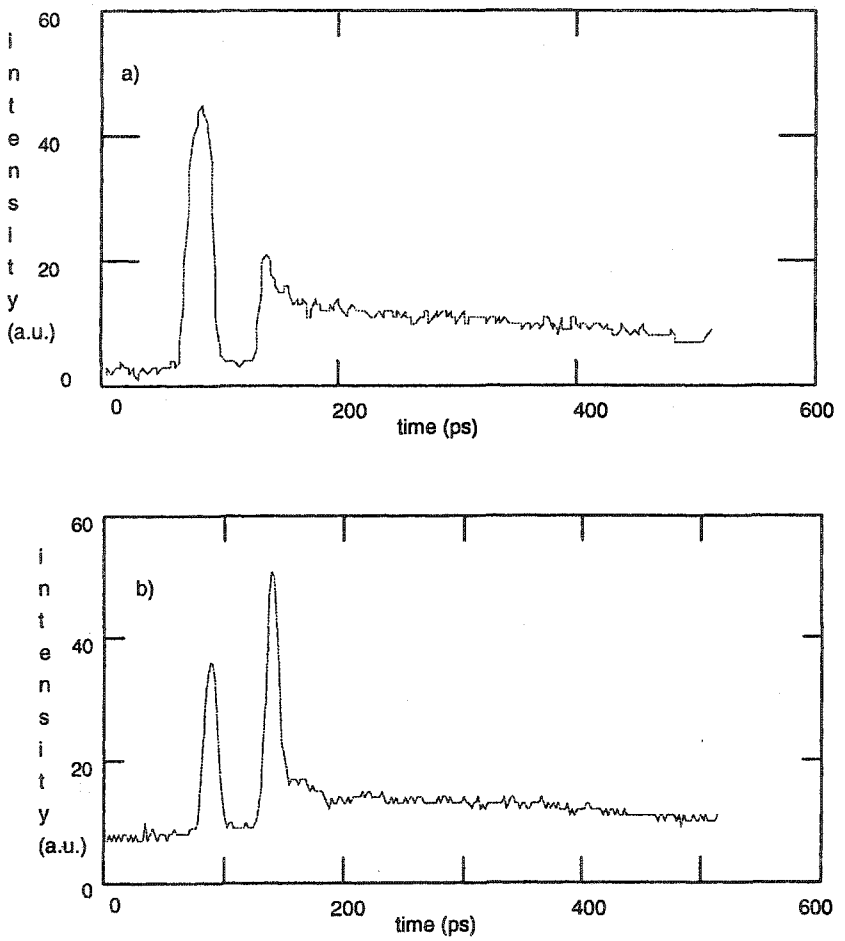


Fig.4.9. Time resolved emission profile of pig fat treated with rhodamine 640 ( $10^{-3}$M); the first pulse in both (a) and (b) is the 10 ps pre-pulse from the exciting source. ( a ) Long duration emission (greater than 4 ns) due to spontaneous emission at low intensity excitation (50 μJ ) . ( b ) Pulse shortening ( less than 50 ps ) due to increased input excitation intensity (400 μJ/pulse).

# CHAPTER 5

# TRANSMISSION OF ULTRAFAST OPTICAL PULSE THROUGH TRANSPARENT HOST MEDIUM CONTAINING ABSORPTIVE AND NON-ABSORPTIVE SCATTERERS

## 5.1 Introduction

Over the past decade, the propagation of ultrafast optical pulses through highly scattering media has drawn considerable attention due to its wide range of diverse applications in the medical, commercial and military fields. Understanding light propagation in a scattering medium remains one of the most challenging problems in optical physics. A better understanding of the fundamental physics behind the propagation of optical pulses in active scattering media is needed to improve imaging and to transmit information through scattering media such as in clouds, fog and tissues[1-4]. A coherent optical pulse traveling through disordered medium undergoes multiple scattering and absorption. The incident optical pulse, characterized by its properties such as intensity, direction, polarization, coherence and temporal width is scattered and absorbed by the surrounding host medium and by the scatterers. The temporal profile of such a pulse is distinguishably altered into two main components: the coherent (ballistic) and the incoherent (diffuse) components[1]. The ballistic component is the portion of the incident pulse that propagates unscattered in the same direction as the incident pulse, traverses the shortest linear path and maintains its directional memory, temporal and spatial coherence. The ballistic component retains most of its initial characteristics of the incident pulse and carries maximum information for use in imaging and communications. The diffuse component consists of the scattered photons that travel over longer paths and

therefore emerge later than the ballistic component. The diffuse light loses most of its initial characteristics such as polarization, directional memory, coherence and temporal duration and acts mainly as the undesirable corrupting noise, which degrades the useful signal in applications such as communications and imaging through cloudy media. The key parameters that characterize the propagation of an optical pulse in a disordered scattering medium are: the scattering length, $l_s$ - the average distance traveled by the photons between two consecutive scattering events; absorption length, $l_a$ - the average distance a photon travels before being absorbed; and the transport mean free path length, $l_t$, - the average distance traveled by a photon before it loses its directional memory.

The scattering of an optical pulse in disordered medium arises mainly from the temporal and spatial variations of the index of refraction in the microscopic and the mesoscopic structures of the medium and increases strongly as the wavelength becomes comparable to the size of scattering elements. The photons in the incident pulse spend different times in transit through the intervening scattering medium, which results in the temporal broadening of the transmitted pulse such that the ballistic portion of incident pulse arrives earlier than the diffuse component. In past research, time-space polarization gating techniques have utilized the fact that the ballistic component arrives earlier[2]. The ballistic photons are thus separated from the diffuse photons by time-space gating techniques and used to reconstruct the image or to transmit information from within or behind the scattering medium. The image of an object illuminated by light can be reconstructed from its shadow in the forward direction or from the backscattered portion of the incident light. When the medium through which the information is being carried contains scatterers, the intensity of the information-carrying component decreases as the

pulse travels farther into the transparent scattering medium. The image is lost when the incident light has traveled far enough into the medium such that most of the temporal and spatial coherence is lost and cannot be distinguished from the haze of the diffuse component so that the signal-to-noise ratio decreases beyond a certain acceptable limit. In our past work[5], a technique was used to recover the image by increasing the absorption of the host medium, which contained non-absorptive scattering particles only. It was shown that an increase in the absorption of the host medium preferentially decreased the intensity of the longer path of diffuse light in comparison to the ballistic light.

In this chapter, a study of the fundamental processes is presented which involves the propagation of an ultrashort optical pulse through a medium containing absorptive and nonabsorptive scatterers in a transparent host medium. The diffuse and ballistic components of the scattered pulse are expected to experience different rates of absorption. The inclusion of absorption in a scattering particle should reduce the probability of absorption for a photon due to the probability of a scattering event. The scattering nature of an ultrashort optical pulse in a scattering medium containing absorptive and non-absorptive scatterers differs from earlier work[5] where the absorption was added to the host medium only such that a scattered photon had the same probability of absorption as the ballistic photons. In an absorptive host medium the ballistic and the diffuse photons experience the same rate of absorption.

The knowledge gained from the current experiments gives further insight and understanding into the fundamental physics behind the propagation of light in scattering media containing a fractional content of absorbent particles to produce new applications. In earlier work[5], the absorption was added to the host medium such that a photon had a

fixed probability of absorption proportional to the time spent in the medium. The present experiment is fundamentally different from the previous one in that the absorption comes from the absorptive scattering particle only after a scattering event where a photon has a probability of scattering without absorption.

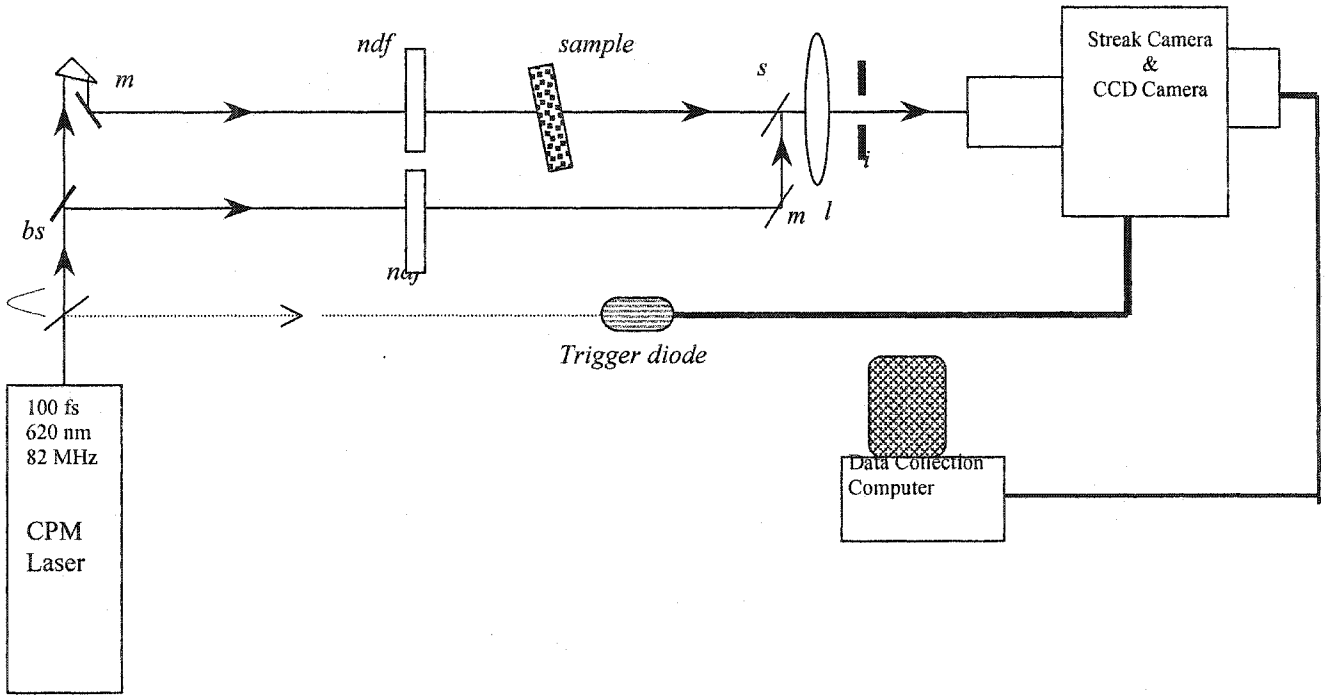


Figure 5.1. Experimental setup.
m: mirror, ndf: neutral density filter, s: glass slide, bs: beam splitter, l: lens, i: iris

## 5.2 Experimental Method and Setup

The temporal profiles of the ballistic and diffuse light were measured by the angle and time resolved technique using a colliding pulse mode-locked (CPM) as a source of ultrafast optical pulses. The experimental layout is shown in figure 5.1. A Hamamatsu synchroscan streak camera with a cooled CCD was used to collect and record the spatial

and temporal profiles. The CPM laser operated at 82 MHz repetition rate giving an output pulse of 100 fs at a wavelength of 620 nm. A lens of 5 cm diameter was placed at the focal length of 10 cm from the entrance slit (10 μm) of the streak camera to collect the optical emission from the exit point of the cuvette holding the sample scattering medium. The angle and time-resolved profile obtained by the streak camera was imaged by the CCD camera and recorded for display on the computer system.

The sample used to model a disordered scattering media was prepared by suspending polystyrene beads of 0.21 μm in diameter in 40 ml of water. The density of total number of scatterers was held constant at $2.06 \times 10^{11}$ $cm^{-3}$. Experimental measurements of the temporal profiles of transmitted light were carried out for different fraction of absorptive versus non-absorptive particles in a transparent host medium to study the effect of absorptive scatterers on the pulse propagation through the disordered scattering media. The number of absorptive particles was varied from 0% to 8% of the total number of scattering particles while keeping the total number of particles constant. The absorption spectrum of the absorptive polystyrene beads was measured to be 100 nm wide with the center at 620 nm, which is the laser wavelength. No measurable fluorescence was observed from the absorptive beads from excitation at 620 nm. A transparent plastic cuvette of 27 mm x 27 mm x 55 mm was used to hold the scattering medium. The linear optical path between the incident and the exit points was 27 mm long.

**5.3 Results**

A series of temporal profiles of the ultrafast optical pulses after traveling through the disordered scattering medium with varying content of absorptive scattering particles

between 0% and 8% in water were measured and displayed in figures 5.2a and 5.2b . Both components of the scattered ultrafast pulse, the ballistic component (early, narrow pulse) and the diffuse component (trailing broad pulse) are evident in these profiles as shown in figure 5.2a. As the absorptive particle density increases, the total energy in the diffuse component decreases at a higher rate than energy of the ballistic component. The same curves are normalized for the ballistic component and shown in figure 5.2b to provide a better visual comparison of the relative change of the diffuse component for the same fractional absorptive particle content as shown in figure 5.2a. The diffuse component is affected, both, in the position of the peak and in the duration and extinction time of the tail portion of the profile.

The energy in each component, ballistic and diffuse, was calculated by integrating the intensity over time for each set of absorptive particle concentration. The normalized extinction rates for the ballistic and diffuse components are shown in figure 5.3. The energy calculated from the measured profiles for the ballistic and the diffuse components is marked by asterisks and crosses respectively for increasing percentage content of absorptive particles. The solid lines are the interpolated values from these points to give a better indication of the rate of extinction for each component. Both the ballistic and the diffuse component decrease in magnitude as the number of absorptive particles is increased. The rates of extinction shown in figure 5.3 indicate that the diffuse pulse loses its energy faster than the ballistic pulse. The diffuse component is seen to decrease by an order of magnitude more than the ballistic pulse and becomes indistinguishable from background noise when about 5% of the total scatterers are replaced by absorptive particles. At a density concentration of 5% of absorptive particles, only the ballistic

component survives after traveling through the scattering medium in a straight optical path. The corrupting noise introduced by the presence of scattering particles is reduced to a great degree by the presence of the absorptive particles, making the recovery of the information carrying ballistic pulse in free space communications much more practical and convenient as it propagates though a virtual noise-free regime.

**5.4 Discussion**

The physical nature of absorption effect in disordered media containing absorptive discrete scattering particles is different from case when the absorption is added to the host medium as shown in this work. The absorption is added to a fraction of the total number of scattering particles, such that a photon has a higher chance of survival even after spending a longer length of time in the medium by not interacting with the absorptive particles.

The temporal distribution of the diffuse photons, $I_z(t)$, arriving at the point opposite to the point of incidence can be predicted by the diffusion theory[6] when $z > 10l_t$ as:

$$I_z(t) = \frac{D}{\pi z^2} \sum_{m=1}^{\infty} m(\pi z / d)^2 \sin(m\pi z / d) \exp(-Dt(m\pi / d)^2) \exp(-vt / l_a) \quad (5.1)$$

where, D is the diffusion constant given by $D = vl_t/3$, $d = z + 2z_0$, $z_0 = 0.71l_t$, $v$ is the speed of the photons in the neat host medium, $z = 2.7$ cm, is the thickness of the sample and $l_a$ is the absorption length.

The intensity of the ballistic component, traversing a distance $z$, is reduced by

$$I_{ballisitc} = f \exp\{-z(1/l_s + 1/l_a)\} \quad (5.2)$$

where $I_{ballistic}$ is the intensity of the ballistic component and $f$ is the fraction of the ballistic light collected depending on the experimental geometry[5]. The scattering length, $l_s$ and absorption length $l_a$, were calculated using the relationships, $l_s=1/n_0\sigma_s$ and $l_a=1/n_a\sigma_a$ respectively, where $\sigma_s$, $\sigma_a$ ,$n_0$ and $n_a$ are the measured scattering cross section, absorption cross section, the total number density of purely scattering particles and the total number density of absorptive particles, respectively. The transport mean free path for this medium was measured to be $l_t$ = 2.5x10$^3$ μ by fitting the experimentally measured temporal profile of the diffuse component shown in figure 5.2a to equation (5.1). The scattering length of the medium was calculated to be $l_s$ =1.94x10$^3$ μ, using the relationship, $l_s = l_t$ (1-$g$), where $g$ is the average cosine calculated using Mie theory. The scattering cross-section and the transport cross-section of the nonabsorptive particles was measured to be, $\sigma_s$ = 2.5 x 10$^{-3}$ μ$^2$ and transport cross-section, $\sigma_t$ = 1.8x10$^{-3}$ μ$^2$ respectively. The absorption cross-section, $\sigma_a$, of the absorptive particles was measured to be $\sigma_a$ = 7.5 x10$^{-3}$ μ$^2$.

The measured value of $\sigma_a$ from the extinction rate of ballistic pulse does not fit the measured temporal profiles of the diffuse component using equation 5.1, as illustrated by the dashed curve in figure 5.4 calculated for 5% content density of absorptive scatterers as marked. The diffuse component experiences a reduced absorption cross section as compared with the absorption cross-section for the ballistic component contrary to prediction by diffusion theory using equation 5.1. Figure 5.4 shows calculated fit of the same temporal profiles shown in figure 5.2b, using a reduced absorption cross-section for the diffuse component as shown by the solid lines passing through each measured

profiles. The effective absorption cross-section given by $\sigma_{eff} = 0.45\sigma_a$, had to be used to obtain the best fit for the diffuse component profile to fit in equation 5.1. The $\sigma_{eff}$ used fits the diffuse curves exactly as shown by the dashed lines passing through the measured profiles in figure 5.4. This results differs markedly from our previous work[5] where absorption is added to the host medium only, the absorption cross-section derived from equation 5.2 fits both the ballistic and the diffuse components of the transmitted pulse as shown in figure 5.5. The graphs in solid lines are the measured temporal profiles of the transmitted pulse through a scattering medium where the absorption was added to the host medium. The dashed lines are the calculated profiles of the diffuse pulse using equation 5.1 where the absorption coefficient was the same for the ballistic and diffuse components of the transmitted pulse. In the present case of a transparent non-absorptive host medium containing absorptive and non-absorptive scattering particles the absorption coefficient calculated using the Mie sphere calculations[7] did not fit the measured $\sigma_a$.

The justification for the, $\sigma_{eff} = 0.45\sigma_a$ , for diffuse component is that the ballistic component is scattered only in the forward direction on a ballistic path and is attenuated by both the scattering and absorption whereas the diffuse component is scattered at wide range of angles. The photons scattered in the forward direction, as in the case of ballistic photons, interact with absorptive particles in direct proportion to the fractional density content of absorptive particles and thus experience the same net absorption cross-section as the fractional density of the absorptive particles, whereas the scattered photons have a probability of remaining unabsorbed. A pictorial depiction of the possible trajectories of photons traversing the scattering medium is given in figure 5.6. There is a fraction of the total number of paths available to a scattered photon where the photon can reach the exit

point without interacting with an absorptive particle. The scattered photons can thus experience less net absorption as compared with the photons in the ballistic path[10].

To get a better estimate for the reduction of absorption for the diffuse component, consider a medium containing *p* fraction of absorptive and (1-*p*) fraction non-absorptive scatterers, the intensity of ballistic component is given by:

$$I_{ballisitc} = I_0 \exp[-(\mu_s + p\mu_a)L] \qquad (5.3)$$

where $\mu_s$ *and* $\mu_a$ are the scattering and absorption coefficients of a medium containing only non-absorptive and absorptive scatterers respectively only. The albedo of an absorptive particle is given by: $w = \mu_s/(\mu_s + \mu_a)$ and the probability, *P*, of absorption of a scattered photon in a medium containing *p* fraction of absorptive scattering particles is:

$$P(pw) = \sum_{b=0}^{n} C_n^b (wp)^b (1-p)^{n-b} = (1-p+wp)^n = \varpi^n \qquad (5.4)$$

where $C_n^b$ is number of arrangements for having *b* number of absorptive balls in *n* number of scattering particles, $\varpi = \mu_s/(\mu_s + \mu_{a,effective})$ is the effective albedo of the medium and $\mu_{a,effective}$ is the effective absorption coefficient of the scattering medium containing absorptive and non-absorptive scattering particles. The effective absorption coefficient $\mu_{a,effective}$ of the medium for the diffuse component can be calculated using the probability distribution given above as:

$$\varpi = \frac{\mu_s}{\mu_s + \mu_{a,effective}} = 1 - p + p\frac{\mu_s}{\mu_s + \mu_a}. \qquad (5.5)$$

The $\mu_{a,effective}$ is given by $\mu_{a,effective} = \frac{p\mu_a}{1+(1-p)(\mu_a/\mu_s)} < p\mu_a$. Using the 5% density content of absorptive particles used in the experiments, $\mu_{a,effective} = 0.25\ \mu_a$ giving a good first order fit to the measured profiles.

A controversy exists about the form of the diffusion coefficient D in media in coexistence with scattering and absorption. In traditional derivations of the diffusion equation, the diffusion coefficient is obtained[11] as,

$$D = \frac{1}{3(\mu_s' + \mu_a)} \tag{5.6}$$

where $\mu_s'$ is the reduced scattering coefficient. Furutsu[8] and Cai[9] suggested another derivation that leads to

$$D = \frac{1}{3(\mu_s')} \tag{5.7}$$

which is independent of absorption. In this formulation, where D is independent of absorption and the absorption coefficient is added to the intensity by an exponential in the RTE. The photon distribution function at position $\vec{r}$, in the direction s at time t is written as:

$$I(\vec{r},\hat{s},t) = I(\vec{r},\hat{s},t)\exp(-c\mu_a t) \tag{5.8}$$

The measurements presented in this chapter did not fit the temporal profiles using equations 5.1 or 5.6 by using the absorption coefficient measured by the ballistic component and absorption cross section had to be modified to fit the profiles as shown in figure 5.4

The effective absorption coefficient for the scattered photons is less than the absorption coefficient experienced by the photons in the ballistic component traveling in

the forward direction only. A photon interacting with an absorbing and scattering particle has a probability of on the order of $\sigma_s/(\sigma_s+\sigma_a)$ of being absorbed. In the present case, the extinction rate of diffuse light arriving at the exit point after spending extended time in the scattering medium is a measure of the extinction experienced by the light scattered at angles. The absorption cross-section $\sigma_a$ is reduced by $\sim\sigma_s/(\sigma_s+\sigma_a)$ approximately, where the term $(\sigma_s+\sigma_a)$ is the total extinction cross section of the absorptive particle. An effective absorption cross-section of $\sigma_{eff} = 0.45\sigma_a$ was used to fit the measured temporal profiles as shown by the solid lines in figure 5.3 whereas the measured $\sigma_a$ was used to fit ballistic component. The adjustment factor $\sigma_s/(\sigma_s+\sigma_a) \approx 0.25$ is not an exact relationship but a first order estimate. The presence of absorption effects the scattering properties of a scattering particle. Relative change in the scattering parameters for a scattering particle with and without absorption is given in Table 5.1 .

The reasonably good fit was obtained using an adjusted parameter for effective absorption cross section, using $\sigma_{eff} = 0.45\sigma_a$, indicates the need to make improvement in the diffusion theory presently used to predict the temporal behavior of diffuse light for scattering medium where $z/l_t > 10$, when a fraction of the scattering particles out of the total number of scattering particles are absorptive and sheds further light on the

Table 5.1

Relative scattering parameters for a scattering particle (dia = 0.21μ, $n_{particle} = 1.59$) with and without absorption using Mie theory

| RELATIVE COMPLEX INDEX OF REFRACTION $n_{particle}/n_{host}$ | g | $\sigma_{ext}$ ($10^{-3}$ $\mu^2$) | $\sigma_s$ ($10^{-3}$ $\mu^2$) | $\sigma_{abs} = \sigma_{ext} - g\sigma_s$ ($10^{-3}$ $\mu^2$) | $\frac{\sigma_s}{\sigma_{abs} + \sigma_s}$ |
|---|---|---|---|---|---|
| Non-absorptive 1.18+i0 | 0.38 | 2.8 | 2.8 | 0 | 1 |
| Absortive particle 1.18+i0.0064 | 0.364 | 2.8 | 2.8 | 0.92 | 2.7 |

independence of absorption on the diffusion constant D[8,9]. The diffusion theory accounts for absorption by adding absorption component only in the exponential in equation 5.1.

The ballistic component of an ultrashort optical pulse, traveling through a highly scattering medium was shown to be preferentially enhanced over the diffuse component when part of the scattering particles in a transparent host medium were replaced by absorptive scattering particles of the same size. The ballistic component was seen to traverse the medium while the diffuse component was preferentially eliminated. The parameters used to predict the temporal behavior of the transmitted optical pulse by using the diffusion theory were adjusted to match this special case; indicating the need to develop better theoretical model for the propagation of optical pulses in absorptive disordered media containing discrete absorptive scattering particles in transparent host. The diffusion model equation needs to be revaluated for the case of an ultrafast optical pulse propagating through a scattering medium consisting of absorptive scattering

particles in a transparent host, as opposed to the way it is currently formulated where absorption is assumed to be uniform.

## 5.4 Conclusion

The implementation of the knowledge gained from this chapter can be of importance in the improvement in free space optical (wireless) communications and certain imaging applications with scattering. An example of practical application can be in optical communications through clouds or traffic handling in foggy environment. The scattering in these cases comes mainly from water droplets. By selecting a wavelength in the absorption spectrum of water from 1.2μ to 1.5μ, with appropriate absorption cross-section, the ballistic pulse penetrates through scattering media such as clouds or fog while the diffuse light gathering in its wake will be preferentially eliminated.

References


1. K. M. Yoo and R. R. Alfano, Opt. Lett. 15, 320 (1990)
2. L. Wang, P.P. Ho, C. Liu, G. Zhang and R. R. Alfano, Science, 253, 769 (1991)
3. D.J.Pine, D.A. Weitz, P.M. Chaikin and E. Herbolzheimer, Phys. Rev. Lett, 60, 1134 (1988)
4. D.A. Weitz, D.J.Pine, P.N. Pusey and R. J. A. Tough, Phys. Rev. Lett, 63, 1747 (1989)
5. K. M. Yoo, Feng Liu and R. R. Alfano, Optics Letters, 16, 1068, (1991).
6. Melvin Lax, Reviews of Modern Physics, 23, 287, (1951).
7. Van Der Hulst, '*Light scattering by small particles*', Dover, (1981)
8. Koichi Furutsu, Yokio Yamada, Phys. Rev. E, Vol. 50, 3634, (1994)
9. Wei Cai, M. Xu, Melvin Lax and R. R. Alfano, Optics Letters, 27, 731, (2002)
10. Private communications with M. Xu;
11. A. Ishimaru, "*Wave propagation and scattering in random media*", (Academic, New York, 1978), vol. 1

Figure 5.2a

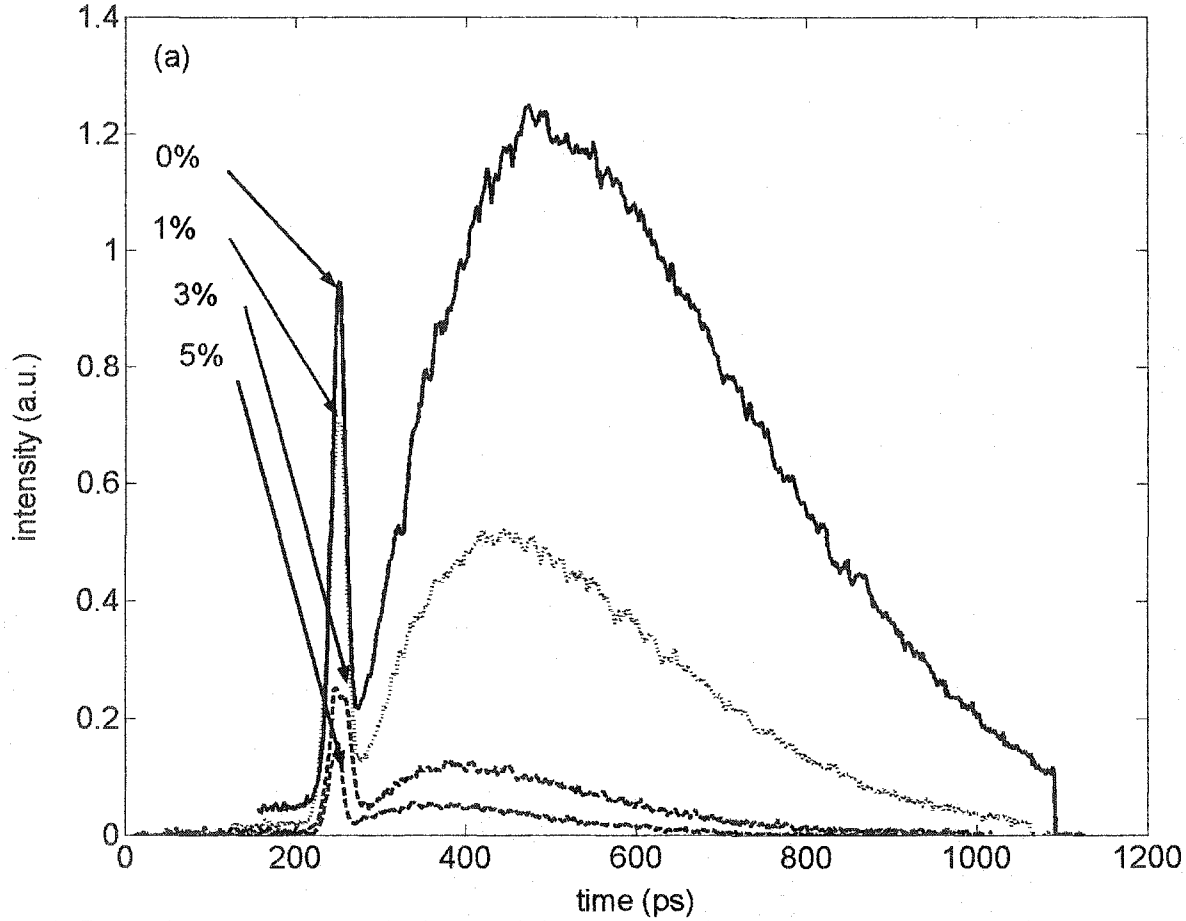


Figure 5.2a.Temporal profiles of transmitted pulse through disordered scattering medium containing discrete absorbent particles. The peak of the coherent ballistic component is marked by the corresponding percentage of absorbent scattering particles in the medium. Solid line: 0%: dotted line: 1%, dash-dot line: 3%, dashed line: 5% absorbent particles of total number of scattering particles in the disordered medium;

Figure 5.2b

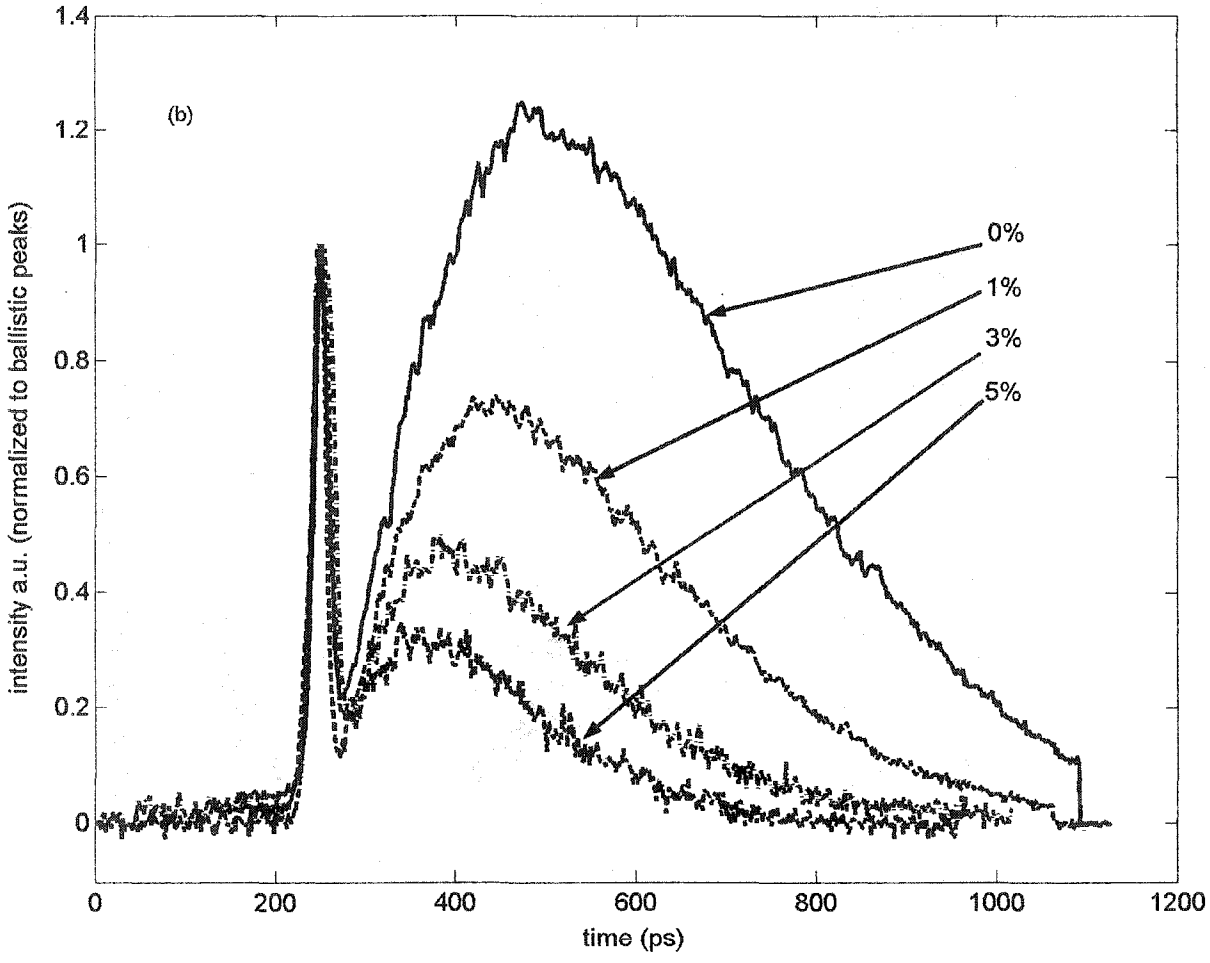


Figure 5.2b.Temporal profiles of transmitted pulse through disordered scattering medium containing discrete absorbent particles. Temporal profile normalized for the peaks of the ballistic component. The diffuse component of the transmitted pulses is marked according to the corresponding percentage of absorbent scattering particles in scattering medium.

Figure 5.3

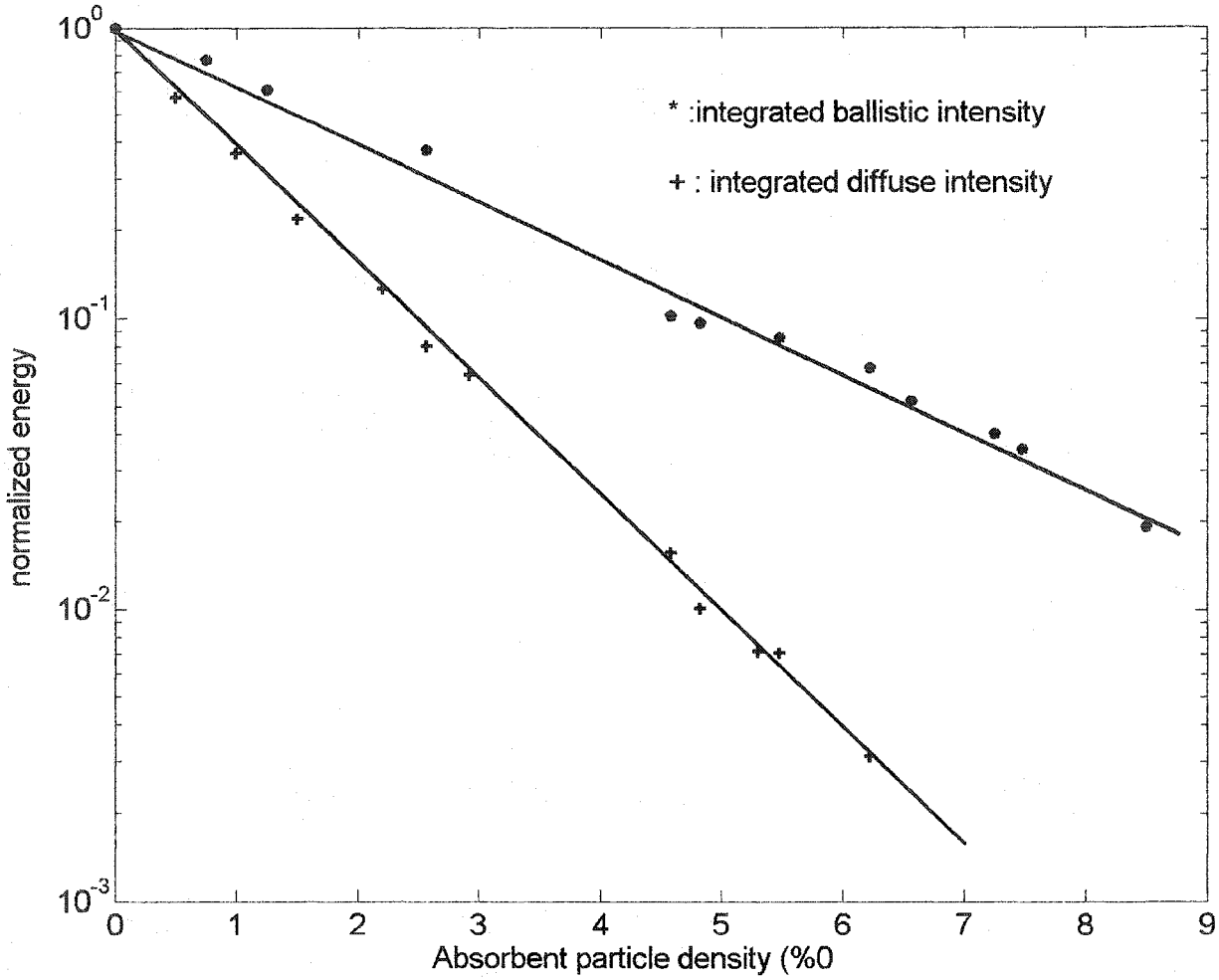


Figure 5.3 Relative rates of extinction of the ballistic and diffuse component energy as a function of percentage content of absorbent particles. The diffuse component energy goes below the noise level of $10^{-2}$ at around 4% concentration; the ballistic component travels practically unscattered thereafter

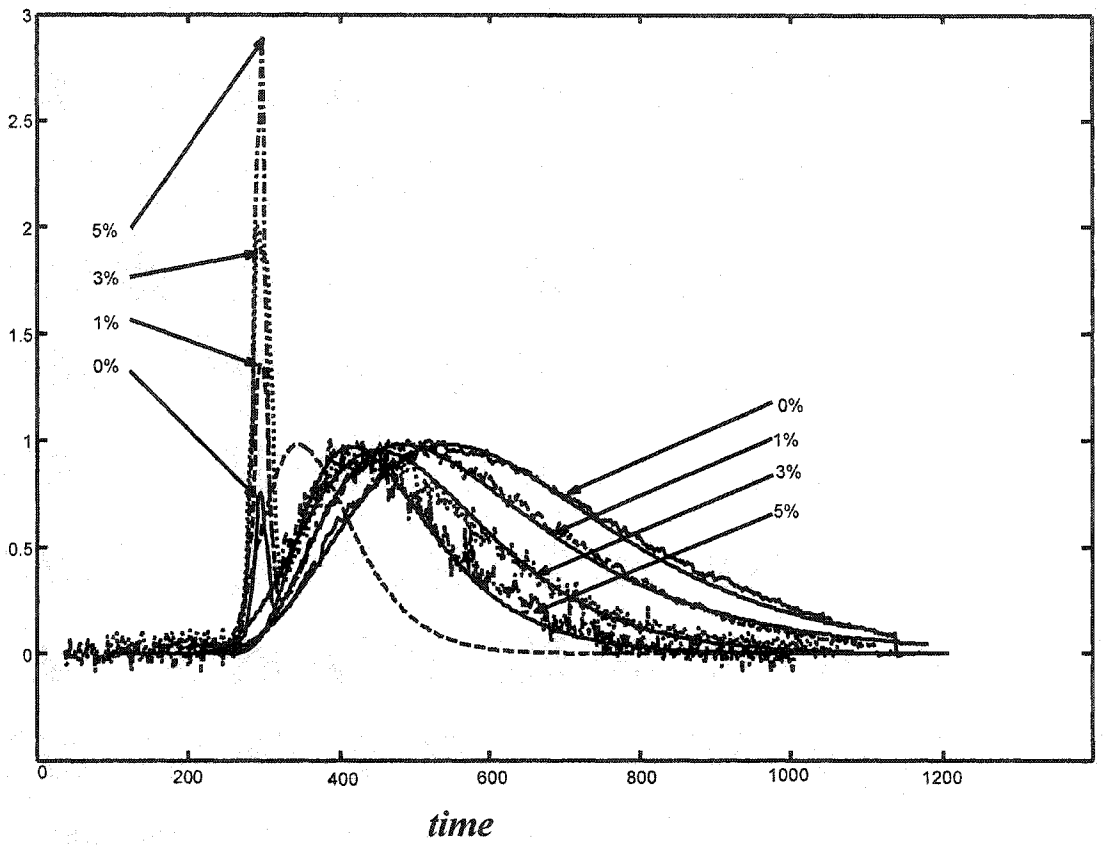


Figure 5.4 Temporal profiles of transmitted pulse from figure1a, normalized for diffuse component. The percent content of absorptive particles in the medium is indicated for each diffuse component. The dashed lines through the curves are the calculated using $\sigma_{eff}$ for diffuse profiles using equation 1. The non-fitting dashed line is the calculated diffuse profile for 5% absorptive particle, marked by an arrow content using $\sigma_a$ using equation 2 for comparison (over estimating the effect of absorption).

Figure 5.5

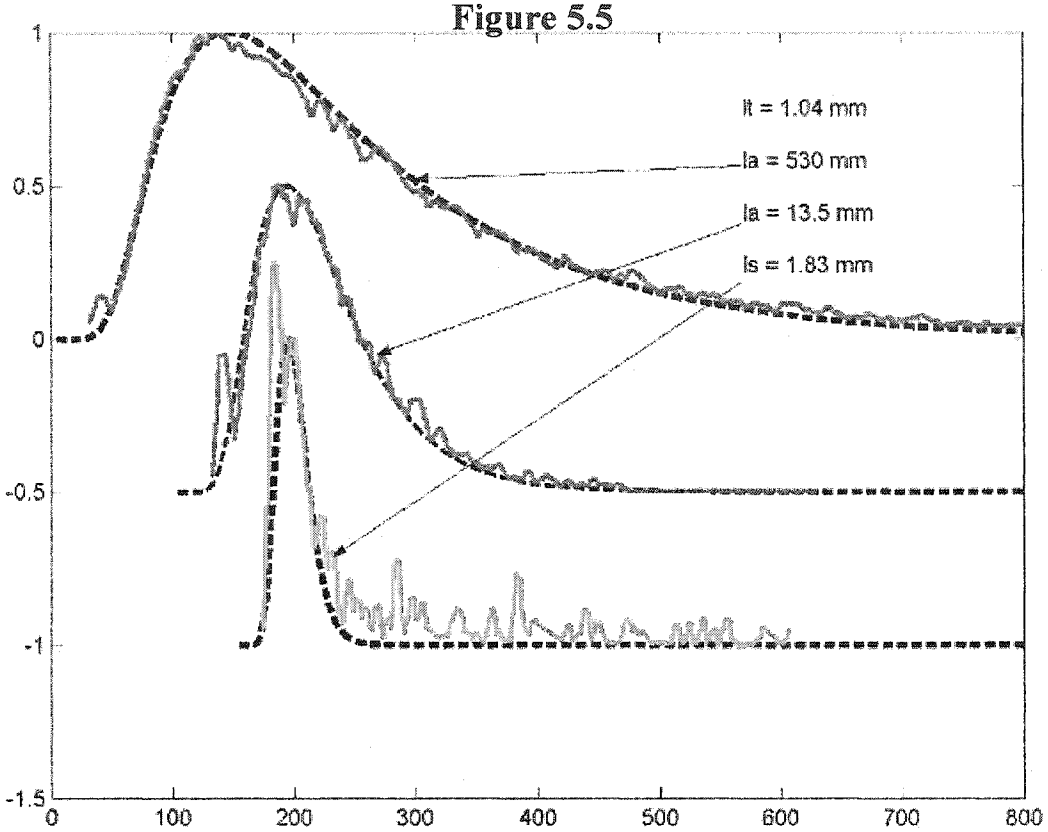


Figure 5.5 Fitting equation 5.1 to the experimentally measured transmission profiles from reference5. The absorption coefficient was kept the same as measured for the ballistic component.

**Figure 5.6**

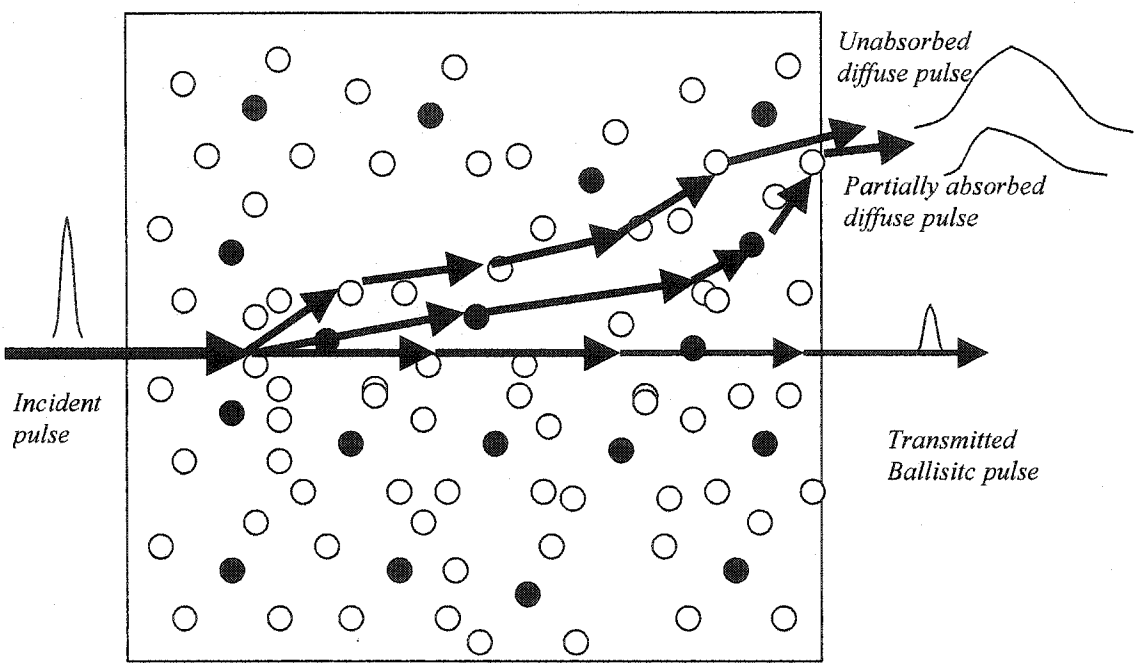


Figure 5.6 Possible photon trajectories experiencing different absorption rate in a scattering medium containing absorptive and non-absorptive scattering particles in a transparent non-absorbing host

# CHAPTER 6

# SUMMARY AND FUTURE RESEARCH DIRECTION

The physics behind the propagation of light in active scattering materials is still not well understood. The temporal and spectral dynamics of an ultrafast optical pulse propagating in materials where either the host material or the scattering particles have absorption or optical again have not been specified according to well-defined physical laws. More research is needed to better understand the processes involved in how light is transported in optically active scattering media. The two main processes studied in this thesis involve:

*i)* the absportion of incident light by the scattering media and reemission in form of intense short bursts of laser-like radiation,

*ii)* the transmission of ultrafast optical pulse in absortive scattering medium.

The lasing action in scattering media was investigated in disordered media consisting of scattering partices in various host medium with optical gain. The scattering media investigated were discretely scattering homogeneous media and continuously scattering heterogeneous bio-medical media. the intensity and pulse width of the emission radiation were shown to be dependent on the scatterer densiy and the absorption and gain length of the optically active portion of the medium.

The temporal dynamics of the transmitted ultrashort pulse through a scattering medium where some of the discrete scattering particles had absorption in a transparent host medium were investigated. The diffuse component of the transmitted pulse was found to follow a different absorption coefficient than the ballistic component.

The experimental investigations into the nature and effects of ultrafast optical interaction in active disordered media presented in this thesis explored the physics of the processes that govern evolution of the temporal and spectral dynamics of the emitted ultrafast optical pulses. These investigations lead to further questions and the need to explore other aspects of the phenomena arising from the optical interactions in optically active materials.

In the following sections, future directions for further work are discussed.

## 6.1 Random lasers

Further investigations into the evolution of laser-like radiation from scattering media with gain is needed to establish the nature of emission and the physical processes that give rise to the lasing action. The experiments would investigate the following:

### 6.1.1 Measurement of Time Delay between excitation and emission

The time of emission can be measured using a reference pulse. The delay of emitted pulse characterizes the nature of the processes involved in the evolution of short intense laser-like radiation from the long-lived spontaneous emission.

The time delay for the lasing process depends on optical gain of the material and the length of the excited medium the spontaneously emitted photon will travel. The length of the excited medium depends on the absorption length of the active medium at the excitation wavelength. The path length, $z$, an emitted photon travels in the excited medium depends on the scattering particle density, given by

$$z = \frac{L^2}{2l_t} \qquad (6.1)$$

where L is the depth of the excited medium.

For the case of stimulated emission resulting from cooperative interaction between excited atom such as superradiance emission, the time delay will depend on the density of excited atoms in the system as given in equation 3.31 as,

$$t_0 \equiv \tau_N \ln(N\mu) \qquad (6.2)$$

### 6.1.2 Time-Resolved Coherence and Angular Distribution of Emitted Emission

The temporal and spatial coherence of the emitted laser-like from excited scattering media depends on the process that leads to the emission of the observed intense and ultrashort pulse. The coherence depends on the the nature of feedback that gives rise to stimulated emission. There are three processes that have been invstigated in this theis:

a) Diffusion induced gain with incoherent feedback proposed by Letokhov[1], as mentioned in section 3.5. In case of incoherent feedback, the cohernce would be minimal and should vanish as more scatterers are added to the medium.

b) Coherent feedback forming micorcavites, as proposed by Lawandy[2], Cao[3] and Vadeny[3] in sections 3.4.3, 3.4.5 and 4.3 respectively and the reflective walls models[4], should lead to temorally cohernt emission at spatially localized areas.

c) Superradiant/Superfluorescence emission process where the emission should be highly coherent

## 6.2 Absorptive particles

The effect of absorption due to discrete absorptive particle on the diffuse component of a scattered ultrashort pulse needs to be investigated further to address the validity of diffusion equation. The spatial and temporal profile of the transmitted radiation, after passing through a scattering medium consisting of absorptive and non-absorptive scatterers in a tranparent host, needs to be measured by imaging the exit

surface on the input slit of the streak camera. The image of the transmitted radiation gives simultaneous profiles of the dissuse components as the function of distqnce from the center where the ballistic pulse exits form the sample. The size and the density of the scattering particles needs to be varied over the three regimes where the diameter of the particles is greater than, same as and much smaller than the incident wavelength.

## Reference

1. R.V. Ambartsumyan, P.G. Kryukov and V.C. Letokhov,

Sov. Phys. JETP 26 ( 1968 ) 835

2. N.M. Lawandy, R.M. Balachandaran, A.S.L. Gomes and E. Sauvian,

Nature 368 (1994) 436.

3. Soukoulis C. M, Jiang X., Xu J Y and Cao H *Phys, Rev.* B 65 R041103, 2002

4. Randal C. Polson G. Levina and Z. Valy Vardeny, App. Phys. Lett. V76, 3858 (2000)

5. Masood Siddique, Q.Z.Wang, R. R. Alfano, *J. Biomedical Opt.* 1, 442, 1996

# APPENDIX A

# CALCULATION OF SCATTERING PARAMETERS USING MIE THEORY

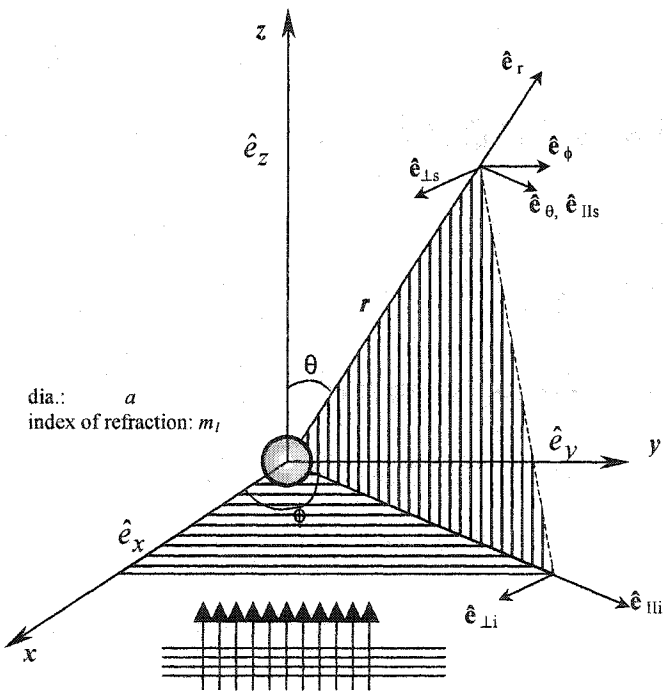


**Figure A.1**, Pictorial model of a plane wave scattering of a spherical scattering particle of diameter a and index of refraction $m_1$.The scattered light is described in terms of the plane and perpendicular polarization.

## A.1 Mie theory

G. Mie obtained the exact solution of the scattering of a plane electromagnetic wave by an isotropic, homogeneous sphere. [Ann. Phys. 25, 377-445, (1908)]. In this section a brief account of the Mie theory is presented sufficient to make numerical

calculations of key parameters to characterize light scattering of a particle. The computer program to calculate the scattering, absorption and transport cross-section is given in Appendix B.

A sphere of radius $a$ and relative dielectric constant $\varepsilon = \varepsilon_r\varepsilon_0$, where $\varepsilon_0$ is the and $\varepsilon_r$ is the relative dielectric constant scatters an incident plane wave propagating in z direction and polarized in x direction is given by,

$$\mathbf{E}_{incident} = e^{ikz}\hat{\mathrm{x}} \qquad \text{(A.1)}$$

Where $E_{incident}$ is the incident electromagnetic field and $k$ is the wave vector as shown in Fig. A.1. The Mie theory derives exact mathematical expressions for the scattered external and internal fields. The incident plane wave can be written in spherical coordinates as two scalar functions $\Pi_1$ and $\Pi_2$ as the radial and components of the electromagnetic hertz vectors as,

$$\Pi_{electric} = \Pi_1\mathbf{r} \quad \text{and} \quad \Pi_{magnetic} = \Pi_2\mathbf{r}. \qquad \text{(A.2)}$$

The $\Pi_1$ and $\Pi_2$ satisfy the scalar wave equation:

for the field outside the sphere and

$$\left(\nabla^2 + k^2\right)\Pi = 0 \qquad \text{(A.3)}$$

$$\left(\nabla^2 + k^2m^2\right)\Pi = 0 \qquad \text{(A.4)}$$

for the field inside the sphere.

The electric and the magnetic fields are given by,

$$\mathrm{E} = \nabla\times\nabla\times\left(r\Pi_1\hat{\mathrm{r}}\right)+i\omega\mu_o\nabla\times\left(r\Pi_2\hat{\mathrm{r}}\right)$$
$$\mathrm{H} = -i\omega\varepsilon\nabla\times\left(r\Pi_1\hat{\mathrm{r}}\right)+\nabla\times\nabla\times\left(r\Pi_2\hat{\mathrm{r}}\right) \qquad \text{(A.5)}$$

where the dielectric constant give by $\varepsilon = \varepsilon_0$ for medium outside the sphere and $\varepsilon = \varepsilon_r\varepsilon_0$ inside the sphere.

The incident field (1) can be derived from the two scalar functions $\Pi_{1i}$ and $\Pi_{2i}$ in terms of spherical harmonics form as,

$$r\Pi_{1i} = \frac{1}{k^2}\sum_{n=1}^{\infty}\frac{i^{n-1}(2n+1)}{n(n+1)}\psi_n(kr)P_n^1(\cos\theta)\cos\phi \qquad \text{(A.6)}$$

$$r\Pi_{2i} = \frac{1}{\eta k^2}\sum_{n=1}^{\infty}\frac{i^{n-1}(2n+1)}{n(n+1)}\psi_n(kr)P_n^1(\cos\theta)\sin\phi \qquad \text{(A.7)}$$

Where $\psi_n(\rho)$ is the Ricatti-Bessel function given by , $\psi_n(\rho) = \rho\sqrt{\frac{\pi}{2\rho}}J_{n+1/2}(\rho)$, $\mathrm{J_n}$ is the Bessel function of the first kind and $\eta = (\mu_0/\varepsilon_0)^{1/2}$.

The general expressions for the scattered fields outside the sphere ($r > a$) can be written as

$$r\Pi_{1scatter} = \frac{(-1)}{k^2}\sum_{n=1}^{\infty}\frac{i^{n-1}(2n+1)}{n(n+1)}a_n\zeta_n(kr)P_n^1(\cos\theta)\cos\phi \qquad \text{(A.8)}$$

$$r\Pi_{2scatter} = \frac{(-1)}{\eta k^2}\sum_{n=1}^{\infty}\frac{i^{n-1}(2n+1)}{n(n+1)}b_n\zeta_n(kr)P_n^1(\cos\theta)\sin\phi \qquad \text{(A.9)}$$

where $a_n$ and $b_n$ are two arbitrary constants and $\xi_n$ is the Ricatti-Bessell,

$\xi_n(\rho) = \rho\sqrt{\frac{\pi}{2\rho}}Y_{n+1/2}(\rho)$ given $\mathrm{Y_n}$ is the Bessel function of the third kind.

The arbitrary constants $a_n$ and $b_n$ can be calculated by applying the boundary conditions where $E_\theta$, $E_\phi$, $H_\theta$ and $H_\phi$ are continuous across the boundary at $r = a$;

$$a_n = \frac{m\psi_n(mx)\psi_n'(x) - \psi_n(x)\psi_n'(mx)}{m\psi_n(mx)\xi_n'(x) - \xi_n(x)\psi_n'(mx)} \tag{A.10}$$

and

$$b_n = \frac{\psi_n(mx)\psi_n'(x) - m\psi_n(x)\psi_n'(mx)}{\psi_n(mx)\xi_n'(x) - m\xi_n(x)\psi_n'(mx)} \tag{A.11}$$

where $x = ka$ and $m = \frac{m_1}{m_0}$, $m_1$ and $m_0$ are the indices of refraction of the medium inside the particle and the medium outside respectively.

## A.2 Scattering amplitude function

The amplitude and the phase of a scattered wave can be described the complex amplitude function $S(\theta,\phi)$ as,

$$E = S(\theta,\varphi)\frac{e^{-ikz+iwt}}{ikr}E_i \tag{A.12}$$

where the incident wave is given by $E_i = e^{-ikz+iwt}$ and $r$ is the radial distance from the particle as shown in figure A.1. From equation A.12 the intensity of the scattered field, $I_s$, can directly be defined n terms of the scattering amplitude function $S(\theta,\varphi)$ and the incident intensity $I_i = E_I E_I^*$, as ,

$$I_s = \frac{s^2(\theta,\varphi)}{k^2r^2}I_i \tag{A.13}$$

For an unpolarized incident wave, the scattering in any direction can be described by four amplitude functions $S_1$, $S_2$, $S_4$ and $S_4$ in form of a scattering matrix $S(\theta,\varphi)$ of four elements for the incident parallel polarization $E_{II}^{i}$ and perpendicular polarization $E_{\perp}^{i}$ as;

$$\begin{bmatrix} E_{II} \\ E_{\perp} \end{bmatrix} = \begin{pmatrix} S_2 & S_3 \\ S_4 & S_1 \end{pmatrix} \bullet \frac{e^{-ikr+ikz}}{ikr} \begin{bmatrix} E_{\Pi}^{i} \\ E_{\perp}^{i} \end{bmatrix} \tag{A.14}$$

For a spherical particle, $S_3 = S_4 = 0$, and $S_1(\theta)$ and $S_2(\theta)$ are functions of $\theta$ only. Only two realtions are required to describe the scattered light as;

$$E_{\perp} = S_1(\theta)\frac{e^{-ikr+ikz}}{ikr} E_{\perp}^{i} \tag{A.15}$$

and

$$E_{\Pi} = S_2(\theta)\frac{e^{-ikr+ikz}}{ikr} E_{\Pi}^{i} \tag{A.16}$$

The intensity of the scattered wave for parallel and perpendicular polarization is given by taking the squares of the moduli of from equation A.14 as

$i_1 = |S_1(\theta)|^2$ and $i_2 = |S_2(\theta)|^2$ where $i_1$ and $i_2$ are the scattering functions for the perpendicular and the parallel polarized scattered waves.

The values of $S_1(\theta)$and $S_2(\theta)$ can be calculated in terms of the constants $a_n$ and $b_n$ from the Mie theory in equations A.10 and A.11 as

$$\begin{aligned} S_1 &= \sum_n \frac{2n+1}{n(n+1)}(a_n\pi_n + b_n\tau_n) \\ S_2 &= \sum_n \frac{2n+1}{n(n+1)}(a_n\tau_n + b_n\pi_n) \end{aligned} \tag{A.17}$$

The amplitude scattering patterns for particles of three sizes for x= 1, x=1 and x=1 are displayed in figure A.1

The polarization ratio, P, is called the polarizability.

$$P = \frac{i_1 - i_2}{i_1 + i_2} \qquad \text{(A.18)}$$

When an incident plane wave scatters off a scattering particle, a part of the incident power is scattered out and the remaining part is absorbed by the particle. The characteristics of the scattering particle which determine these two phenomena, scattering and absorption, can be conveniently described in terms of the appropriate cross-sections, $\sigma_s$, the scattering cross-section and $\sigma_a$, the absorption cross-section, of the particle. The cross-section values of a scattering particle is determined by the wavelength $\lambda$ of the incident field, the radius $a$ of the particle and the indices of refraction of the host medium, $m_0$ and the scattering medium $m_1$. The incident wave is scatters off the scattering particle whose realtive dielectric constant is given by $\varepsilon = \varepsilon_r \varepsilon_0$ where $\varepsilon_r$ is complex in general.

## A.3 Forward Scattering Theorem and the Extinction cross-section $\sigma_{ext}$

The forward scattering theorem, also known as the optical theorem is related to the behavior of the scattering particle in the forward direction. The forward scattering theorem relates the total power loss from the incident wave due to scattering and absorption by the particle. The forward scattering theorem states that the total cross section is related to the imaginary part of the scattering amplitude in the forward direction $f(\hat{i}, \hat{i}')$ as;

$$\sigma_{ext} = \sigma_s + \sigma_a \qquad \text{(A.19)}$$

the $\sigma_{ext}$ is given in terms of constants $a_n$ and $b_n$ from Mie theory as

$$\sigma_{ext} = \frac{2\pi}{k^2} \sum_{n=1}^{\infty} (2n+1) \mathrm{Re}(a_n + b_n) \qquad \text{(A.20)}$$

### A.4 Scattering Cross-section $\sigma_s$

The scattered field behaves as a spherical wave. The scattered power flux at at a distance R from the particle in the direction $\hat{o}$ as shown in figure X is defined in terms of the differential cross section as

$$\sigma_d(\hat{o},\hat{i}) = \lim_{R\to\infty}\left[\left(R^2 S_s\right)/S_i\right] = \left|f(\hat{o},\hat{i})\right|^2 = (\sigma_t/4\pi)p(\hat{o},\hat{i}) \qquad \text{(A.21)}$$

Where $\sigma_d$ is the differential cross-section, $\sigma_t$ is the total cross-section and $f(\hat{i},\hat{i}')$ is the amplitude scattering function. The differential cross-section and the amplitude scattering function represent the the cross-section of a particle which would produce the observed power $S_s$ in the direction o. The scattering cross section $\sigma_s$ represents the total scattered power at all angles surrounding the particle and is given by

$$\sigma_s = \int_{4\pi}\sigma_d d\omega = \int_{4\pi}\left|f(\hat{o},\hat{i})\right|^2 d\omega = \frac{\sigma_t}{4\pi}\int_{4\pi}p(\hat{o},\hat{i})d\omega. \qquad \text{(A.22)}$$

The scattering cross-section of a particle can be calculated from the Mie theory by

$$\sigma_s = \frac{2\pi}{k^2}\sum_{n=1}^{\infty}(2n+1)\left(|a_n|^2 + |b_n|^2\right) \qquad \text{(A.23)}$$

where the constants $a_n$ and $b_n$ are as given by equations A.10 and A.11.

### A.5 Absorption Cross-section $\sigma_a$

the absorption cross-section $\sigma_a$ of a dielectric particle is given by the volume integral of loss inside the scattering particle.

$$\sigma_a = \left( \int_V \frac{1}{2} \omega \varepsilon_0 \varepsilon'' |E|^2 dV \right) \Big/ S_i \qquad \text{(A.24)}$$

where $\varepsilon''$ is the imaginary part of the dielectric constant. The absorption cross-section is calculatedin terms of the Mie theory constants $a_n$ and $b_n$ given by Mie theory as;

$$\sigma_a = \sigma_{ext} - \sigma_s \qquad \text{(A.25)}$$

where $\sigma_{ext}$ is the extinction cross section of the particle.

## A.6 Anisotropy factor, *g*, and Momentum Transfer Cross-Section $\sigma_{tr}$

An incident wave of irradiance $I_i$ interacting with scattering particle with an absorption cross-section of $\sigma_a$, will transfer momentum to the particle proportion to $I_i\sigma_a$. and eleastically scatter energy proportional to $I_i\sigma_s$. The net rate of momentum transferred in the direction of propagation of the incident beam will be proportion to $I_i\sigma_s\left(1-\langle\cos\theta\rangle\right)$. Thus the total rate of momentum transfer will be proportion to $I_i\left(\sigma_{ext}-\sigma_s\langle\cos\theta\rangle\right)$, therefore the momentum transfer cross-section for the particle is defined as;

$$\sigma_{tr} = \sigma_{ext} - \sigma_s\langle\cos\theta\rangle \qquad \text{(A.26)}$$

The factor $\sigma_s\langle\cos\theta\rangle$ can be calculated from Mie theory as;

$$\sigma_s\langle\cos\theta\rangle = \frac{2\pi}{k^2}\left[\sum_{n=1}^{\infty}\frac{n(n+2)}{n(n+1)}\mathrm{Re}\left(a_n a_{n+1}^* + b_n b_{n+1}^*\right) + \sum_{n=1}^{\infty}\frac{(2n+1)}{n(n+1)}\mathrm{Re}\left(a_n b_n^*\right)\right] \qquad \text{(A.27)}$$

The average cosine, $\langle\cos\theta\rangle$, of the amplitude scattering function is a measure of the directional scattering amplitude of incident light at a given wavelength. It is defined as

$$g = \langle \cos\theta \rangle = \int_{4\pi} p \cos\theta d\Omega \qquad \text{(A.28)}$$

where ***g*** is the anisotropy factor and ***p*** is the phase factor. The ***g*** vanishes for a particle scattering light isotropically, is positive for forwardly scattering and negative for incident wave scattered mainly is backward direction. The anisotropy factor is independent of polarization of the incident wave. The value of g can be calculated from the Mie theory from equation a.23 and equation A.27 given above as;

$$g = \sigma_s \langle \cos\theta \rangle / \sigma_s \qquad \text{(A.29)}$$

# Appendix B

This program calculates scattering parameters for a single spherical particle using Mie theory. The parameters calculated are:

$\sigma_s$: the scattering cross section

$\sigma_{ex}$: the extinction cross section

$\sigma_a$: the absorption cross section

g: average cosine

S11: The scattering amplitude function as a function of angle, for perpendicular polarization

S22: The scattering amplitude function as a function of angle, for parallel polarization

This program was written for Matlab V5.2

```
%*****************************************************************
tic
clear theta costheta ang g P P2 Pe mm jj phinmx dphinmx dphinx
clear wl Cscat a1 a2 a b1 b2 b Cs Ce Q Qe Qe1 phinx x r k m mx ll wl S1
S2 S G g1 g2 k1 k2 Ga Sa S11 S12 S33 S34
clear dsynmx dsynx synmx synx tao
clear no nfact1 nfact2 fact1 fact2 qcos sigmas sigmatr

Ce = 0;
%wl = input('input wavelength in microns -> ')
%dia = input('input diameter of the particle (microns) -> ')
%m0 = input('host medium index of refraction -> ')
%m1 = input('scattering medium index of refraction -> ')
wl = 0.62; %1.2;
m0 = 1.33;
m1 = 1.59
k = 2*pi*m0/wl;
   r = 1.2; %1.2; %0.152; %dia/2;
x = (2*pi*r*m0)/wl; % wl(g);
%k = x/0.26;
%m = m1/m0;
m = 1.1806; %-.5i;  %-1.5i; %1.33+1e-8i; %1.19;

mx = m*x;
```

```
area = pi*r^2
ll = sqrt(pi/(2*x));
llm = sqrt(pi/(2*mx));
NSTOP =  round(x+4*x^(1/3)+2)
fprintf('NSTOP value, pausing ... press return to proceed \n')
pause
theta11 = pi/1000:pi/1000:2*pi;
theta = theta11(1:end-1);
[l jj ] = size(theta);
%jj =ltheta-1;
d = theta(2) - theta(1);
costheta = cos(theta(1:jj));
ang = theta*180/pi;
sintheta = sin(theta);


S1 = zeros(1,jj);
S2 = zeros(1,jj);

for n = 1:NSTOP
     phinmx = (mx)*llm*besselj(n+.5,mx);
phinx = x*ll*besselj(n+.5,x);
dphinmx = mx*llm*besselj(n-1+.5,mx)-(n/mx)*phinmx;
dphinx = x*ll*besselj(n-1+.5,x)-(n/x)*phinx;
synx = x*ll*besselh(n+.5,x);
synmx = mx*llm*besselh(n+.5,mx);
dsynx = x*ll*besselh(n-1+.5,x)-(n/x)*synx;
dsynmx = (mx)*llm*besselh(n-1+.5,mx)-(n/mx)*synmx;


a1(n) = m*phinmx*dphinx-phinx*dphinmx;
a2(n) = m*phinmx*dsynx-synx*dphinmx;
a(n) = a1(n)/a2(n);

b1(n) = phinmx*dphinx-m*phinx*dphinmx;
b2(n) = phinmx*dsynx-m*synx*dphinmx;
b(n) = b1(n)/b2(n);
Cextn(n)=(2*n+1)*real((a(n))+ (b(n)));
Cscan(n)=(2*n+1)*(abs(a(n))^2+ abs(b(n))^2);
P = legendre(n,costheta);
    %P2 = legendre(n+1,costheta);
    Pe(n,:) = -P(2,:)./sintheta;
```

```
    tao(n,1:jj-1) = -(P(2,2:end)-P(2,1:end-1))./d;
    %tao(n+1,1:89) = -(P2(n+1,2:end)-P2(n+1,1:end-1))./d;
    tao(n,jj)= tao(n,jj-1);
    %tao(n+1,90)= tao(n+1,89);
    %k = k+1;
    %S(n) = ((2*n+1)/(n*(n+1))).*((a(n).*Pe(n,:)).+(b(n).*tao(n,:)));
    Sa(n) = ((2*n+1)/(n*(n+1)));
    k1(n,1:jj) = (a(n)*Pe(n,:));
    k2(n,1:jj) = b(n)*tao(n,:);
    S(n,1:jj) = ((k1(n,:)+k2(n,:))*Sa(n));
    Ga = (2*n+1)/(n*(n+1));
    g1(n,1:jj) = b(n)*Pe(n,:);
    g2(n,1:jj) = a(n)*tao(n,:);
    G(n,1:jj) = ((g1(n,:)+g2(n,:))*Ga);

    %S(k) =
((2*k+1)/(k*(k+1))).*((a(k,:).*Pe(k,:)).+(b(k,:).*tao(k,:));
 if n == 100, fprintf('100 down \n'), end
 if n == 50, fprintf('100 down \n'), end
end
 %Cext = (2*pi/k^2)*sum(Cextn);
 %Csca = (2*pi/k^2)*sum(Cscan)
 for mm = 2:jj

    S1(mm) = sum(S(:,mm));
    S1(1) = S1(2);
    S1(1000) = S1(999);
    S2(mm) = sum(G(:,mm));
     S2(1) = S2(2);
    S2(1000) = S2(999);
%    S1(numz) = S1(numz-1);
 %   S2(numz) = S2(numz-1);
end
%************************************************************
% Radiation Pressure
%************************************************************

for scatnum = 1: NSTOP-1
   no = scatnum;
   nfact1 = (no*(no+2))/(no+1);
   nfact2 = (no*2+1)/(no*(no+1));
```

```
    fact1(no) = nfact1*real( a(no)*conj(a(no+1))+ b(no)*conj(b(no+1)));
    fact2(no) = nfact2*real(a(no)*conj(b(no)));
    nfact(no) = 2*n+1;
    nscat(no) = nfact(no)*(abs(a(no))^2+abs(b(no))^2);
    nextinct(no)   = real(a(no)+b(no));


end
%n0 = 1:NSTOP;
%sigma = sum( (2.*n0+1).*(abs(a).^2 +abs(b).^2))
%sigmas = (2*pi/k^2)*sigma

%qcos = (4/x^2)*(sum(fact1)+sum(fact2))
%sigmas = area*(2*pi/k^2)*(sum(nscat))
%sigmas = (2/x^2)*(sum(nscat))
%sigmas = (2*pi/k^2)*(sum(nscat));
%sigmatr = (2/x^2)*sum(nfact.*nextinct);
%***********end of crossections ******************************

    S11(1:jj) = .5*((abs(S2.^2))+(abs(S1.^2)));
    S12(1:jj) = .5*((abs(S2.^2))-(abs(S1.^2)));
    S33(1:jj) = .5*(conj(S2).*S1 + (conj(S1).*S2));
    S34(1:jj) = .5i*(conj(S2).*S1 - (conj(S1).*S2));

    n0 = 1:NSTOP;
    n01 = 1:NSTOP-1;
    %acb = a(n01).*conj(a(n01+1))+b(n01).*conj(b(n01+1));
    % ******** Scattering cross section ************
    nn0 = 2*n0+1;
    absfact = abs(a).^2 + abs(b).^2;
    sigmas = (2*pi/k^2)*sum(nn0.*absfact)
    % ********* Extinction Cross section ********
    sigmaex = (2*pi/k^2)*sum(nn0.*real(a+b))

    %calculating  *****   Qscatter<cos> ******
    %real(a(n) x conjugate (a(n+1)) + b(n) x conjugate(b(n+1))) ::
part1 of Qscatter
    acb = real(a(n01).*conj(a(n01+1))+b(n01).*conj(b(n01+1)));
    % part II of Qscatter<cos> :: real(a(n) x b(n))
    ab = real(a(n01).*conj(b(n01)));
    nn1 = n01.*(n01+2)./(n01+1);  %n(n+2)/n+1
    nn2 = (2.*n01+1)./(n01.*(n01+1)); %2n+1/n(n+1)
```

```
    f1 = nn1.*acb;
    f2 = nn2.*ab;
    Qcos = (4/x^2).*(sum(f1)+sum(f2));


    Qsigmas = sigmas/area;
    g = Qcos/Qsigmas
    sigmatr = sigmas*(1-g)

toc
```

# APPENDIX C

# CALCULATION OF AVERAGE COSINE, *g*, AS A FUNCTION OF PARTICLE DIAMETER

```
%***********************************************

tic
clear gindex
for nnn = 1:100

clear theta costheta ang g P P2 Pe mm jj phinmx dphinmx dphinx
clear wl Cscat a1 a2 a b1 b2 b Cs Ce Q Qe Qe1 phinx x r k m mx ll wl S1 S2 S G g1 g2
k1 k2 Ga Sa S11 S12 S33 S34
clear dsynmx dsynx synmx synx tao
clear no nfact1 nfact2 fact1 fact2 qcos sigmas sigmatr

Ce = 0;
%wl = input('input wavelength in microns -> ')
%dia = input('input diameter of the particle (microns) -> ')
%m0 = input('host medium index of refraction -> ')
%m1 = input('scattering medium index of refraction -> ')

wl = .250 +nnn*.01; %1.2;
m0 = 1.33;
m1 = 1.59;
k = 2*pi*m0/wl;
  r = 1; %1.2; %0.152; %dia/2;
x = (2*pi*r*m0)/wl; % wl(g);

%k = x/0.26;
%m = m1/m0;
m = 1.1806; %-.5i;  %-1.5i; %1.33+1e-8i; %1.19;

mx = m*x;
area = pi*r^2;
```

```
ll = sqrt(pi/(2*x));
llm = sqrt(pi/(2*mx));
NSTOP =  round(x+4*x^(1/3)+2)
nnn
%fprintf('NSTOP value, pausing ... press return to proceed \n')
%pause
theta11 = pi/1000:pi/1000:2*pi;
theta = theta11(1:end-1);
[l jj ] = size(theta);
%jj =ltheta-1;
d = theta(2) - theta(1);
costheta = cos(theta(1:jj));
ang = theta*180/pi;
sintheta = sin(theta);


S1 = zeros(1,jj);
S2 = zeros(1,jj);

for n = 1:NSTOP
    phinmx = (mx)*llm*besselj(n+.5,mx);
phinx = x*ll*besselj(n+.5,x);
dphinmx = mx*llm*besselj(n-1+.5,mx)-(n/mx)*phinmx;
dphinx = x*ll*besselj(n-1+.5,x)-(n/x)*phinx;
synx = x*ll*besselh(n+.5,x);
synmx = mx*llm*besselh(n+.5,mx);
dsynx = x*ll*besselh(n-1+.5,x)-(n/x)*synx;
dsynmx = (mx)*llm*besselh(n-1+.5,mx)-(n/mx)*synmx;


a1(n) = m*phinmx*dphinx-phinx*dphinmx;
a2(n) = m*phinmx*dsynx-synx*dphinmx;
a(n) = a1(n)/a2(n);

b1(n) = phinmx*dphinx-m*phinx*dphinmx;
b2(n) = phinmx*dsynx-m*synx*dphinmx;
b(n) = b1(n)/b2(n);
Cextn(n)=(2*n+1)*real((a(n))+ (b(n)));
Cscan(n)=(2*n+1)*(abs(a(n))^2+ abs(b(n))^2);
P = legendre(n,costheta);
```

```
   %P2 = legendre(n+1,costheta);
   Pe(n,:) = -P(2,:)./sintheta;
   tao(n,1:jj-1) = -(P(2,2:end)-P(2,1:end-1))./d;
   %tao(n+1,1:89) = -(P2(n+1,2:end)-P2(n+1,1:end-1))./d;
   tao(n,jj)= tao(n,jj-1);
   %tao(n+1,90)= tao(n+1,89);
   %k = k+1;
   %S(n) = ((2*n+1)/(n*(n+1))).*((a(n).*Pe(n,:)).+(b(n).*tao(n,:)));
   Sa(n) = ((2*n+1)/(n*(n+1)));
   k1(n,1:jj) = (a(n)*Pe(n,:));
   k2(n,1:jj) = b(n)*tao(n,:);
   S(n,1:jj) = ((k1(n,:)+k2(n,:))*Sa(n));
   Ga = (2*n+1)/(n*(n+1));
   g1(n,1:jj) = b(n)*Pe(n,:);
   g2(n,1:jj) = a(n)*tao(n,:);
   G(n,1:jj) = ((g1(n,:)+g2(n,:))*Ga);

   %S(k) = ((2*k+1)/(k*(k+1))).*((a(k,:).*Pe(k,:)).+(b(k,:).*tao(k,:));
 if n == 100, fprintf('100 down \n'), end
 if n == 50, fprintf('100 down \n'), end
end
 %Cext = (2*pi/k^2)*sum(Cextn);
 %Csca = (2*pi/k^2)*sum(Cscan)
 for mm = 2:jj

   S1(mm) = sum(S(:,mm));
   S1(1) = S1(2);
   S1(1000) = S1(999);
   S2(mm) = sum(G(:,mm));
    S2(1) = S2(2);
   S2(1000) = S2(999);
%    S1(numz) = S1(numz-1);
 %   S2(numz) = S2(numz-1);
end
%*************************************************************
% Radiation Pressure
%*************************************************************

for scatnum = 1: NSTOP-1
  no = scatnum;
```

```
  nfact1 = (no*(no+2))/(no+1);
  nfact2 = (no*2+1)/(no*(no+1));

  fact1(no) = nfact1*real( a(no)*conj(a(no+1))+ b(no)*conj(b(no+1)));
  fact2(no) = nfact2*real(a(no)*conj(b(no)));
  nfact(no) = 2*n+1;
  nscat(no) = nfact(no)*(abs(a(no))^2+abs(b(no))^2);
  nextinct(no)  = real(a(no)+b(no));


end
%n0 = 1:NSTOP;
%sigma = sum( (2.*n0+1).*(abs(a).^2 +abs(b).^2))
%sigmas = (2*pi/k^2)*sigma

%qcos = (4/x^2)*(sum(fact1)+sum(fact2))
%sigmas = area*(2*pi/k^2)*(sum(nscat))
%sigmas = (2/x^2)*(sum(nscat))
%sigmas = (2*pi/k^2)*(sum(nscat));
%sigmatr = (2/x^2)*sum(nfact.*nextinct);
%***********end of crossections ******************************

  S11(1:jj) = .5*((abs(S2.^2))+(abs(S1.^2)));
  S12(1:jj) = .5*((abs(S2.^2))-(abs(S1.^2)));
  S33(1:jj) = .5*(conj(S2).*S1 + (conj(S1).*S2));
  S34(1:jj) = .5i*(conj(S2).*S1 - (conj(S1).*S2));

  n0 = 1:NSTOP;
  n01 = 1:NSTOP-1;
  %acb = a(n01).*conj(a(n01+1))+b(n01).*conj(b(n01+1));
  % ******** Scattering cross section ***********
  nn0 = 2*n0+1;
  absfact = abs(a).^2 + abs(b).^2;
  sigmas = (2*pi/k^2)*sum(nn0.*absfact)
  % ********* Extinction Cross section ********
  sigmaex = (2*pi/k^2)*sum(nn0.*real(a+b))

  %calculating *****  Qscatter<cos> ******
  %real(a(n) x conjugate (a(n+1)) + b(n) x conjugate(b(n+1))) :: part1 of Qscatter
  acb = real(a(n01).*conj(a(n01+1))+b(n01).*conj(b(n01+1)));
```

```
  % part II of Qscatter<cos> :: real(a(n) x b(n))
  ab = real(a(n01).*conj(b(n01)));
  nn1 = n01.*(n01+2)./(n01+1);  %n(n+2)/n+1
  nn2 = (2.*n01+1)./(n01.*(n01+1)); %2n+1/n(n+1)
  f1 = nn1.*acb;
  f2 = nn2.*ab;
  Qcos = (4/x^2).*(sum(f1)+sum(f2));


  Qsigmas = sigmas/area;
  g = Qcos/Qsigmas
  sigmatr = sigmas*(1-g)

  gindex(nnn,1) = wl;
  gindex(nnn,2) = g;
 toc
end
toc
```

# APPENDIX D

## LIST OF PUBLICATIONS

1. Masood Siddique, R. R. Alfano, G. A. Berger, M. Kempe and A. Z. Genack, "*Time-Resolved Studies Of Stimulated Emission From Colloidal Dye Solutions*", Optics Letters, 21, 450 (1994)

2. Masood Siddique, Li Yang, Q. Z. Wang and R. R. Alfano, "*Mirrorless Laser Action From Optically Pumped Dye-Treated Animal Tissues*", Optics Communications, 117, 475, (1995)

3. Masood Siddique, Q. Z. Wang and R. R. Alfano, "*Laser action in condensed disordered media of active dye-stained animal tissues and sandy colloidal scattering walls*", Journal of Biomedical Optics, 1, 442, (1996)

4. Masood Siddique and R. R. Alfano, "*Transmission Of Ultrafast Optical Pulse Through Transparent Host Medium Containing Absorptive And Non-Absorptive Scatterers*" submitted for publication

5. Alimova A., Katz, A., Siddique, M., Minko, G., Savage, H. E., Shah, M., Rosen, R. B. and Alfano R. R., "*Native Changes Induced by Bactericidal Agents*", accepted in IEEE sensor Journal, (2005)

## CONFERENCES AND PRESNETATIONS

1. Masood Siddique, Li Yang, Q. Z. Wang And R. R. Alfano, "*Ultrafast Temporal Behavior Of Of Laser Action Of Dyes In Sand-Like Powders*", Optical Society Of America, Annual Meeting, Baltimore, MD, (1995)

2. Masood Siddique, Li Yang, Q. Z. Wang And R. R. Alfano, "Time-Resolved Studies Stimulated Emission From Colloidal Dyes" OSA, Annual Meeting Dallas, TX, (1994)

3. Masood Siddique, Q. Z. Wang And R. R. Alfano, "Laser Action In Animal Tissues", OSA Annual Meeting, Dallas TX, (1994)

4. Masood Siddique And R. R. Alfano, "*Laser Action In Random Media*", OSA, Long Island, NY (1998)

5. Masood Siddique And R. R. Alfano, "*Laser Action Animal Tissues*", Annual Meeting , NASA, JPL, Pasadena, CA, (1994)

## List Of Sponsors

1. New York State Science And Technology Foundation
2. New York State Center for Advanced Technology for Lasers and Materials
3. Air Force Office Of Scientific Research
4. National Science Foundation

# BIBLIOGRAPHY

## CHAPTER 1


1. Rayleigh, Lord, *Phil. Mag.* 41, 107 (1871)
2. A. Schuster, *Astrophys. J.* 21, 1 (1905)
3. K. Schwarzchild, *Göttinger Nachrichten*, p. 41 (1906)
4. Mie, G., *Ann. Phys.*, 25, 377-445 (1908)
5. S.Chandrasekhar, "Radiative transfer", Dover 1960
6. H. C. van de Hulst, "Light scattering by small particles", Dover, 1981
7. C. F. Bohren and D. R. Huffman, "Absorption and scattering of light by small particles", Wiley-Interscience, 1983
8. A. L. Schawlow and C. H. Townes, *Phys. Rev.* 112, 1940-1949 (1958)
9. Lawandy, N. M. and Balachandran R. M., Gomes A.S.L., and Sauvain, E., *Nature*, 368, 436 (1994)
10. Sha, W.L., Liu C-H. and Alfano, *Opt. Lett.* 19, 1922 (1995)
11. Masood Siddique, Alfano R.R, Berger G.A. Kempe A. and Genack A.Z., *Opt. Lett.*, 21,450, 1996
12. Letokhov,v. S.*et al, "Non-resonant feedback in Lasers"*, Pergamon Press Ltd, (1970)
13. Markushev V NI, Zolin V F ,Briskina Ch. 1986 Sov: .1. Quantum *Electron.* 16 28
14. Gouedard C., Husson D., Sauteret C., Auzel F and Migus A, *J. Opt. Soc. Am. B* 10 2358, 1993
15. Cao, H., *Waves in random media*, 13, R1, (2003)
16. Auzel F and Goidner P, *J. Alloys Compounds* 300, 2000

17. Wiersma D S. and Lagendijk A, *Phys. Rev. E* 54 4256,

18. Berger, G.A., Kempe M and Genack A.Z., *Phys. Rev.E,* 56, 6118,1997

19. K. M. Yoo, Feng Liu and R. R. Alfano, Optics Letters, 16, 1068, (1991)

20. Wei Cai, M. Xu, Melvin Lax and R. R. Alfano, Optics Letters, 27, 731, (2002)Cai

21. Koichi Furutsu, Yokio Yamada, Phys. Rev. E, Vol. 50, 3634, (1994)

## CHAPTER 2

1. C. F. Bohren and D. R. Huffman, "*Absorption and scattering of light by small particles*", Wiley-Interscience, 1983

2. Ishimaru, Akira, "*Wave propagation and scattering in Random Media*", IEEE Press, (1997)

3. H. C. van de Hulst, "*Light scattering by small particles*", Dover, 1981

4. S.Chandrasekhar, "*Radiative transfer*", Dover 1960

5. Siegman, Anthony, "*Lasers*", University Science Books, (1986)

6. Duarte F.J., Hillman, L.W., "*Dye laser Principles*", Academic Press, 1990

7. Milne, E. A. , Philos. Trans. Roy. Soc. (London), A, 223, 201 (1922)

## CHAPTER 3

1. A. L. Schawlow and C. H. Townes, "Infrared and optical masers," Phys. Rev.112,1940-1949 (1958).

2. R. H. Dicke, Phys. Rev. 93, 99 (1954)

3. Maiman, T.H.,*Nature,* Vol. 187, No. 4736, pp. 493-494. 1960

4. R.V. Ambartsumyan, P.G. Kryukov and V.C. Letokhov,

Sov. Phys. JETP 26 ( 1968 ) 835.,V.M. Markushev, V.F. Zolin and Ch.M. Briskina, Sov. J. QuantumElectron. 16 (1986) 281;

6. N.E. Ter-Gabrielyan, V.M. Markushev, V.M. Belan, Ch.M. Briskina, O.V. Dimitrova, V.F. Zolin and A.V. Lavrov, Sov. J.Quantum Electron. 21 ( 1991 ) 840, and references therein.

7. N.M. Lawandy, R.M. Balachandaran, A.S.L. Gomes and E. Sauvian, Nature 368 (1994) 436.

8. W. Sha, C.H. Liu and R.R. Alfano, Optics Lett. 19 (1994).

9. M. Siddique, Li Yang, Q.Z. Wang and R.R. Alfano, Opt. Soc. Am. Annual Meeting, Dallas, Texas, October 1994;

10. M. Siddique, Q.Z. Wang and R.R. Alfano, Opt. Soc. Am., Annual Meeting, Dallas, TX, October 1994;

11. W. Sha, C.H. Liu and R.R. Alfano, Opt. Soc. Am., AnnualMeeting, Dallas, TX, October 1994.

12. Masood Siddique, R. R. Alfano, G.A.Berger, M. Kempe and A. Z. Genack, *Opt. Lett. 21, 450, 1996*

13. Masood Siddique, Q.Z.Wang, R. R. Alfano, *J. Biomedical Opt.* 1, 442, 1996

14. M. Balachandran and N.M. Lawandy, Opt. Soc. Am.,Annual Meeting, Dallas, TX, October 1994.

15. Noginov M. A., Caulfield H J. Noginova N E and Venkateswarlu P, *Opt. Commun.* 118, 430 1995

16. Noginov M. A., Egarievwe S U, Noginova N E., Caulfield H. and Wang J C, *Opt. Mater.* 12 127, 1999

17. Noginov M. A, Egarievwe S U. Noginova N E, Wang J C and Caulfield H J, *J. Opt. Soc. Am.* B, 15, 2854, 1998

18. Noginov M A, Noginova N E, Egarievwe S U., Caulfield H J, Cochrane C., Wang J C., Kokta M R, and Paitz J, *Opt. Mater,:* 10 ,297, 1998

19. Noginov M A, Noginova N E, Egarievwe S U., Caulfield H J., Venkateswarlu P., Thompson T, Mahdi M and Ostrumov V, *J. Opt. Soc. Am.* B 13 2024, 1996

20. Noginov M A., Noginova N E, Egarievwe S U, Caulfield H J., Venkateswarlu P., Williams A and Mirov S B, *J. Opt. Soc. Am..* B 14, 2153, 1997

21. Gouedard C., Husson D., Sauteret C., Auzel F and Migus A, *J. Opt.* Soc. Am. B 10 2358, 1993

22. Briskina Ch M., Markushev V M, and Ter-G Gabrielyan N E, *Quantum Electron.* 26 23, 1996

23. Auzel F and Goidner P, *J. Alloys Compounds* 300, 2000

24. Zyuzin A Yu, *Europhys. Let.* 26 5 7, 1994

25. Zyuzin A Yu, *Phys. Rev:* E 51 5274, 1995

26. Zyuzin A Yu, JETP 86 445, 1998

27. Wiersma D S. and Lagendijk A, *Phys. Rev. E* 54 4256, 1997

28. Zolin V F, *J. Alloys Compounds* 300 214, 2000

29. Markhushev V, Ter-Gariclyan N E. Briskina Ch NI. Belan V R and Zolin V F 1991) Sov. J. *Quantum Electron.* 20 773

30. Markushev V NI, Zolin V F tilts! Briskina Ch. 1986 Sov: .1. Quantum *Electron.* 16 281

31. Cao H. Jiang X. Ling Y. Xu J *Y* and Soukoulis C M 2003 *Preprint* cond-

mat/0301461

32. Cao H. Ling Y., Xu J Y and Burin A L, 2002 *Phys. Rev: E,* 66 R25601

33. Cao H., Ling Y., Xu J Y., Cao C Q and Kumar P, 2001 *Phys. Rev Lett.* 86 4524

34. Cao H., Xu J Y., Chang S-H and Ho S T, 2000 *Phys. Rev.* E 61 1985

35. Cao H., Xu J Y. Chang S-H., Ho S T, Seelig F W., Liu X and Chang R P H *Phys.Rev. Lett.* 84 5584, 2000

36. Cao H. Xu J Y, Seelig E W and Chang R P H *Appl. Phys. Lett.* 76 2997, 2000

37. Cao H., Zhao Y G, Liu X., Seelig E W and Chang R P H, *Appl. Phys. Lett.* 75 1213, 1999

38. Cao H., Zhao Y G., Ong H C and Chang R P H *Phys. Rev.* B 59 15107, 1999

39. Cao H., Zhao Y G., Ong H C., Ho ST., Dai J Y, Wu J Y and Chang R. P.H., *Appl. Phys. Lett.* 73 3656, 1998

40. Cao H., Zhao Y G., Ong H C, Ho S T., Seelig E. Q., Wang Q H., and Chang R.P.H., Phys. Rev. Lett. 82 2278, 1999

41. Frolov S V., Vardeny Z V., Yoshino K. Zakhidov A A, and Baughman R H, *Phys. Rev.* **B 59** R5284, 1999

42. Frolov S V., Vardeny Z V, Yoshino K. Zakhidov A A, and Baughman R H, Opt. *Commun.* 162 241, 1996

43. Yoshino K, Tatsuhara S., Kawagishi Y and Ozaki M, *Appl Phys. Lett.* 74 2590, 1999

44. Soukoulis C. M, Jiang X., Xu J Y and Cao H *Phys, Rev.* B 65 R041103, 2002

45. Zacharakis G., Heliotis G., Filippidis G., Anglos D and Papazoglou T G,

*Appl. Opt.*, 38 6087, 1999

46. Zacharakis G, Papadogiannis N A., Filippidis G and Papazoglou T G, *Opt. Lett.* 25 923, 2000

47. Zacharakis G., Papadogiannis N A and Papazoglou T. G., *Appl. Phys. Lett.* 81 2511, 2002

48. A.Z. Genack and J.M. Drake, Nature 368 (1994) 400.

49. Ling Y., Cao H., Burin A L., Ratner M A., Liu X and Chang R P H., *Phys. Rev.* A 64 063808, 2001

50. John S., *Phys. Today*, 44, 32, 1991

51. John S and Pang G, *Phys. Rev.* A 54 3642, 1996

52. A. A Lisyansky, J.H. Li, N. Garcia. T.D. Cheung and A. Z. Genack, *"Photonic Band Gaps and Localization", Ed. C. M. Soukoulis, Plenum Press, New York, 1993*

## Chapter 4

1. F. Duarte, Dye laser principles (Academic Press, Boston, MA,1990).
2. N.M. Lawandy, R.M. Balachandaran, A.S.L. Gomes and E. Sauvian, Nature 368 (1994) 436.
3. W. Sha, C.H. Liu and R.R. Alfano, Optics Lett. 19 (1994).
4. Masood Siddique, R.R. Alfano, G.A. Gerber, M. Kempe and A.Z. Genack, *Opt. Lett.*, 21, 450 (1996)
5. M. Siddique, Li Yang, Q.Z. Wang and R.R. Alfano, Opt. Soc. Am. Annual Meeting, Dallas, Texas, October 1994;

6. M. Siddique, Q.Z. Wang and R.R. Alfano, Opt. Soc. Am., Annual Meeting, Dallas, TX, October 1994;

7. W. Sha, C.H. Liu and R.R. Alfano, Opt. Soc. Am., AnnualMeeting, Dallas, TX, October 1994.

8. R.V. Ambartsumyan, P.G. Kryukov and V.C. Letokhov, Sov. Phys. JETP 26 ( 1968 ) 835.

9. V.M. Markushev, V.F. Zolin and Ch.M. Briskina, Sov. J. QuantumElectron. 16 (1986) 281.

**10.** N.E. Ter-Gabrielyan, V.M. Markushev, V.M. Belan, Ch.M. Briskina, O.V. Dimitrova, V.F. Zolin and A.V. Lavrov, Sov. J.Quantum Electron. 21 ( 1991 ) 840, and references therein.

11. Gouedard C., Husson D., Sauteret C., Auzel F and Migus A, *J. Opt. Soc. Am. B* 10 2358, 1993

12. Cao, H., *Waves in random media*, 13, R1, (2003)

13. Pradhan and N. Kumar, Phys. Rev. B 50 ( 1994 ) .

14. )Randal C. Polson and Z. Valy Vardeny, App. Phys. Lett. V85, 1289 (2004)

**15.** Randal C. Polson G. Levina and Z. Valy Vardeny, App. Phys. Lett. V76, 3858 (2000) Lihong Wang, Da Liu, Nancy He, Steven L. Jacques and Sharon L. Thomsen, Applied Optics, V35,1775 (1996

**CHAPTER 5**

1. K. M. Yoo and R. R. Alfano, Opt. Lett. 15, 320 (1990)

2. L. Wang, P.P. Ho, C. Liu, G. Zhang and R. R. Alfano, Science, 253, 769 (1991)

3. D.J.Pine, D.A. Weitz, P.M. Chaikin and E. Herbolzheimer, Phys. Rev. Lett, 60, 1134 (1988)

4. D.A. Weitz, D.J.Pine, P.N. Pusey and R. J. A. Tough, Phys. Rev. Lett, 63, 1747 (1989)

5. K. M. Yoo, Feng Liu and R. R. Alfano, Optics Letters, 16, 1068, (1991).

6. Melvin Lax, Reviews of Modern Physics, 23, 287, (1951).

7. Van Der Hulst, '*Light scattering by small particles*', Dover, (1981)

8. Koichi Furutsu, Yokio Yamada, Phys. Rev. E, Vol. 50, 3634, (1994)

9. Wei Cai, M. Xu, Melvin Lax and R. R. Alfano, Optics Letters, 27, 731, (2002)

10. Private communications with M. Xu;

11. A. Ishimaru, "*Wave propagation and scattering in random media*", (Academic, New York, 1978), vol. 1

## Chapter 6

1. R.V. Ambartsumyan, P.G. Kryukov and V.C. Letokhov,

Sov. Phys. JETP 26 ( 1968 ) 835

2. N.M. Lawandy, R.M. Balachandaran, A.S.L. Gomes and E. Sauvian,

Nature 368 (1994) 436.

3. Soukoulis C. M, Jiang X., Xu J Y and Cao H *Phys, Rev.* B 65 R041103, 2002

4. Randal C. Polson G. Levina and Z. Valy Vardeny, App. Phys. Lett. V76, 3858 (2000)

5. Masood Siddique, Q.Z.Wang, R. R. Alfano, *J. Biomedical Opt.* 1, 442, 1996